REPUBLIC OF TÜRKİYE

YILDIZ TECHNICAL UNIVERSITY

GRADUATE SCHOOL OF SCIENCE AND ENGINEERING

TECHNO-ECONOMIC ANALYSIS OF HYBRID RENEWABLE ENERGY SYSTEMS FOR THE OPTIMAL DESIGN OF A HYDROGEN REFUELLING STATION IN GERMANY

Berna Burcu KALYONCU

DOCTOR OF PHILOSOPHY THESIS

Department of Chemical Engineering

Program of Chemical Engineering

Supervisor

Prof. Dr. Hasan SADIKOĞLU

Co-Supervisor

Assist. Prof. Dr. Yavuz KIRIM

December, 2025

REPUBLIC OF TÜRKİYE

YILDIZ TECHNICAL UNIVERSITY

GRADUATE SCHOOL OF SCIENCE AND ENGINEERING

TECHNO-ECONOMIC ANALYSIS OF HYBRID RENEWABLE ENERGY SYSTEMS FOR THE OPTIMAL DESIGN OF A HYDROGEN REFUELLING STATION IN GERMANY

A thesis submitted by Berna Burcu KALYONCU in partial fulfillment of the requirements for the degree of **DOCTOR OF PHILOSOPHY** is approved by the committee on 25.12.2025 in Department of Chemical Engineering, Program of Chemical Engineering.

Prof. Dr. Hasan SADIKOĞLU Yildiz Technical University Supervisor	Assist. Prof. Dr. Yavuz KIRIM Siirt University Co- supervisor

Approved By the Examining Committee

Prof. Dr. Hasan SADIKOĞLU, Supervisor
Yildiz Technical University _____

Prof. Dr. Nil ACARALI, Member
Yildiz Technical University _____

Assist. Prof. Dr. Abdullah Bilal ÖZTÜRK, Member
Yildiz Technical University _____

Prof. Dr. Mustafa ÖZİLGEN, Member
Yeditepe University _____

Assoc. Prof. Dr. Özgün YÜCEL, Member
Gebze Technical University _____

I hereby declare that I have obtained the required legal permissions during data collection and exploitation procedures, that I have made the in-text citations and cited the references properly, that I haven't falsified and/or fabricated research data and results of the study and that I have abided by the principles of the scientific research and ethics during my Thesis Study under the title of "Techno-economic Analysis of Hybrid Renewable Energy Systems for the Optimal Design of a Hydrogen Refuelling Station in Germany" supervised by my supervisor, Prof. Dr. Hasan SADIKOĞLU. In the case of a discovery of false statement, I am to acknowledge any legal consequence.

Berna Burcu KALYONCU

Dedicated to my beloved children,

Can and Melisa

ACKNOWLEDGEMENTS

I would like to express my sincere gratitude to my supervisor, Prof. Dr. Hasan SADIKOĞLU, for his guidance and continuous support throughout my doctoral studies. I am truly grateful for the opportunity to work under his supervision.

I would like to sincerely thank my co-supervisor, Assist. Prof. Dr. Yavuz KIRIM, for his close collaboration, motivation, and valuable contributions during our work together. His perspective has played an essential role in strengthening the quality of my research.

I would also like to thank Assist. Prof. Dr. Mert Akın İNSEL for his support throughout my thesis, as he always answered my questions and provided valuable help whenever I encountered difficulties.

I am deeply grateful to my family for their endless love, patience, and support throughout this journey. Their support has given me the strength and determination to complete this thesis.

Berna Burcu KALYONCU

TABLE OF CONTENTS

LIST OF SYMBOLS viii
LIST OF ABBREVIATIONS ix
LIST OF FIGURES x
LIST OF TABLES xii
LIST OF MAPS xiv
ABSTRACT xv
ÖZET xvii
1 INTRODUCTION 1
1.1 Literature Review 1
1.2 Objective of the Thesis 9
1.3 Original Contribution 10
2 HYBRID RENEWABLE ENERGY SYSTEMS AND HYDROGEN TECHNOLOGIES 12
2.1 Hybrid Renewable Energy Systems 12
2.1.1 Classification of Hybrid Renewable Energy Systems by Grid Connectivity 14
2.1.2 Sources of Renewable Energies for Hybrid System Utilization 16
2.1.3 Integration of Thermal Components into Hybrid Renewable Energy Systems 23
2.2 Hydrogen Technologies 26
2.2.1 Hydrogen Production Methods 27
2.2.2 Hydrogen Cost 28
2.2.3 Green Hydrogen Production 30
2.2.4 Green Hydrogen Applications and Integration Pathways 31
2.2.5 Hydrogen Roadmap of Germany 33
3 FUNDAMENTALS OF REGULARIZATION AND REGRESSION MODELS 36
3.1 Fundamentals of Regularization 36

3.1.1 Multicollinearity 36
3.1.2 Bias and Variance 37
3.1.3 Overfitting and Underfitting 38
3.1.4 Cross Validation 40
3.1.5 Root Mean Square Error and Coefficient of Determination 41
3.2 Regression Models 42
3.2.1 Linear Regression Model 42
3.2.2 Ridge Regression Model 43
3.2.3 Lasso Regression Model 43
3.2.4 Elastic Net Regression Model 44
4 METHODOLOGY, DATA AND ECONOMIC ANALYSIS 46
4.1 Methodology and Data for Hybrid Systems 46
4.1.1 Definition of Hybrid Systems 46
4.1.2 HOMER Pro Analysis 47
4.1.3 Description of the selected site 49
4.1.4 Hybrid System Components 51
4.1.5 Hydrogen Load Data 55
4.1.6 Electric Load Data 56
4.1.7 Thermal Load Data 57
4.1.8 Biomass Load Data 57
4.2 Methodology and Data for Regression Models 59
4.3 Economic Analysis 62
4.3.1 Net Present Cost 62
4.3.2 Levelised Cost of Energy 62
4.3.3 Levelised Cost of Hydrogen 62
4.3.4 Operating Cost 63
4.3.5 Initial Capital Cost 63
4.3.6 Operational and Maintenance Cost 63
4.3.7 Replacement Cost 63
5 RESULTS AND DISCUSSION 64
5.1 Techno-economic Results of Hybrid Systems 64
5.1.1 Optimization Results of the Systems with Four Different Wind Turbines 64

5.1.2 Optimization Results of the Systems without Recovering Excess Energy 66
5.1.3 Optimization Results of the Systems with Thermal Components 70
5.1.4 Sensitivity Analysis of Capital Costs, O&M Costs, and Electrolyser Efficiency on System Performance 78
5.1.5 Optimization Results of the Systems with Biogas generator 83
5.2 Regression Model Results 94
5.2.1 Linear Regression Results 94
5.2.2 Ridge, Lasso, Elastic Net Regression Results 95
5.2.3 Model Comparison 99
6 CONCLUSION **101**
6.1 Conclusion 101
REFERENCES **104**
PUBLICATIONS FROM THE THESIS **114**

LIST OF SYMBOLS

$	American Dollar
m^3	Cubic Meter
°	Degree
°C	Degree Celsius
E	East
€	Euro
GW	Gigawatt
kg	Kilogram
km	Kilometer
kW	Kilowatt
kWh	Kilowatt-hour
MJ	Megajoule
m	Meter
M	Million
mio.mt	Million metric tons
'	Minute
N	North
%	Percentage
s	Second
m^2	Square meter
TWh	Terawatt-hour

LIST OF ABBREVIATIONS

CO_2	Carbon Dioxide
EE	Excess Electricity
ENR	Elastic Net Regression
HOMER	Hybrid Optimization of Multiple Energy Resources
HRES	Hybrid Renewable Energy Systems
LCOE	Levelized Cost of Energy
LCOH	Levelized Cost of Hydrogen
LR	Lasso Regression
MGT	Micro Gas Turbine
NPC	Net Present Cost
O&M	Operational and Maintenance
PV	Photovoltaic
R	R programming language
R^2	Coefficient of determination
RR	Ridge Regression
RMSE	Root Mean Square Error
TLC	Thermal Load Controller
WT	Wind Turbines

LIST OF FIGURES

Figure 2.1 A scheme for a grid-connected HRES system [48] **15**
Figure 2.2 A scheme for an off-grid HRES system [48] **16**
Figure 2.3 Global installed solar PV capacities throughout the years [56] **18**
Figure 2.4 Global installed wind energy capacities throughout the years [56] **19**
Figure 2.5 A PV-wind hybrid system scheme **21**
Figure 2.6 Global installed bioenergy capacity over the years [56] **23**
Figure 2.7 A scheme of HRES with TLC and boiler for hydrogen production **24**
Figure 2.8 A scheme of HRES with MGT and boiler for hydrogen production .. **26**
Figure 2.9 Flow diagram of green hydrogen production and transportation processes [72] **31**
Figure 2.10 Hydrogen demand growth in Germany over years [40] **34**
Figure 2.11 Hydrogen refuelling stations in Germany by year [40] **35**
Figure 3.1 Bias and variance scheme using a bulls-eye diagram [94] **38**
Figure 3.2 The graphs for (a) underfitting, (b) good fit, (c) overfitting [96] **39**
Figure 3.3 Representation of k-fold cross validation [99] **41**
Figure 4.1 Flow Chart of HOMER Pro Optimization Process Steps **48**
Figure 4.2 The monthly solar radiation and clearness index of Schleswig-Holstein **50**
Figure 4.3 The monthly average wind speed at Schleswig-Holstein **50**
Figure 4.4 Hydrogen load profiles of the systems: (a) daily; (b) seasonal; (c) yearly profiles **56**
Figure 4.5 Electric load profiles of the systems: (a) daily; (b) seasonal; (c) yearly profiles **56**
Figure 4.6 Thermal load profiles of the systems: (a) daily; (b) seasonal; (c) yearly profiles **57**
Figure 4.7 Monthly straw biomass distribution of the Schleswig-Holstein in HOMER Pro software **58**
Figure 5.1 HOMER Pro schemes of HRES with various WT **65**

Figure 5.2 The monthly electricity production of: (a) PV/XANT L-36 WT/Battery; (b) PV/XANT L-36 & Vestas V47 WT/Battery systems **67**

Figure 5.3 HOMER Pro schemes of HRES with thermal components **71**

Figure 5.4 CO2 emissions of the thermal component integrated HRES **78**

Figure 5.5 HOMER scheme of the biomass-only system..... **84**

Figure 5.6 HOMER scheme of the PV/XANT L-36 WT /Biogas gen. system **86**

Figure 5.7 HOMER scheme of the PV/ XANT L-36&Vestas V47 WT/Biogas gen. system **90**

Figure 5.8 Mean squared error vs log (λ) for the train data in (a) RR; (b) LR **97**

Figure 5.9 Coefficients vs log (λ) for the train data in (a) RR; (b) LR; (c) ENR **98**

LIST OF TABLES

Table 2.1 Carbon footprint and hydrogen production technology for different types of hydrogen [70] **27**

Table 2.2 Hydrogen production costs by energy source [70] **29**

Table 4.1 Techno-economic data of the system components [10], [12], [22], [112], [113], [114] **51**

Table 4.2 Daily Biomass Availability Profile Based on 504,000 tons of Annual Straw Supply, Distributed Inversely to Solar Radiation **58**

Table 4.3 Annual variable values used in regression analysis [56], [117], [118], [119], [120], [121], [122] **61**

Table 5.1 Renewable fraction and EE results of the HRES with different WT **66**

Table 5.2 Optimum configuration of HRES with different WT **67**

Table 5.3 Techno-economic analysis results of the HRES with different WT **68**

Table 5.4 The costs of each component for the PV/XANT L-36 WT/Battery system **68**

Table 5.5 The costs of each component for the PV/XANT L-36 & Vestas V47 WT/Battery system **69**

Table 5.6 Hydrogen, gasoline replacement, and CO2 emission reduction values **70**

Table 5.7 Optimum configuration of thermal component integrated systems with XANT L-36 WT **72**

Table 5.8 Optimum configuration of thermal component integrated systems with XANT L-36 & Vestas V47 WT **72**

Table 5.9 The costs of each component for the PV/XANT L-36 WT/TLC/Boiler system **73**

Table 5.10 The costs of each component for the PV/XANT L-36 WT/TLC/ Boiler/MGT system **74**

Table 5.11 The costs of each component for the PV/XANT L-36 & Vestas V47 WT/TLC/Boiler system **74**

Table 5.12 The costs of each component for the PV/XANT L-36&Vestas V47 WT/TLC/Boiler/MGT system **75**

Table 5.13 Techno-economic analysis results of the HRES with XANT L-36 WT **77**

Table 5.14 Techno-economic analysis results of the HRES with XANT L-36&Vestas V47 WT **77**

Table 5.15 Sensitivity Analysis: Effects of Capital and O&M Cost Changes on System Cost **79**

Table 5.16 Sensitivity Analysis of Electrolyser Efficiency for PV/XANT L-36 WT System **82**

Table 5.17 Sensitivity Analysis of Electrolyser Efficiency for PV/XANT L-36 &Vestas V47 WT System **83**

Table 5.18 Techno-economic analysis results of biomass-only system **85**

Table 5.19 Techno-economic analysis results of PV/XANT L-36 WT /Biogas gen. System **87**

Table 5.20 Techno-economic analysis results of PV/XANT L-36 WT /Biogas gen. (2000kW) system with different electrolyser capacities **88**

Table 5.21 The costs of each component for the PV/XANT L-36 WT /Biogas gen. system **89**

Table 5.22 Techno-economic analysis comparison of PV/XANT L-36 WT system with/without biogas generator **90**

Table 5.23 Techno-economic analysis results of PV/ XANT L-36&Vestas V47 WT/Biogas gen. system **91**

Table 5.24 Techno-economic analysis results of PV/XANT L-36&Vestas V47 WT/Biogas gen. (1000kW) system with different electrolyser capacities **92**

Table 5.25 The costs of each component for the PV/XANT L-36 WT/Vestas V47 WT/Biogas gen. system **93**

Table 5.26 Techno-economic analysis comparison of PV/XANT L-36 WT/Vestas V47 WT system with/without biogas generator **93**

Table 5.27 Linear regression model results created in R **94**

Table 5.28 RR, LR and ENR model results created in R **96**

Table 5.29 Comparison of Model Performance Based on Different Regression Parameters **99**

LIST OF MAPS

Map 4.1 Map of the selected site, Schleswig-Holstein, Germany [110].....**49**

ABSTRACT

Techno-economic Analysis of Hybrid Renewable Energy Systems for the Optimal Design of a Hydrogen Refuelling Station in Germany

Berna Burcu KALYONCU

Department of Chemical Engineering

Doctor of Philosophy Thesis

Supervisor: Prof. Dr. Hasan SADIKOĞLU

Co- supervisor: Assist. Prof. Dr. Yavuz KIRIM

This study investigates the optimal configuration of stand-alone hybrid renewable energy systems (HRES) for green hydrogen production at a hydrogen refuelling station in Schleswig-Holstein, Germany. The Hybrid Optimization of Multiple Energy Resources (HOMER) Pro software is utilized to simulate different configurations and perform techno-economic analyses.

In the first part, several HRES configurations powered by photovoltaic (PV) panels and different wind turbines (WT) were examined to achieve 100% renewable fraction. Simulation results indicated that the systems with XANT L-36 and XANT L-36 & Vestas V47 WT could prevent more than 700 tons of carbon dioxide (CO_2) emissions annually. Additionally, econometric analysis of global green hydrogen production was conducted using linear, ridge regression (RR), lasso regression (LR), and elastic net regression (ENR) models in R programming language (R). The RR model demonstrated the best predictive ability based on the root mean square error (RMSE) and the coefficient of determination (R^2) value. The final

model highlighted that global hydrogen refuelling stations had the most significant influence on green hydrogen production.

In the second part, a thermal load controller (TLC) and boiler were integrated, along with a micro gas turbine (MGT) to manage surplus electricity and provide heat. Results showed that systems with TLC and boiler were not feasible, while MGT integration significantly reduced the costs by recovering waste heat. The optimum system includes PV, XANT L-36, Vestas V47, electrolyser, hydrogen storage, battery, TLC, boiler, and MGT, with $6.28 M net present cost (NPC), $0.249/kWh levelized cost of energy (LCOE), and $2.14/kg levelized cost of hydrogen (LCOH).

In the third part, biomass-based HRES were analysed. The configurations include a straw-fuelled biogas generator with PV and WT. The results demonstrated that integrating a biogas generator with PV and WT achieved lower NPC and LCOH values while minimizing excess electricity (EE) to below 1-2%.

Keywords: Solar energy, wind energy, hydrogen, econometric analysis, biomass.

ÖZET

Almanya'da Bir Hidrojen Yakıt Dolum İstasyonunun Optimum Tasarımı için Hibrit Yenilenebilir Enerji Sistemlerinin Tekno-ekonomik Analizi

Berna Burcu KALYONCU

Kimya Mühendisliği Anabilim Dalı

Doktora Tezi

Danışman: Prof. Dr. Hasan SADIKOĞLU

Eş-Danışman: Dr. Öğr. Üyesi Yavuz KIRIM

Bu çalışmada, Almanya'nın Schleswig-Holstein bölgesinde bir hidrojen dolum istasyonunda yeşil hidrojen üretimi için hibrit yenilenebilir enerji sistemlerinin (HRES) optimum konfigürasyonunu tasarlamak amaçlanmıştır. Çoklu Enerji Kaynakları Hibrit Optimizasyon (HOMER) Pro yazılımı, farklı konfigürasyonları modellemek ve tekno-ekonomik analizler gerçekleştirmek için kullanılmıştır.

Birinci bölümde, fotovoltaik (PV), çeşitli rüzgar türbinleri (WT) ile %100 yenilenebilir oranında çalışan çeşitli HRES konfigürasyonları incelenmiştir. Simülasyon sonuçları, XANT L-36 ve XANT L-36 & Vestas V47 rüzgar türbinleri içeren sistemlerin yıllık 700 tondan fazla karbondioksit (CO_2) emisyonunu önleyebileceğini göstermiştir. Ayrıca, küresel yeşil hidrojen üretiminin ekonometrik analizi, doğrusal, ridge (RR), lasso (LR) ve elastic net regresyon (ENR) modelleri kullanılarak R programında (R) gerçekleştirilmiştir. Kök ortalama kare hatası (RMSE) ve belirleme katsayısı (R^2) değerlerine göre RR modeli en iyi

tahmin performansını göstermiştir. Nihai model, küresel hidrojen dolum istasyonlarının yeşil hidrojen üretimini en çok etkilediğini göstermiştir.

İkinci bölümde, bir ısıl yük kontrolörü (TLC), kazan ve mikro gaz türbini (MGT) fazla elektriği kullanmak ve ısı elde etmek için sistemlere ilave edilmiştir. Sonuçlar, TLC ve kazan kullanılan sistemlerin ekonomik olarak uygun olmadığını, MGT entegrasyonunun ise atık ısı geri kazanımı sayesinde maliyetleri önemli ölçüde azalttığını göstermiştir. Optimum sistem; PV, XANT L-36, Vestas V47, elektrolizör, hidrojen depolama tankı, batarya, TLC, kazan ve MGT'den oluşmakta olup, $6.28 milyon net bugünkü maliyet (NPC), $0.249/kWh seviyelendirilmiş enerji maliyeti (LCOE) ve $2.14/kg seviyelendirilmiş hidrojen maliyeti (LCOH) değerlerine sahiptir.

Üçüncü bölümde, biyokütle destekli HRES analiz edilmiştir. Konfigürasyonlar, saman yakıtlı bir biyokütle jeneratörünün PV ve rüzgar türbinleriyle birlikte kullanılmasını içermektedir. Sonuçlar, biyokütle jeneratörünün PV ve rüzgar türbinleriyle entegrasyonunun daha düşük NPC ve LCOH değerleri sağladığını ve fazla elektriği (EE) %1–2'nin altına indirdiğini göstermiştir.

Anahtar Kelimeler: Güneş enerjisi, rüzgar enerjisi, hidrojen, ekonometrik analiz, biyokütle.

1
INTRODUCTION

1.1 Literature Review

Today, the amount of energy used globally has increased dramatically [1]. However, a large population of people lacks adequate energy sources [2]. Fossil fuels form the main part of electricity production on an immense scale. The combustion of fossil fuels leads to ecological harm and contributes to global climate issues as a result of the greenhouse emissions released [3]. Notably, the transportation sector accounts for a significant share of global fossil fuel consumption. Consequently, this contributes to the continuous increase in pollutant emissions into the atmosphere [4].

Although nuclear power provides low-carbon energy, its risks such as long-lived radioactive waste, catastrophic accidents (e.g., Fukushima, 2011), and high costs have led many countries to abandon it due to safety concerns and the growing competitiveness of renewables. France remains an exception, relying on nuclear for 67% of its electricity [5]. Radioactive waste and accident risks continue to pose health and environmental threats, including long-term cancer risks [6].

The demand for alternative energy sources for generating electricity has increased due to decreasing fossil fuel resources, unreliable fossil fuel costs, rising electricity consumption, and the risks of global warming [7]. The world needs a substantial change towards more environment-friendly energy sources to counterbalance the destructive impacts on the environment [8]. The adoption of these sources for energy depends on location or site since these sources of energy cannot deliver continuous power to the load due to site limitations. When there are insufficient

supplies of these energy sources, a load's primary power requirement cannot be satisfied by them [9].

Hydrogen fuel has low emission level and high energy efficiency. Hence, this fuel has the highest energy density when compared to various fuels per weight [10]. The suitability of hydrogen as an electricity storage solution when derived from renewable energy resources has been particularly emphasized [11]. Hydrogen can be generated via two principal methods: water electrolysis and natural gas reforming. Water electrolysis has a high efficiency of above 70%. The reliance on renewable sources to generate hydrogen significantly helps the environment by reducing gas emission levels [12]. Therefore, green hydrogen has been rapidly finding applications in the energy industry domains, particularly in the transport industry. In transport sectors, hydrogen fuel cells serve as power sources for fuel cell electric cars. As fuel cell vehicles increase on roads, the demand for refuelling stations based on renewable hydrogen fuels continually increases [13].

Modelling a renewable energy system is important to carry out accurate feasibility evaluation [12]. It can be designed both off-grid and grid-connected energy configurations with comprehensive results of the techno-economical, sensitivity and environmental assessments [14]. Although various studies have been performed to design HRES, only limited studies address simulating green hydrogen production for hydrogen refuelling stations via renewable sources in HOMER Pro software.

Gökçek et al. proposed a hydrogen refuelling station driven by HRES on Gökçeada, Turkey, utilizing a hybrid system combining wind, solar, and battery storage. The design, modelled with HOMER Pro software, aimed to support up to 25 vehicles daily, each with a 5 kg hydrogen storage. Their analysis indicated that the hydrogen production costs varied between $8.92/kg and $11.08/kg, depending on the system configurations [12]. The authors later carried out a techno-economical assessment for a hydrogen refuelling station utilizing a PV-wind renewable energies in İzmir-Çeşme, Turkey. The results showed that İzmir-Çeşme was a more favorable location for establishing a hydrogen refuelling station compared to Gökçeada Island. In this new study, the LCOH was lower, ranging from $7.53/kg to $7.87/kg

and indicating a more feasible option for hydrogen generation in the region [13]. Siyal et al. examined the economic feasibility of hydrogen refuelling stations utilizing wind energy at three different regions in Sweden, using two V82 and V112 WT. The refuelling station was proposed to serve 200 vehicles/day, with simulations performed using HOMER Pro software. The study revealed that green hydrogen could be steadily produced by wind energy at selected areas. When using the V112 WT, the LCOH ranged from $5.18/kg to $7.25/kg, while with the V82 turbine, the costs were higher, ranging from $6.52/kg to $9.62/kg [14]. A similar study focusing solely on wind energy was conducted by Ayodele et al. in South Africa. The study evaluated a hydrogen refuelling station designed for 25 fuel cell electric vehicles, each with a 5 kg tank and an annual hydrogen demand of 45.63 tons. The NPC of the system ranged between $3.74 M and $5.38 M, with LCOE between $0.098/kWh and $0.140/kWh. The LCOH was found to be between $6.34/kg and $8.97/kg [4]. Barhaumi et al. performed a techno-economic analysis for hydrogen generation using a PV grid-connected system. The proposed refuelling station would operate 24 hours a day, supplying an average of 6.67 kg of hydrogen/hour. The optimized system was found as a viable alternative with an LCOH of 5.5 kg at a total NPC of €4.17 M [11]. Okonkwo et al. carried out research work to simulate a hybrid energy system at Al-Kharj in Saudi Arabia that uses solar and wind energies for hydrogen production. The total daily demand was estimated as 20 kg of hydrogen. The optimized hybrid energy system had the lowest LCOH of $9.34/kg, LCOE of $0.6208/kWh, and a total cost of $484,360 [15]. The research carried out by Praveenkumar et al. aimed to supply the electricity demand of five major Indian cities. The hydrogen demand for a refuelling station was defined for 20 hydrogen vehicles that require 5 kg of hydrogen. The minimum LCOH of $3.00/kg had been obtained by Mumbai as against $3.22/kg by Ludhiana. The remaining four cities had LCOH of $3.11/kg, $3.16/kg, and $3.17/kg [10]. Chen et al. had designed a hydrogen refuelling system for 50 vehicles that had 5 kg of hydrogen capacity. The various route options had LCOE that varied from 0.28 to 0.83 Renminbi/kWh. The LCOH values were given as 40 to 50 Renminbi/kg [16]. The research paper presented by Micena et al. proposed a hydrogen refuelling system that was powered by a PV power system at a Brazilian city. The paper

outlined the various options of replacing the existing taxis by fuel cell buses that were suggested as a next step. The daily demand of hydrogen had varied from 20 to 185 kg depending on replacement of 10% to 100%. The paper showed that the LCOE varied from $0.27 to $0.41/kWh and the LCOH varied from $8.96 to $13.55 [17].

A notable expansion in the installation of hydrogen refuelling stations has been observed for transportation in recent years. So, it is important to develop hydrogen refuelling stations that rely on renewable energy sources for fuel cell vehicles [12]. In addition, the HRES produces substantial excess energy while meeting the power requirement in off-grid situations. However, the only a few references that deal with hydrogen and thermal loads are those that use EE for hydrogen refuelling stations.

Jahangiri et al. focused on the utilization of biomass, wind, and solar energy in HRES system for the concurrent generation of electricity and heat in Zarrin Shahr, Iran. They used four scenarios: two were on-grid, with one of them converting EE to heat, while the other two scenarios were off-grid, with one of them also has heat conversion. The results showed that connection to the national grid was most cost-effective scenarios with LCOE of 0.014 $/kWh. However, for sites beyond 2.8 km away from the grid, off-grid scenarios were suggested. The optimal off-grid hybrid system resulted in an LCOE of $1.019/kWh [18]. The author later examined a combine heat and power system integrating solar energy, WT, biogas generator, fuel cell, boiler and grid to meet both electric and heating demands simultaneously. Among different system configurations, the optimum configuration showed a minimum LCOE of $1.16 per kWh [19]. Das et al. proposed a model that evaluates excess energy utilization and waste heat recovery through HOMER Pro software. They studied PV, WT, TLC, MGT and Li-ion battery configurations. Scenarios both including and excluding waste heat recovery options, as well as the TLC, were analysed to assess their effectiveness in meeting heating demand. The hybrid systems with both the TLC and the heat recovery unit had lower energy costs (LCOE was 0.178 $/kWh for Cyclic Charging (CC) strategy and 0.212 $/kWh for Load Following (LF) strategy) compared to the systems using only the TLC (LCOE was 0.192 $/kWh for CC strategy and 0.218 $/kWh for LF strategy) [20]. The author later carried out research to obtain a hybrid renewable energy system that

utilized excess energy to meet the electric and thermal demands of a rural region. The system comprised a solar energy, WT, battery, TLC, gas boiler, and diesel generator, and was analysed for techno-economic feasibility using a hybrid optimization model. The study compared different configurations to meet electric and thermal demand. The results showed that the PV/Wind/Battery hybrid system achieved a lower LCOE of $0.255/kWh when meeting thermal demand, compared to $0.274/kWh when not utilizing excess energy [21]. Akhtari et al. performed the techno-economic analysis of a hybrid system by combining solar panel, WT, diesel, electrolyser, and battery to fulfil electrical, heating, and hydrogen demands of in 5 different cities in Iran. A TLC powered by EE was incorporated to satisfy thermal demand. The results demonstrated that recovering surplus electricity could increase the renewable fraction up to 35%, while simultaneously reducing the LCOE and CO_2 emissions by 7.1% and 10.6%, respectively [22]. Micco et al. performed their research for an off-grid hybrid system simulated to operate with WT, a fuel cell, electrolyser, battery, hydrogen tank and boiler. The system's objectives were to meet industrial electrical and thermal demands; to produce 100 kg of hydrogen/day to fuel 20 fuel cell vehicles; and to provide electricity for fast-charging 50 battery electric vehicles each day. The levelized costs were estimated at $0.048 to $0.054/kWh for electricity, $3.14 to $3.49/kg for hydrogen and $0.037 to $0.048/kWh for thermal energy [23]. Isa et al. designed a grid-dependent combined heat and power system containing PV, fuel cell, and battery technologies via HOMER Pro software. The resulting configuration had the minimum LCOE at $0.091 per kWh, with a NPC of $106,551. The electrical energy was not utilized to meet the thermal demand in this research. Instead, waste heat recovery via fuel cell was employed. If the thermal demand could not be met, it was provided by an electric water heating system via grid electricity [24]. Ramesh et al. carried out optimization research for HRES with PV, wind, hydro, diesel, and battery technologies to provide electricity to a remote village in India. They utilized lead-acid and lithium-ion battery systems in the HOMER Pro optimizer for their analysis. The results showed LCOE values ranging from $0.10 to $0.162/kWh, NPC values between $465,790 and $716,658, and annual CO_2 emissions varying from 30,934 to 89,911 kg [25].

Biomass is readily available and abundant source in rural areas. Moreover, the massive amounts of biomass materials produced by farming, animal husbandry, and forestry in isolated rural areas must be consumed to maintain production. When biomass resources are converted into organic fertilizer by natural fermentation processes like composting and returning to the field, considerable amounts of CO_2 gases are released simultaneously. Thus, it is also necessary and feasible to use biomass in remote rural locations in an environmentally friendly way [26]. Schleswig-Holstein's strong agricultural sector provides significant biomass potential, particularly straw from wheat cultivation, which is plentiful, cheap, and never competes with food production. For this reason, straw biomass is considered as an additional renewable source for HRES to reduce costs while maintaining sustainability [27]. Therefore, biomass-based HRES scenarios were analysed by integrating a straw-fuelled biogas generator with PV and WT, and the related literature studies are presented below.

Sanni et al. assessed a hybrid solar PV/Biogas/Diesel power system for supporting an unreliable energy supply from the grid at an abattoir site in Ado-Ekiti, Nigeria. The biogas fuel from anaerobic processing of cattle paunch manure was used as a supplementary source to solar PV. Two optimum configurations were proposed using the HOMER software as Grid/PV/Biogas and Grid/PV/Diesel. The results indicated that the solar system and biogas fuel combination provides lower LCOE of \$0.164/kWh and an NPC of \$67,616. Furthermore, this configuration reduced carbon emissions by 61.5% compared to the diesel system. The results show that solar power integrated with biogas fuel provides viable economic and environmental considerations as an alternative solution to using a diesel power system [28]. Sigarchian et al. designed and proposed a hybrid power system that incorporated PV panels and a wind system integrated with a biogas engine for supporting electricity for a village community located in Kenya. The monthly average and peak power needs were 8 kW and 16.5 kW. In addition, it is proposed that cattle and sheep manures were used as biological sources of gas. The study used HOMER simulation analysis to perform the economic assessment of a system that integrated a power system which used a gas engine as an alternative to diesel fuel. The system showed better economic viability that gave a LCOE of \$0.25/kWh

when compared to a diesel-powered system that gave a higher cost by 20%. In addition, capital cost and NPC are lowered by 30% and 18%, and CO_2 emissions are reduced by 17 tons/year [29]. Al-Najjar et al. examined hybrid Solar PV/Biomass power system integration that included Solar PV power and biomass power that were designed to supply energy needs of a household. The study included research from Gaza that have adequate solar power, and it used HOMER PRO analysis that examined a community of 1074 kWh of daily demand. The data showed improved NPC of $2.30 M with an LCOE of $0.438/kWh [30]. Li et al. performed a techno-economic assessment of an off-grid HRES designed to provide rural electrification for a village located in western China. In the selected village, maize straw from 180 ha of cultivated land provided about 3000 tons/year of freely available biomass, which was utilized by converting it into biogas for energy production. Simulations and optimization studies resulted that the most economical and stable configuration included 104 kW of PV, three 10 kW WT, a 50 kW biogas generator, 331 kWh of battery storage, and a 99 kW converter, generating about 322,158 kWh/year and supplying electricity at a COE of $0.201/kWh, making the village independent of the main grid [31]. Kirim et al. conducted novel modular HRES combining biogas and solar PV for dairy cattle barns in Konya, Erzurum, and Izmir cities in Turkey. In this study, dairy cattle barns were assumed to be the source of cattle manure (CM), which was utilized as the primary biomass feedstock for biogas production. The results demonstrated that grid-connected systems with PV and biomass were more feasible than stand-alone biomass systems in terms of NPC, return on investment, LCOE, and annual worth. The lowest NPC values for five different barn capacities ranged from $36,942 to $3,097,716 [32]. The author further designed a hybrid system combining solar PV and biogas co-firing for a hazelnut cracking plant in Ordu, Turkey. The study compared different HRES configurations and analysed the impact of government incentives on NPC and LCOE. Sensitivity analysis considered factors such as biomass price, discount rate, inflation, and grid sellback rate. The optimal scenario achieved the lowest NPC ($3.0 M) and LCOE ($0.098/kWh) with a renewable fraction of 73.6%, while CO_2 and NO_x emissions were minimized in another scenario. The study was notable for evaluating the co-firing potential of hazelnut shells with natural gas and estimating

the electricity generation potential of the facility [33]. Boghdady et al. analysed a hybrid system combining PV and biomass as a energy supply for a poultry farm in Egypt. Poultry litter is considered as a biomass material. The proposed system was tied to a grid network and enhanced reliability and mitigated issues associated with surplus power. The analysis indicated that a 400 kW power-generating system and a 500 kW PV system can provide power to a poultry farm all day and was more economical as it cuts costs to a lower value of $0.0894/kWh when compared to a power-generating system that relied on grid connections [34]. Sarkar et al. proposed a microgrid that combined a renewable system including a PV energy and a wind energy in addition to a biomass power system and a vanadium redox battery. The microgrid supplied a rural village with a steady power supply. The study utilized biogas generated from biodegradable waste from canteen and kitchen residues. The quantity of biogas generated was calculated to produce 1 m^3 biogas through 25 kg of biodegradable waste. The HOMER Pro program was utilized to simulate and evaluate the system, and it demonstrated in a practical scenario that combined a microgrid consisting of a 10 kW solar PV, 1 kW wind, and 15 kilovolt-amper biogas generator. The significance of the study is to highlight how biomass can synergistically work with solar and wind energy in a microgrid for a sustainable energy supply in a rural setup [35]. Rad et al. conducted the evaluation of economic feasibility for a hybrid power generation system that combined hydrogen with other renewables in a rural area in Iran. The study proposed a power system that included PV, wind energy, and a biogas system that used cow dung as its biomass material. The results showed that a system that combined PV, wind power, and biogas was more economical but another system that employed fuel cells increased costs by 33-37%. Stand-alone power systems that employed a reformer had LCOE that ranged between $0.164-0.233/kWh. Others that were grid connected had LCOE that ranged between $0.096-0.125/kWh [36]**.** H. El-houari et al. designed an off-grid power system that was a combination of hybrid renewable energy sources that could provide power to a village in Morocco that was far away from the power grid. The design involved a power system from sun energy. The study used biogas generated from anaerobic digestion of cow dung that came from 27 domestic reindeers. In this study, all generated power came from renewable sources, with 48% derived from

biomass balance, 41% from solar power, and the remaining 11% from wind energy. The LCOE of the optimum configuration that included PV, wind and biomass resources was calculated as 0.20 $/kWh. The proposed study reduced carbon emissions to a maximum of 28.8 tons annually compared to power generated from diesel and grids [37]. Malik et al. proposed a techno-economic and feasibility study for an off-grid hybrid systems in the western Himalayan region, India. The optimized system consisted of a PV array, a biomass gasifier, and a battery bank. The share of power generated from biomass and solar is 59% and 41%, respectively. The biomass considered is pine needle biomass resource. The availability of total biomass was given 690 tons/year with the cost of $14.57/ton. The optimum LCOE was estimated to be $0.185/kWh with significant decrease of CO_2 emissions compared to the diesel-based power system [38].

1.2 Objective of the Thesis

In this study, techno-economic analyses of green hydrogen production for an on-site hydrogen refuelling station in Schleswig-Holstein, Germany, have been conducted. The PV and two different WT sources are used in the HRES. The study compares various system configurations to meet electrical, hydrogen, and thermal demands, including the use of waste heat and electricity recovery in the HRES. The CO_2 emissions avoided by the systems with a 100% renewable fraction, and the CO_2 emissions produced by the systems with lower renewable fractions, are also determined. Additionally, sensitivity analyses are conducted to examine the effects of variations in capital costs, O&M costs, and electrolyser efficiency on system performance and costs.

Besides, the econometric analyses can help future research make better predictions and create more effective strategies to reduce risks in green hydrogen energy investments. Recently, machine learning algorithms have exhibited remarkable advancements in energy systems and various other research disciplines. Within the energy sector, these algorithms are particularly applied in areas such as energy production and demand forecasting [39]. Kirim et al. carried out a regression analysis to estimate the effect of electricity production on Turkey's gross domestic

product by creating four regression models in R. Thirteen independent variables, related to renewable energies were used for prediction in linear regression, RR, LR and ENR models. The results indicated that total installed cost of solar energy variable had the most significant impact [32]. Therefore, an econometric analysis is performed in this study using machine learning methods to predict global green hydrogen production values using R. Twelve independent variables, which significantly impact global green hydrogen production, are used for the econometric assessment with four different regression models: Linear regression, RR, LR, and ENR.

Moreover, this study evaluates the role of biomass as a supplementary renewable energy in a HRES for hydrogen generation. Availability and sustainability of wheat straw biomass in Schleswig-Holstein render it a cheap and valuable resource that can easily be harnessed as an energy resource. Thus, the study evaluates the techno-economic feasibility of multiple configurations and determines the most efficient design for green hydrogen production at a refuelling station integrating biomass, solar PV, and wind energy systems. The study also examines system reliability, renewable fraction, and the reduction of EE.

1.3 Original Contribution

The original contributions of the study are outlined as follows:

- A considerable research gap exists in the literature related to innovative hybrid systems that can address both hydrogen and thermal loads effectively. In this context, while addressing both energy requirements together, the aim of this study is to design a more economical and effective system for hydrogen refuelling and hence assist in the development of sustainable energy infrastructure. Therefore, the proposed research tries to contribute to the efforts to lower hydrogen production costs by developing more efficient and better integrated hybrid energy system designs.

- The hydrogen is produced through various methods in Germany, but only 28% of this hydrogen is produced through green methods [40]. Thus, by modelling an on-site hydrogen refuelling station, the study aims to model cheap, safe and

efficient production of green hydrogen in Schleswig-Holstein, Germany which is important to help the country's environment strategy of releasing zero CO_2 emissions.

- Reliable forecasts can be generated to guide investments, research and development, and market expansion by collecting relevant data and selecting appropriate models. So, the regression model examines how significant factors can assist future research in generating reliable predictions for renewable energy systems. Since the production of green hydrogen is still relatively low compared to its potential and the rising demand, econometric models can be applied to predict global green hydrogen production. While HOMER determines the optimal configuration for green hydrogen production, the regression model provides insight into the market changes that might impact this production. Accordingly, the study intends to perform a novel econometric analysis that has not been reported in the literature to determine the factors influencing green hydrogen production using regression models.

- Biogas generators are not weather-dependent and are fully dispatchable. This property enables them to compensate for the intermittent nature of PV and wind energy sources, because these renewable sources can lead to fluctuating power supply and unstable electrolyser operation. Biogas generators can adjust their output according to the availability of PV and wind sources by providing on-demand power. So, they can ensure continuous and stable electrolyser operation. This approach minimizes EE and reduces the need for large-scale energy storage. However, few research in the literature have examined the use of biomass specifically for hydrogen production. Therefore, it is aimed to integrate biomass as an alternative energy source to enhance both the economic efficiency and environmental sustainability of HRES for green hydrogen production.

2
HYBRID RENEWABLE ENERGY SYSTEMS AND HYDROGEN TECHNOLOGIES

2.1 Hybrid Renewable Energy Systems

The significance of environment friendly power generation technologies in the future scenario is highlighted by an increasing awareness regarding environmental concerns and actions focused on minimizing the use of fossil fuels for electricity production [41]. Although renewable sources are vital for a sustainable future scenario, energy fluctuations in natural resources like sun and wind result intermittent and inefficient operation for power generation. However, by utilizing the comparative advantages of these energy sources, a hybrid system that includes renewable energies could reduce dependency on unstable grids and other fossil fuel-based power sources [42].

Hybrid systems are primarily characterized by the combination of different renewable energy sources for electricity production [43], [44], [45], [46]. The HRES play a vital role in sustainable energy transition as they make optimal use of renewable resources. They ensure a sustainable energy shift away from fossil fuels and can address growing demands for clean energy. Furthermore, HRES can mitigate intermittency associated with stand-alone renewable energy resources and can provide a stable power supply through the integration of different resources [46].

The common type of hybrid power combines both solar and wind energy. The sun provides power through solar panels during daytime hours. The excess power generated is stored in batteries. To ensure that there is a steady power supply even during nighttime hours when there is no power from solar energy, wind energy is

used as a supplementary resource to produce electricity and charge batteries. In a setup that combines solar and hydro power, for instance, power generated during sun hours is used to pump water. The water serves as a battery that is released during nighttime hours to flow through a turbine to generate energy since solar panels are not producing power during this time. Thus, combining different sources of power in a hybrid setup improves power efficiency and ensures a stable power supply compared to a system that employs one power-generating source [43].

Battery storage is a key component for HRES and has been incorporated to address the two key operational challenges. The first one is to provide adequate power to satisfy the peak load demand even in periods where solar and wind resources are not contributing to the power supply for electricity generation. The next key challenge addressed using battery storage is to deal with the mismatch between peak load demand hours and the maximum output hours of solar and wind resources [47]. This not only overcomes the most challenging issues but can allow the utilization of solar/wind resources in an efficient manner, thereby decreasing the LCOE substantially [43].

Hybrid technologies offer an even better alternative for modern grids with integrated economic, environmental, and social benefits [48]. Due to these advantages, they work best in areas with limited or no grid access [43]. In such areas, through careful selection of the most applicable renewable resources based on the geographical location, it is possible to significantly reduce dependence on fossil fuels. This would not only strengthen the long-term reliability of the power supply but would also enhance the energy independence of countries that currently depend on other countries to satisfy their power needs [44].

The advantages of the HRES are summarized as follows [49], [50]:

- Provides a continuous and reliable supply of energy to meet the demand.
- Optimizes the utilization of available renewable resources for maximum productivity.
- Requires minimal ongoing O&M costs.
- Shows good performance in converting natural resources into usable energy.
- Enables the most effective matching of supply to consumer load requirements.

- Provides greater flexibility in managing and directing power distribution.
- Reduces the harmful impacts resulting from fossil fuel combustion on the environment.
- Strengthens the overall reliability and resilience of the energy system.
- Reduces total ownership costs for applications with peak demands or growing energy needs.
- Delivers electrical power that meets higher standards of quality and stability.
- Provides inherent flexibility for capacity expansion.
- The combination of various other sources may be achieved based on the resource availability.
- The setup for wind and PV systems is easily accomplished because they are easy to install and modular.

2.1.1 Classification of Hybrid Renewable Energy Systems by Grid Connectivity

HRES are designed to function in either stand-alone or grid-connected mode [51]. This fundamental distinction between stand-alone and grid-connected configurations is important, as it directly influences key decisions about how renewable sources are integrated and how the overall system is managed [52].

The techno-economic feasibility of the usage of HRES in standalone or remote areas has been remarkably improved. This can be the result of the concurrent advancements in the area of renewable energy resources and the effective power electronic converters needed to appropriately convert the energy variations of the renewable sources into a useful form of energy for the application [51]. Therefore, in standalone hybrid system design, the need of extensive technical and economic studies is crucial. This is primarily because, despite the intermittent nature of available renewable resources, standalone power arrangements should be self-sufficient in terms of managing the maximum demand while offering a continuous supply of electricity. In contrast, for grid-connected systems, understanding the nature of connection provides the researcher to simulate different scenarios and to evaluate the benefits of HRES integrating with the existing power network [52].

2.1.1.1 Grid-connected Hybrid Renewable Energy Systems

A grid-connected energy system is a decentralized power generation unit that operates while integrated with the main electrical grid. This setup is most practical for areas with existing grid infrastructure [48]. Figure 2.1 illustrates a grid-connected hybrid system with PV and wind turbine energy sources.

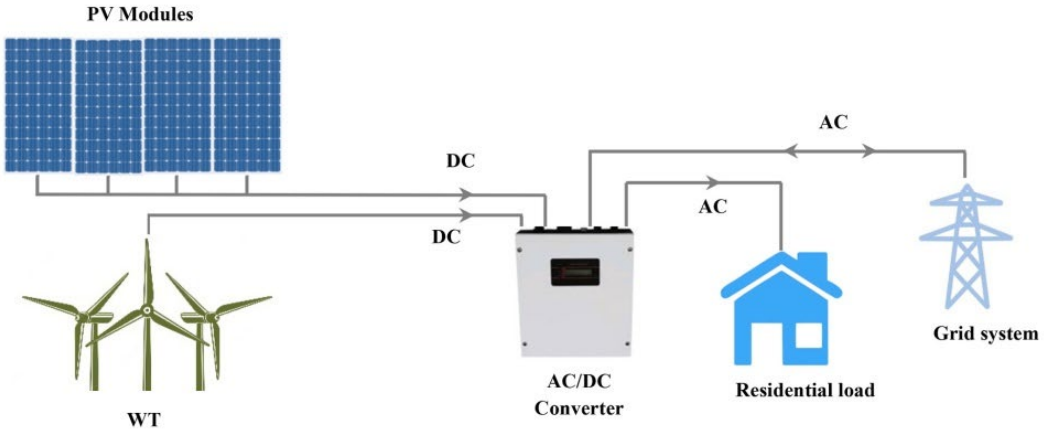


Figure 2.1 A scheme for a grid-connected HRES system [48]

The system may be intended to meet only the local power demand, with any surplus delivered to the grid, or it can be designed to deliver all generated electricity directly to the grid. The availability of the grid enables the construction of larger systems which can achieve higher capacity factor values, thereby making them economically viable. Indeed, in this situation, the grid acts as if it has an unlimited battery with effortlessly handling the supply and demand in various seasonal periods. However, aside from the initial installation cost, there would also be the additional installation cost of the equipment employed in connecting to the grid. Furthermore, for systems based on renewable sources such as solar and wind, their large-scale operation may require the use of biomass or other supplementary resources to maintain continuous functioning [53].

2.1.1.2 Stand-alone Hybrid Renewable Energy Systems

The standalone HRES can generate electricity without relying on the grid power supply and are known to require a storage system for a stable operation. The systems are very useful and applicable in remote locations that are away from any

grid electricity supply [48]. Figure 2.2 illustrates an off-grid hybrid system with PV and wind turbine energy sources.

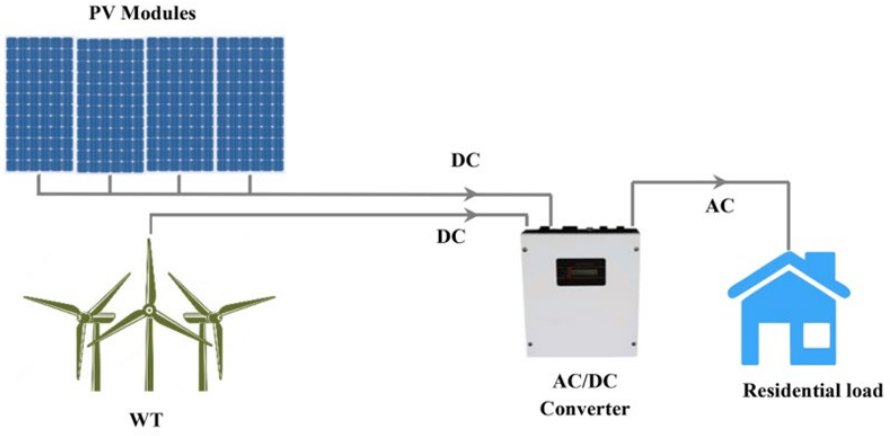


Figure 2.2 A scheme for an off-grid HRES system [48]

Standalone systems are commonly chosen in remote regions across the world because they provide a practical solution where conventional power stations are located far from the main grid. These systems prioritize the demands of the area by designing the energy producing capacity to meet to the specific local demand. They are an ideal solution for remote locations where the power station does not have to operate at full capacity all the time. Since they are disconnected from the utility grid, stand-alone systems require batteries to store electricity produced when demand is low. This results in additional costs for batteries and storage; otherwise, any surplus power that is generated is wasted [53].

2.1.2 Sources of Renewable Energies for Hybrid System Utilization

Various renewable sources can be used for hybrid power systems, including wind, PV, micro-hydro, biomass, geothermal, and ocean wave or tidal energy [41]. Each source has different levels of availability, development, and ease of integration. This study specifically focuses on wind, PV, and biomass energy because they can create a synergistic combination, and they are widely applicable, especially for local power generation. Therefore, the following sections present comprehensive information for these resources to provide a technical basis of this research.

2.1.2.1 Solar Energy Source

Solar energy is considered site-specific, unlimited, and clean with significant potential for alternative energy production. The importance and viability of solar power have received considerable attention and intensified development since the global petroleum crisis in the 1970s. The most prominent drawback of solar power is its intermittency and unpredictable nature. This makes it impossible for stand-alone solar PV plants to provide useful power to the load for most parts of the year in isolated areas. Hence, the battery storage components are installed to provide continuous energy supply. The battery storage is sized based on the number of days the system needs to run on its own. This shows how reliably the electrical load can be maintained [47].

The solar radiation received in the global arena is one of the major sources of energy with high capability in terms of promoting the usage of renewable forms of energy and reducing the greenhouse effect in terms of gas emissions. The solar intensity differs on a regional level in terms of geographic locations in the world. Hence, the usable solar intensity of any place is directly proportional to the intensity of solar radiation received at that location [45]. The intensity of total solar power is also correlated with the position of the sun in the sky, that fluctuates seasonally throughout the year [47]. Furthermore, it decreases in terms of geographic factors such as elevation, atmospheric moisture, dust content in the atmosphere, and atmospheric clouds, resulting in an observed irradiance [54].

The solar PV technology is a novel technology area in the renewable energy industry, exhibiting immense growth and continuous technological evolution in the world's energy marketplaces [51]. During 2023, this technology was recognized to be the major contributing factor in the global renewable power installed capability, surpassing hydropower for the very first time in recorded history. At the end of 2024, there was considerable growth in the global solar PV installed capability to 1,865 GW, showing an immense increase in solar PV capability from 710 GW registered in 2020. The new installation capacity of solar PV technology in 2024 registered over 451 GW in the renewable industry, symbolizing the most widely used technology in the renewable industry, accounting for over three-quarters of all

new installed renewable capacity in the global market in 2024 [55]. Figure 2.3 shows the growth of global installed solar PV capacity by year.

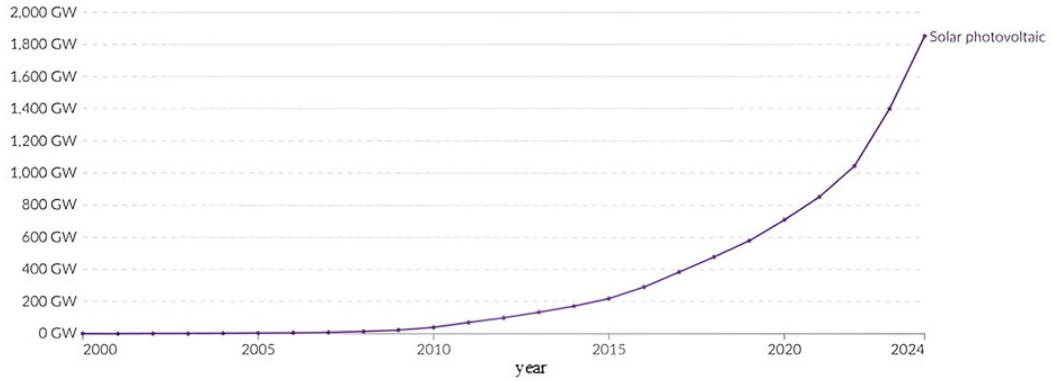


Figure 2.3 Global installed solar PV capacities throughout the years [56]

The manufacturing costs for solar panels have experienced a sharp and consistent reduction during the past decade, establishing solar technology not just as a viable alternative but commonly as the lowest-cost option for power generation. Data shows the LCOE for solar PV fell by almost half just between 2018 and 2023. Examining the broader period from 2014 to 2023 reveals that the global weighted-average LCOE for utility-scale solar PV projects declined sharply, from $0.16/kWh to only $0.044/kWh. By 2023, this significant cost decreases had made solar power 56% more affordable than electricity generated from conventional fossil fuels [55].

2.1.2.2 Wind Energy Source

The conversion of wind energy's kinetic energy into electrical power is the fundamental principle behind wind energy production. Modern WT can harness such energy in the form of rotational mechanical energy via the turbine blades to produce usable electric power [55].

Wind energy can be considered an alternative renewable, site-specific, and clean form of energy with considerable potential. Nonetheless, wind energy production would fulfill only the energy needs if the wind speed can remain within the operational range. Therefore, HRES are designed to include backup energy storage, ensuring that the system can continuously meet load demand regardless of fluctuations in generation [51].

Wind energy potential shows regional differences worldwide, where seasonal and major weather patterns play an essential role on wind speed. There tend to be periods where there is abundant wind in areas, followed by periods of low wind speed [54]. Nonetheless, wind energy has major importance in low-capacity power production in regions with abundant wind resources. Thus, areas with high wind speeds and consistency in wind patterns, such as in offshore and elevated areas, are major fields for wind farms to be installed [45].

The wind power sector has experienced remarkable global growth from the beginning of the century, affected by technological innovation, supportive government policies, and substantial cost reductions. According to IRENA statistics, worldwide installed wind power capacity encompassing both onshore and offshore installations has multiplied nearly 100-fold over twenty years, increasing to approximately 1,131 GW by 2024. The year 2024 saw particularly strong growth with 113 GW of new capacity installations, representing an 11.1% annual increase. Onshore capacity installation has reached 1,053 GW by 2024, with offshore capacity growing six times from the 2015 installed capacity of 11.7 GW to 79.4 GW. Output from the installed capacity in terms of electricity has also grown, reaching 2,098 TWh in 2022 [55]. The growth of global installed wind energy capacity within the years are given in Figure 2.4.

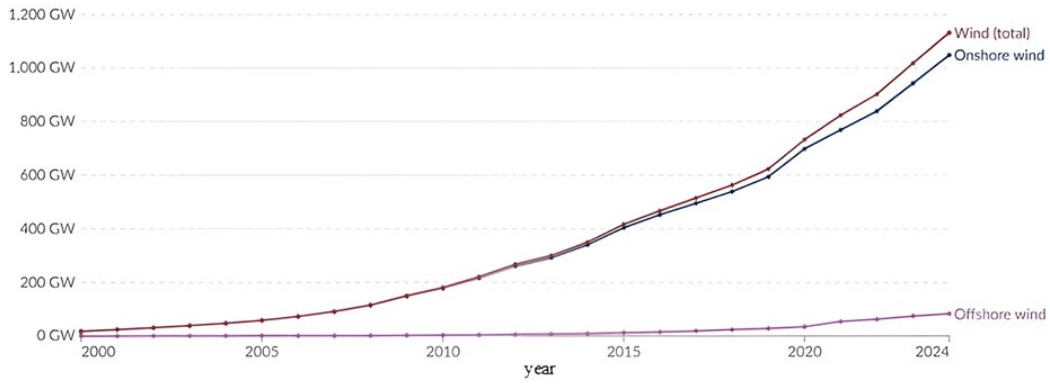


Figure 2.4 Global installed wind energy capacities throughout the years [56]

There have been advances in technology and capacity increases, leading to reduced costs and improved efficiency. Between 2010 and 2023, the global weight-average LCOE in onshore wind fell by 70 %, from $0.089/kWh to $0.033/kWh. Between

2010 and 2023, the LCOE of newly installed offshore projects also fell by 63 %, from $0.203/kWh in 2010 to $0.075/kWh in 2023 [55].

2.1.2.3 Integration of Photovoltaic and Wind Energy Sources

The integration of wind and solar photovoltaic (PV) systems has expanded substantially over recent decades and now plays an important role in the global electricity supply. Nevertheless, both PV and wind systems have weather-dependent nature, because these renewable sources produce unstable output characteristics [49], [50]. This natural intermittency leads to power fluctuations on a large scale, thereby presenting major difficulties to the power management in terms of power quality, load leveling, and reliability of supply and dispatch control [50]. Without the help of storage devices, such as batteries and backup generators, these systems can be considered extremely unreliable in autonomous operation [49].

The integration of PV systems and WT forms a highly effective renewable energy solution, where their naturally complementary generation profiles ensure more consistent power output to meet electrical demand. Since peak generation periods for solar and wind energy generally occur at different times of the day and year, their combination creates a more balanced power output profile [50]. This complementary characteristic enables hybrid systems to generate more consistent energy while reducing dependency on battery storage and backup generators [49]. Figure 2.5 illustrates a scheme of a PV-wind hybrid system with back up components for hydrogen production.

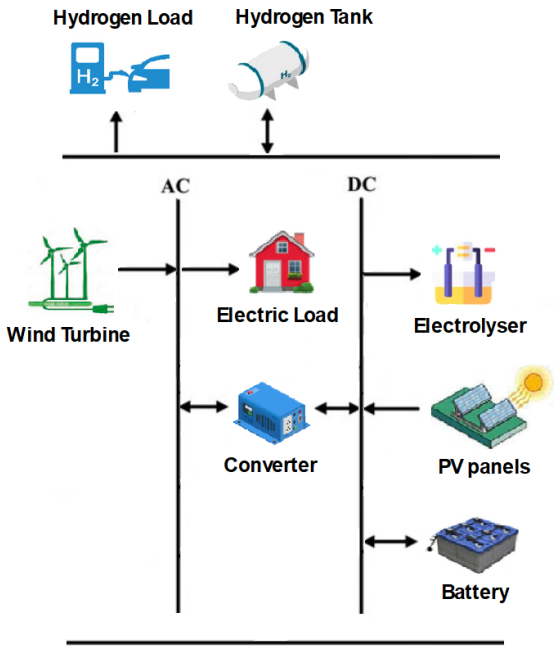


Figure 2.5 A PV-wind hybrid system scheme

Careful sizing of all components, namely the size of the PV array, wind turbine, and batteries, is essential in the efficient functioning of these hybrid systems. The battery size should be enough to provide for the loads in cases where there is cloud cover or low wind. Additionally, the site-specific factors, like the amount of solar irradiation, wind availability, and geographical distance from the point of utilization, are very essential and have significant implications on whether the system is efficient and viable [49].

2.1.2.4 Biomass Energy Source

Biomass is composed of plant-derived organic matter and it is a biological waste that can be converted into productive uses, such as energy production. Biomass has emerged as a prominent alternative to fossil fuel transitioning from fossil fuel-based energy to renewable energy resources in the world today. Biomass consists of primarily three resource forms: agricultural crop harvest residuals, biodegradable wastes such as industry-generated sludges, biological wastes such as animal dungs, and biodegradable wastes in the form of food wastes, and lastly, forest-derived materials for bioenergy production. The most useful form of bioenergy in current practices is agricultural crops harvest residuals, which can be defined as residuals

left behind after harvest processes together with the residuals left behind after food processing in domestic and industrial setups. The agricultural crop harvest residuals include maize residuals, palm fruit residuals, rice residuals, sorghum residuals, millet residuals, coconut residuals, wheat residuals, and sugarcane residuals. Electricity can be currently obtained from these forms of biomass through processes such as gasification, combustion, or pyrolysis methods [45].

There are two major application areas of bioenergy, namely traditional and modern bioenergy. Traditional bioenergy can be defined as the direct combustion of biological matter in the form of wood, animal waste, and charcoal. Alternatively, modern bioenergy can be defined as modern technologies in the application area of bioenergy production in the form of biofuel from bagasse and plant crops, biorefineries, biogas from the anaerobic digestion process of organic substances, wood pellets in automatic heating plants, and other new technologies [55].

Biomass has immense potential in improving the energy independency of growing and densely populated countries like Brazil, India, and the Republic of China. Biomass can be utilized as a fuel source through combustion as a heat and electricity producer or as a raw material for the production of synthetic fuels as a substitute for traditional gas and oil. Among such fuels liquid biofuels are mostly used in the transport sectors as an alternative to the conventional fuels [55].

Bioenergy represents about 75% of total consumption of renewable energy sources. From this overall share, more than 50% comes from traditional uses of biomass. According to IRENA statistics, the world's total capacity of bioenergy power capacity by 2024 has reached 151 GW. This represents 4.4% of the total capacity of the whole renewable energy sources infrastructure [55]. The installed bioenergy capacity progress within the years is presented in Figure 2.6 below.

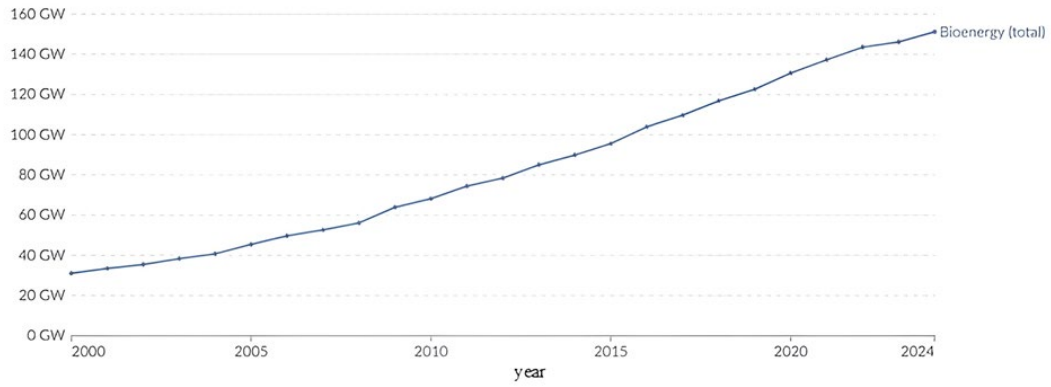


Figure 2.6 Global installed bioenergy capacity over the years [56]

Although cost reduction in bioenergy has progressed more gradually compared to other renewable technologies, the global weighted-average LCOE for bioenergy power projects still achieved a 14% reduction between 2010 and 2023, declining from USD 0.084/kWh to USD 0.072/kWh [55].

2.1.3 Integration of Thermal Components into Hybrid Renewable Energy Systems

Integrating the TLC with waste heat recovery from the MGT allows the system to utilize electrical and thermal energy more efficiently, thereby enhancing overall system performance. The TLC manages the EE produced by renewable sources, whereas the heat recovery unit captures waste heat generated by the MGT [20].

2.1.3.1 Thermal Load Controller and Boiler

A TLC is a control device that manages EE by converting it into heat to meet thermal demands, thereby improving overall system efficiency. It continuously monitors the available surplus electricity and dynamically directs it to heating elements, ensuring that thermal requirements are satisfied effectively. In contrast, a boiler is a conventional thermal unit that combusts fuel to generate heat, providing a continuous thermal supply when EE is insufficient. The boiler operates automatically whenever the thermal load exceeds the heat supplied by renewable sources or the TLC [22].

In off-grid systems, HRES are likely to generate excess energy while ensuring a stable power supply. This surplus capacity that is configurated to meet the

electricity requirements creates larger and more expensive components. Nevertheless, the EE can be strategically employed to meet thermal demands via the TLC and the gas boiler. As a result, EE produced by renewable sources can be converted into thermal energy using the TLC. The component capacities and the associated NPC can be reduced accordingly [21]. Figure 2.7 shows a hybrid hydrogen production system with TLC and boiler thermal components.

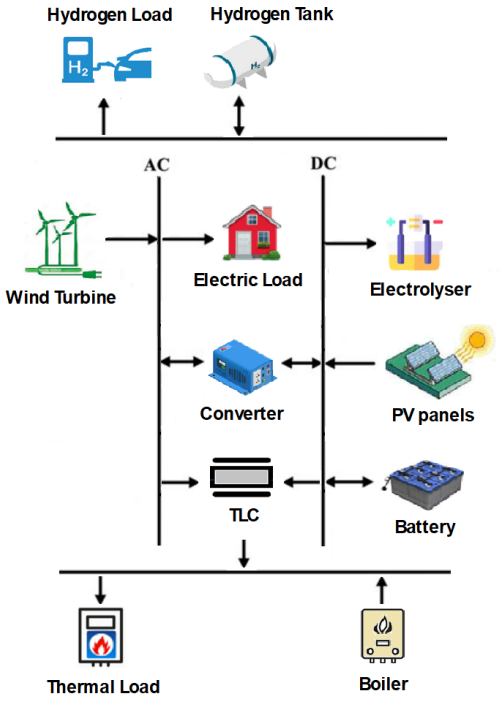


Figure 2.7 A scheme of HRES with TLC and boiler for hydrogen production

When the surplus electrical energy is unavailable, a conventional fuel-fired boiler supplies the necessary heat [20], [21], [22], [57], [58]. Namely, the HOMER software models the boiler as a secondary heat source capable of meeting the entire thermal demand whenever required. While a TLC is optional in systems with thermal loads, its absence results in unused surplus electricity within the HOMER simulation environment [59].

2.1.3.2 Micro Gas Turbine

A MGT is a power generation system that is usually between 30 kW and 250 kW capacity and relies on the same thermodynamic process as traditional open-cycle gas turbines [60]. Fundamentally, the system is composed of three primary

components: the compressor, the combustion chamber, and the turbine. In the Brayton cycle the pressurized air in the compressor goes to the combustion chamber and subsequently the mixture of the air and fuel ignites to produce high-temperature gas [60], [61]. This gas with high pressure and high temperature expands through the turbine, generating mechanical power that drives both the compressor and an integrated electrical generator [60]. MGTs demonstrate suitability for decentralized power applications due to their installation flexibility, simple load integration, quiet operation, and reduced nitrogen oxide emissions compared to conventional alternatives [62].

In order to sustain the generation of electricity, studies mostly focus on the use of local resources based on renewables such as industrial solid waste and hydrogen. In this regard, a MGT can significantly contribute towards improving the flexibility and efficiency of conversion of these energy sources. Moreover, the application of hybrid configurations involving MGT provides stability with respect to variations in renewable resource availability. Namely, the system provides a continuous power output during the period when solar power is not adequate with backup components. In addition, the integration techniques promote a total efficiency greater than the efficiency provided by any energy resource used alone [63]. However, when modelling these systems in HOMER Pro, the HRES configuration cannot operate with an MGT alone because the model requires a boiler to meet the system's thermal load and ensure heat balance.

A MGT works as a backup power source when the total output of the solar systems, the output of the wind turbine, and the stored battery energy is insufficient to meet the total power demand [57]. Their fast response to changing power needs enables them to address demand peaks and support intermittent renewable sources during periods of unavailability [64]. Moreover, the effect of integrating the total energy system of a MGT not only provides solutions for the energy shortages but also enhances overall energy efficiency by the waste heat recovery system [57]. Figure 2.8 demonstrates a hybrid system including MGT and boiler thermal components for hydrogen generation.

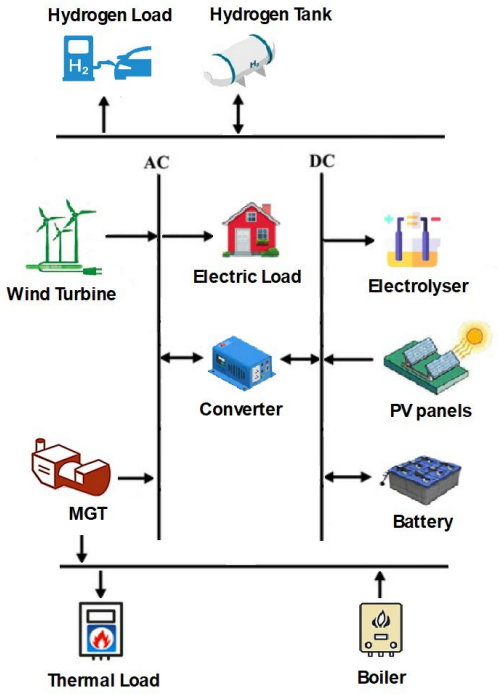


Figure 2.8 A scheme of HRES with MGT and boiler for hydrogen production

2.2 Hydrogen Technologies

It is theoretically achievable to decrease the world's final energy consumption by 60% by 2050 and to secure an acceptable living standard for every person [65]. Despite the difficulty in the efficiency transition necessary for the goal of the net zero energy world, it is possible to construct an equal energy world [66].

Although hydrogen has been conventionally used mainly in the chemical industry, the increasing concern of various countries to move forward the energy transition has made hydrogen regain its attraction as an alternative to the fossil fuel technology [67]. There are key reasons for its attraction due to its versatility, and environment-friendliness [68]. However, until recently, the majority of hydrogen was generated from non-renewable sources such as coal, oil, or natural gas, which negatively impact the environment and exhaust natural resources [69]. Therefore, encouraging hydrogen production from renewable energy sources is essential to reduce environmental impacts and facilitate a sustainable shift in the energy sector.

2.2.1 Hydrogen Production Methods

The type of hydrogen depends on its carbon footprint and the production process. Blue hydrogen is produced from fossil fuels using carbon capture techniques. Green hydrogen, on the other hand, uses renewable energy. Pink hydrogen is generated from nuclear power. Turquoise hydrogen uses the process of fossil fuel pyrolysis. This process does not produce CO_2. Brown hydrogen is produced by coal gasification method. Another type of hydrogen, grey hydrogen is obtained from the natural gas reforming [70]. Different methods of hydrogen production are categorized based on the kind of energy utilization and carbon footprint as shown in Table 2.1 below.

Table 2.1 Carbon footprint and hydrogen production technology for different types of hydrogen [70]

Technology	**Type**	**Energy Source**	**Carbon Footprint (kg CO_2/kg H_2)**
Water Electrolysis	Green Hydrogen	Renewable Energy	<1
Water Electrolysis	Pink Hydrogen	Nuclear Energy	<2
Pyrolysis	Turquoise Hydrogen	Fossil Fuels	<3
Steam Methane Reforming (with Carbon Capture)	Blue Hydrogen	Natural Gas/Coal	<4
Steam Methane Reforming (without Carbon Capture)	Gray Hydrogen	Natural Gas	8-10
Coal Gasification	Brown Hydrogen	Coal	>20

The production of hydrogen comprises different technologies. The main production process involves natural gas and superheated steam. This process is known as the steam reforming of the natural gas. This process uses metal-based catalysts to boost the chemical reactions. This process not only uses metal catalysts for chemical reactions but also must be heated to very high temperatures between 700°C and

1000°C [67]. Most of the world's hydrogen currently comes from the reforming of fossil fuels, specifically natural gas (76%) [71]. This indicates that hydrogen production primarily relies on non-renewable sources and generates large amounts of CO_2 emissions. In fact, the elimination of such emissions is very important since the hydrogen amounts produced only in France is 900,000 tons per year leading to 9 M tons of CO_2 emissions [67]. Other new processes for the generation of sustainable hydrogen involve the methane pyrolysis and water electrolysis processes [71].

The hydrogen chain has four primary steps: the production stage, the storage stage, the transport stage, and the usage stage. All the above steps involve widespread technological innovation to provide a revolution in the hydrogen economy. The transport stage is quite important as the ability to transport the hydrogen from the generation to the consumption point could increase the cost of the whole process [72]. Another important innovation required in the hydrogen chain is the development of safe, efficient and reliable storage systems. This poses a great technological challenge to the hydrogen economy [73].

At present, the percentage of sustainable hydrogen used is very limited because the dominant contributor to the total available hydrogen is obtained from the processes of fossil fuels. This is primarily due to the cost factor involved in electrolysis, the challenges in hydrogen storage and the initial investment for the infrastructure [74]. Despite these challenges, the integration of renewable energy to the green hydrogen production is expected to overcome these challenges. Technological progress seems to create new opportunities for expanding the necessary production, storage, and distribution networks. Achieving this potential, however, depends on a comprehensive understanding of how to effectively integrate renewable energy sources with electricity generation for hydrogen production, which is the main focus of this study [72].

2.2.2 Hydrogen Cost

The cost of hydrogen production can differ greatly depending upon the technology used and the source of the energy [75]. Table 2.2 highlights the cost comparison of the different sources of hydrogen production [70]. Currently, the cost-effective

process of hydrogen production is surely the steam methane reforming process, also recognized as the gray hydrogen process, though its economics are substantially affected by carbon tax applications. [67]. The cost of blue hydrogen production is significantly higher compared to the cost of grey hydrogen production. This main reason for the cost variation between the two hydrogen production methods is the cost of the carbon capture and storage technique. Currently, the highest cost of hydrogen production results when electricity produced from renewable sources is used [75].

Table 2.2 Hydrogen production costs by energy source [70]

Type	**Energy Source**	**Production Cost ($/kg H_2)**
Green Hydrogen	Renewable Energy	4.0 - 9.0
Pink Hydrogen	Nuclear Energy	3.5 - 7.0
Turquoise Hydrogen	Fossil Fuels	1.25 - 2.20
Blue Hydrogen	Natural Gas/Coal	1.5 - 3.0
Gray Hydrogen	Natural Gas	0.5 - 1.70
Brown Hydrogen	Coal	1.0 - 2.2

While fossil fuel-based hydrogen production currently remains the most economical choice, future advancements in technology and the expanded use of renewable energy sources are expected to make green hydrogen a competitive alternative [75]. Historically, the high cost of production has been a factor that has limited the use of green hydrogen in the transport and industrial sectors. The cost of producing hydrogen from electrolysis can significantly differ depending on various factors such as the type of electrolyser, capacity and efficiency. In particular, the cost of green hydrogen has been reduced by 80% between 2002 and 2017. Moreover, the cost will continue to fall through the middle of the century. This cost forecasts depend on the availability of green electricity, and the level of the electrolyser installed capacity which makes renewable power affordable and

feasible hydrogen production [67]. IRENA also projects that combined cost reductions in electricity generation and electrolysis could lower hydrogen production costs by as much as 80%. The production of competitive green hydrogen requires low electricity costs, and cost reductions only in electrolysers are not enough to compensate for the high cost of electricity [76]. Additionally, growing renewable energy integration is set to further reduce electricity prices, while rising CO_2 emission costs are likely to increase the expense of fossil fuel-based hydrogen production [75]. Forecasts expect that green hydrogen is likely to become more cost-effective than blue hydrogen starting in 2030 [77]. Hence, it is crucial to carry out a detailed cost analysis of green hydrogen within this study to scientifically verify these forecasts and provide a solid basis for the assessment of the hydrogen's integration potential.

2.2.3 Green Hydrogen Production

Green hydrogen generation is significant in terms of the global energy sector since it is crucial to find solutions for the global issues like climate change, and it offers crucial benefits to decarbonize various sectors, and sustainable energy development. Hence, green hydrogen has various contributions for the future energy sector as a clean fuel resource [78].

Hydrogen's role in the energy sector is crucial during the transition towards the low-carbon economy, thus contributing immensely to the reduction of greenhouse gas emissions in the following years. However, the forecast reveals that up to 60% of emission reductions during the final phase of the transition process could be provided using renewable energy sources, green hydrogen, and the subsequent electrification. Nevertheless, the substantial investment of governments, industry leaders, investors is needed for an effective realization of the benefits associated with hydrogen [67].

Green hydrogen refers to an 'eco-friendly' carrier fuel produced via the electrolysis of water, where the electricity is sourced only by renewable sources [75]. In the electrolysis reaction, water molecules (H_2O), an electrolytic compound, are split into hydrogen (H_2) and oxygen (O_2) via an electrochemical reaction [71], [79]. In electrolysis, there are no uses of non-exhaustible finite fossil fuels; thus, the

production process does not produce direct greenhouse gases associated with carbon emissions [71]. Green hydrogen, as a zero-emission fuel, plays a crucial role in advancing sustainable fuel infrastructure and reducing emissions from transport networks [75]. Figure 2.9 illustrates process flow of renewable energy conversion to hydrogen and the pathway toward net-zero emissions.

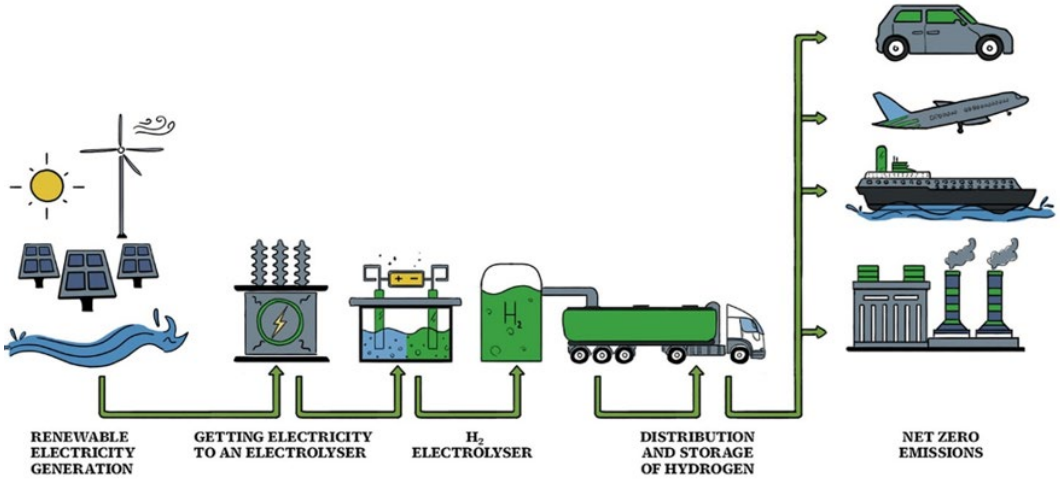


Figure 2.9 Flow diagram of green hydrogen production and transportation processes [72]

2.2.4 Green Hydrogen Applications and Integration Pathways

Green hydrogen shows the revolutionary power in different sectors, especially in transportation infrastructure [78]. Following sections examine the specific application approaches available for green hydrogen deployment: industrial applications, gas grid integration, power system balancing, sustainable transportation, and decentralized power systems.

2.2.4.1 Industrial Sector Integration

Green hydrogen can displace conventional hydrocarbon-derived hydrogen in heavily polluting industrial operations including petroleum refining and chemical manufacturing. These industries characteristically maintain extended procurement agreements with substantial volume commitments, creating favourable conditions for rapid market expansion and improved economic feasibility for green hydrogen projects [67].

2.2.4.2 Gas Grid Incorporation

Green hydrogen can be mixed into existing natural gas infrastructure, reducing the demand for conventional gas and associated emissions for the production of residential and commercial heat. Furthermore, this approach facilitates the advancement of an integrated energy infrastructure by synergistically interconnecting electric, gas, and heat infrastructures. The permissible hydrogen concentrative levels within gas infrastructures demonstrate substantial variation at the country level [67].

2.2.4.3 Power System Balancing

Green hydrogen facilitates the necessary seasoning balance for the electrical grid with high levels of renewable integration. While the changes in intraday electricity may be effectively managed by means of electricity management and modulating demands, the differences in the seasons based upon the climate, such as the need for higher levels of heating in the winter season, require distinct measures for management. Seasonal peak demands could be met by electrolytic hydrogen production during times of high renewable generation without the need for additional conventional power generation capacities [67].

2.2.4.4 Sustainable Transportation

The development of fuel cell cars based on green hydrogen represents an extension of clean transportation alternatives alongside battery electric options, providing an effective alternative for the petroleum fuels used within the transportation sector [67]. The transportation sector consumes about 18% of the primary energy used worldwide and emits about 17% of the total CO_2 emissions, making it one of the most difficult sectors for the process of decarbonization [80]. Green hydrogen provides various important advantages over other hydrogen forms for transportation purposes. Its energy density is comparable to the conventional gasoline, while fuel cell electric vehicles provide superior fuel economy compared to conventional internal combustion engines used in the gasoline engines [81]. Hydrogen refuelling stations, while functionally similar to conventional petrol stations, differ technically through their use of mass flow meters that measure

hydrogen by weight in kilograms [82]. A transportation vehicle carrying 5 kg of hydrogen weight can achieve a driving distance of about 500 km. Also, hydrogen refuelling time is approximately equal when compared to the refuelling time of gasoline and diesel fuel for transportation vehicles. These characteristics make hydrogen particularly well-suited for long-distance and heavy-duty transport applications, including intercity buses and freight delivery services [67]. However, hydrogen refuelling infrastructure and distribution network establishment are needed to carry out hydrogen based transportation systems for the increasing demand of transport [82], [83]. In this context, hydrogen can either be generated on-site or produced in centralized stations to supply hydrogen refuelling stations. Hence, the costs can greatly vary for these stations depending on the site of the hydrogen refuelling station [84].

2.2.4.5 Decentralized Power Systems

Green hydrogen offers a new potential for energy generation, especially in areas which are geographically distant from the grid system [67]. With green hydrogen, these remote areas can produce and store green hydrogen to supply their own energy requirements other than depending on electricity supply from other networks [83].

2.2.5 Hydrogen Roadmap of Germany

The German Government conducts one of the biggest hydrogen transportation and infrastructure pilot projects around the globe [85]. The Federal Government has launched a National Hydrogen Strategy to promote environmentally friendly technology using hydrogen. The establishment of a hydrogen economy that involves all levels of society has facilitated green hydrogen projects and resulted in the development of the National Hydrogen Strategy in 2020. Specifically, this strategy focuses on providing a supportive structure for the development of the hydrogen sector. Major objectives are to facilitate cost-competitive hydrogen production, develop the local hydrogen market while importing hydrogen, assure hydrogen as an attractive energy carrier and sustainable raw material in the industrial sector, improve hydrogen infrastructure for transport and distribution, and advance scientific research and staff training in the hydrogen sector [86]. Furthermore, in the transportation sector, the policy allocates €3.6 billion for the

subsidization of the acquisition of electric and climate-friendly cars and €4.5 billion for the development of electro fuels for the building sector. An additional €50 M targets the enhancement of hybrid planes and ships based on electricity and hydrogen [87]. To monitor the execution and development of the strategy, the federal government formulated an interministerial Committee of State Secretaries for hydrogen [67]. So, this hydrogen plan contributed to the improvement of the long-term plan for the nation's energy transformation [79]. Aligned with this vision, Germany aims to achieve greenhouse gas neutrality by 2045 with the use of renewable energy sources such as green hydrogen [86].

2.2.5.1 Hydrogen Demand in Germany

The demand for hydrogen in the German market shows an impressive increasing trend over the years, reflecting the accelerated transition of the country to the hydrogen economy. As illustrated in the figure, hydrogen consumption increased from 0.9 tons in 2016 to 2.5 tons in 2018, reaching 6.8 tons by 2020 and 16.6 tons in 2022. This rapid growth continued with a significant rise to 44.7 tons in 2023, and the demand is projected to reach 58.3 tons by October 2025, as presented in Figure 2.10. The steady increase demonstrates Germany's expanding industrial and transportation applications of hydrogen, driven by national policies and investments supporting the adoption of green hydrogen technologies.

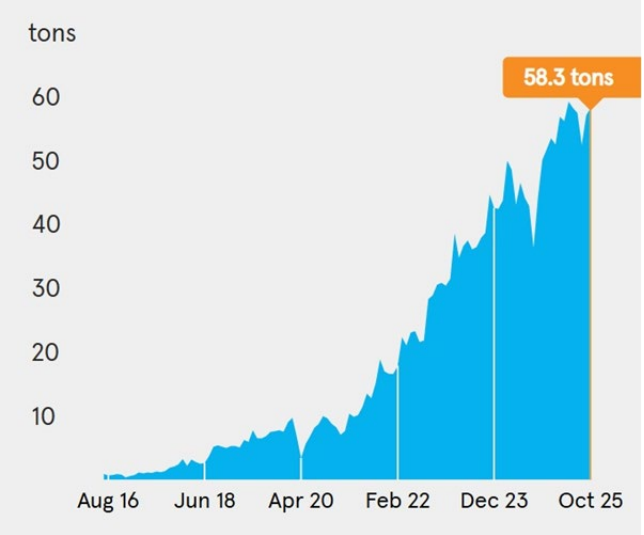


Figure 2.10 Hydrogen demand growth in Germany over years [40]

2.2.5.2 Hydrogen Refuelling Stations in Germany

To facilitate hydrogen mobility, Germany has already established a basic infrastructure for hydrogen refuelling, which currently comprises 72 hydrogen refuelling stations in the country. Figure 2.11 shows the amount of operating hydrogen refuelling stations in Germany.

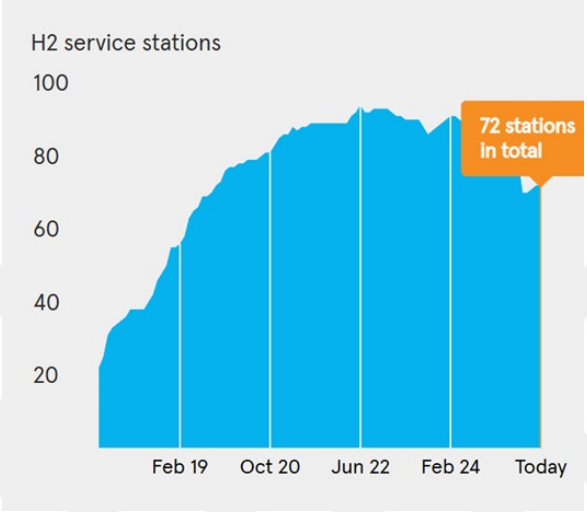


Figure 2.11 Hydrogen refuelling stations in Germany by year [40]

The network serves both passenger cars at 700 bar and commercial transport at 350 bar, as the development focuses on areas expected to grow commercially and to meet the increasing demands of passenger transport. Hydrogen can be transported through specific trailers using pressure of 200, 300 or 500 bar. Alternatively, the transportation of hydrogen can be carried out in cryogenic liquid form. In some regions, high amounts of hydrogen are transported to the demand centers via hydrogen pipelines [40].

The current hydrogen mix comprises only 28% green hydrogen, 30% industrial by-products, and 42% hydrogen from natural gas. Moreover, there is a clear commitment to rapidly scaling up the production of green hydrogen at the national and international levels. The infrastructure development plan includes the installation of 'S' size stations (€1.2 M, H_2 storage of 200 kg), as well as larger commercial stations (€2.5 M, H_2 storage of 400–800 kg), which typically require 12–20 months for approval and execution, benefiting from Germany's world-leading technical expertise in hydrogen station engineering [40].

3
FUNDAMENTALS OF REGULARIZATION AND REGRESSION MODELS

3.1 Fundamentals of Regularization

Regularization plays a crucial role in improving the stability and generalizability of regression models by reducing complexity and preventing overfitting. When evaluating how well a regression model performs, it is not sufficient to focus solely on the results. It is also essential to take into consideration factors influencing the reliability of the model. These include issues such as multicollinearity, overfitting or underfitting, the balance between bias and variance, and the use of cross-validation techniques. In addition, performance indicators like RMSE and R^2 are assessed to better understand how accurately the model represents the data [88].

3.1.1 Multicollinearity

In multiple regression analysis, multicollinearity refers to the condition of linear relationship between independent variables, whereas collinearity refers to the exact relationship between two independent variables. However, multicollinearity may emerge because of having multiple independent variables within a regression equation that are largely correlated to both the variable and the other independent variables [89]. The possible consequences of multicollinearity may result in an unreliable estimate of the regression coefficients, an increase in the standard errors, and the decline in the accuracy of the regression equation predictivity [90], [91]. Therefore, multicollinearity may affect the result of the analysis by increasing the standard errors of the coefficients [89]. Additionally, the multicollinearity problem may not be detected by researchers until after the process of data collection [92].
Linear Regression analysis often serves the relationship between a dependent variable and one independent variable, as well as for two or more independent

variables. However, this regression analysis may have some limitations in practice, where multicollinearity could be the major problem among others, which could affect the results [91]. The best technique to avoid multicollinearity could be the addition of new data, where the major problem associated with multicollinearity lies in the lack of data because the technique does not result from the analysis process. However, acquiring new data may not be possible, especially for studies carried out using convenience sampling techniques [93]. Hence, regularization techniques provide an effective solution by applying shrinkage to regression coefficients in order to avoid multicollinearity. Among the widely adopted methods for regularization purpose are RR, LR, and ENR models [90], [91].

3.1.2 Bias and Variance

The performance of machine learning models is measured by the accuracy of predictions on new, unseen data, which are usually denoted as prediction accuracy, or alternatively, prediction error. Prediction error results from various sources; the major sources are bias and variance [94].

Bias occurs when the resulting model doesn't fit the underlying data well. To be clear, for example, if a nonlinear algorithm is used to solve a classification task where the underlying data needs a nonlinear boundary, the result will be biased. In this context, bias represents the difference between the expected outcome and the predictions made by the model. A prediction model characterized by high bias makes predictions systematically incorrect regardless of the underlying patterns in the input data [94]. Models characterized by high bias generally contain fewer parameters compared to models characterized by low bias, meaning the models are simple and of low capacity. Such models can model a limited set of data only since their parameter size limits them to do so. On the other hand, models characterized by low bias generally contain many parameters, meaning the models are complex and of high capacity. These models can use diverse data since the models are capable of producing more complex patterns within the underlying dataset [95].

Variance measures how sensitive a model to small changes in the training dataset. Large values of variance indicate that the predictions are highly sensitive to the training data, thus affecting the generalization performance of the models by

increasing the possibility of overfitting [94]. In simpler words, the measure represents the difference among models trained on distinct datasets of the same size from one another. For instance, an example could be the training of a machine learning model on a given dataset and assigning the label 'A' to the resultant model. Then, taking a new dataset of the same size and training a new model 'B' based on it, the measure of variance represents the difference between models B and A. Actually, it shows the sensitivity of a learning algorithm to variations in the training data [95]. Figure 3.1 shows a bulls-eye graph, which is a very common technique used to exhibit the balance between bias and variance.

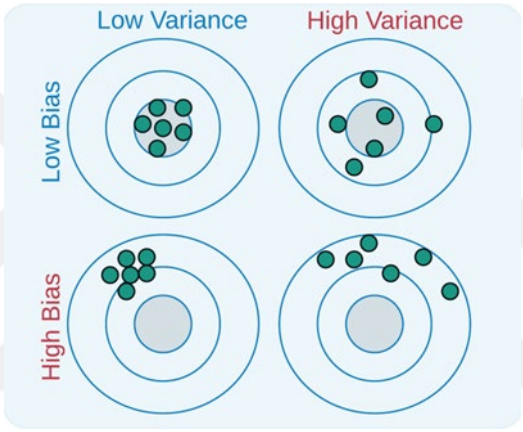


Figure 3.1 Bias and variance scheme using a bulls-eye diagram [94]

3.1.3 Overfitting and Underfitting

Overfitting happens if the algorithm uses a very complex model, resulting in high variance and low bias. High bias occurs when a model interprets random noise in the training data as a real pattern, thereby reducing its ability to accurately predict the new data. In contrary, underfitting happens if the algorithm uses a very simple model, resulting in high bias and low variance. High bias occurs when the modelling algorithm fails to fit the underlying pattern in the data [96]. Figure 3.2 presents examples of underfitting, good fit and overfitting models.

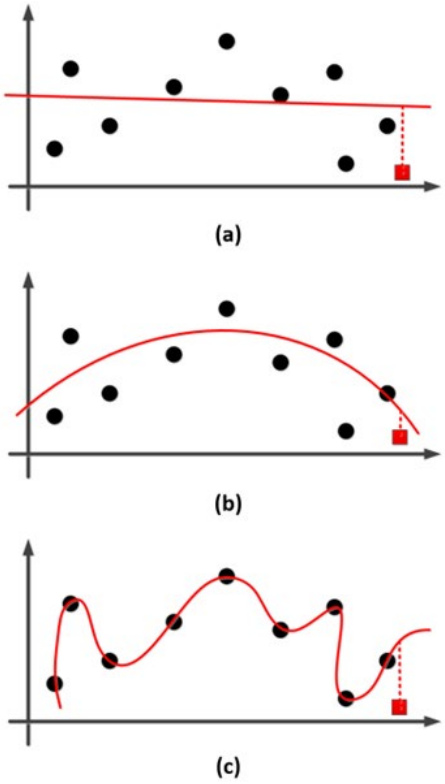


Figure 3.2 The graphs for (a) underfitting, (b) good fit, (c) overfitting [96]

To ensure effective performance of the modelling algorithm and prevent overfitting (high variance) and underfitting (high bias), penalty methods (regularization) and early stopping techniques are used [97].

3.1.3.1 Penalty Methods (Regularization):

In this method, the error function from the training process is penalized by the addition of a lambda (λ). This penalty term increases with the complexity of the function avoiding overdependence on a single feature in a model. Ridge and Lasso Regression models rely on this technique to reduce the coefficients of the models by using this penalty term [97].

3.1.3.2 Early Stopping:

This technique is carried out during the iterative training of models such as the neural networks. The training process uses the training data, while the performance measures the result during the training process on the validation data. Training stops the moment the validation error starts indicating the point of overfitting [97].

3.1.4 Cross Validation

Cross-validation is a widely used data resampling technique for the assessment and selection of models. The process aids in the optimal choice of hyperparameters, reduction of overfitting, assessment of learning algorithms, and calculation of the generalization error of prediction models for effective forecasting [98]. In this process, the dataset is split into two distinct subsets: a training and a test set. The combination of the two represents the entire dataset, while the intersection of the two subsets is the empty set, meaning the two do not share any observation in common for analysis [96]. Furthermore, the data is equally divided into subsets, denoted by the term 'folds'. For every iteration, the algorithm trains the model on all other subsets except the specified fold, whilst the fold acts as the validation set; the process repeats until every subset of the data has been used for validation. Finally, the results from each iteration are averaged to give a reliable assessment of the model's predictive performance [88].

Several cross-validation techniques exist, with K-fold cross-validation being one of the most commonly used [96]. It is a useful technique for performance analysis and researching the capacity of machine learning algorithms for generalisation. After dividing the training data into equally sized folds, one fold is used for model validation while the remaining folds are employed for training in each iteration. The results are subsequently averaged to produce a trustworthy accuracy estimate [99]. To get more reliable machine learning algorithm results, it is important that the k-fold machine learning cross-validation must be repeated several times. To reduce variability and increase the robustness of the validation results, for instance, 10-fold cross-validation is advised [100]. Figure 3.3 shows an illustration of the k-fold cross-validation process.

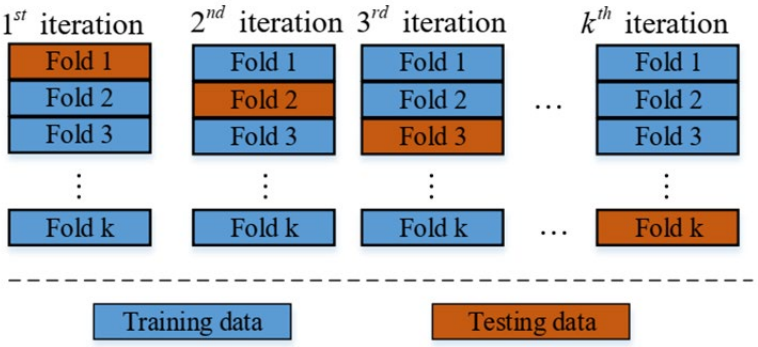


Figure 3.3 Representation of k-fold cross validation [99]

3.1.5 Root Mean Square Error and Coefficient of Determination

The RMSE represents an essential statistical measure for the assessment of the performance of a given model in many disciplines. It measures the mean size of prediction errors, where smaller values indicate higher prediction capability [101]. A clear interpretation of the RMSE requires certain assumptions about the prediction errors, which should be normally distributed and not biased. Therefore, the presentation of the RMSE and the standard error provides useful information about the distribution of prediction errors since it is computed from the equation given below [100]:

$$RMSE = \sqrt{1}/n \sum_{i=1}^{n} (y_i - \hat{y}_i)^2 \quad (3.1)$$

where n is the number of data points in the dataset; yi is the observed value of the dependent variable for the i^{th} data point; $\hat{y}i$ is the predicted value of the dependent variable for the i^{th} data point.

The statistic R^2, also termed the coefficient of determination, measures the proportion of the variation in the response variable explained by the fitted model compared to the simple variation around the mean. Essentially, it indicates how well the model captures the underlying data structure. An R^2 value approaching 1 indicates that the model accounts for nearly all the variability in the response, while a value near 0 suggests the model performs no better than predicting the mean value [102]. In practical terms, R^2 measures how much of the variation in the dependent variable can be explained by the independent variables, with values closer to 1

demonstrating a stronger model fit. R^2 is calculated by the following equation [103]:

$$R^2 = 1 - (RSS/TSS) \tag{3.2}$$

where *RSS* is the residual sum of squares and *TSS* is the total sum of squares.

3.2 Regression Models

A technique used to handle multicollinearity in the data is regularization, which involves shrinking the coefficients obtained from the regression analysis. This process produces smaller coefficients than those obtained using ordinary least squares, thereby increasing the reliability of the regression results [96].

The values of dependent variable are predicted using regression models based on the available independent variables. Regression equations estimate the relationship between the independent and dependent variables, thus enabling the prediction of results based on the given data [104]. In this study, the Linear Regression, RR, LR, and ENR models are used to provide statistics for subsequent research.

3.2.1 Linear Regression Model

In a linear regression model, the dependent variable is estimated using a linear relationship with one or more independent variables. The model's performance depends on balancing bias, which is the difference between observed and predicted values and variance, which reflects how sensitive the predictions are to changes in the data [105].

Multicollinearity may present challenges in the process of linear regression modeling, since measuring the effects of each independent variable on the dependent variable may be problematic. The high variances result in overfitting the model [88]. The objective of linear regression is to minimize the sum of squared errors, and it is given by the function below:

$$\sum_{i=1}^{n}(y_i - \hat{y}_i)^2 \tag{3.3}$$

yi is the observed value of the dependent variable for the i^{th} data point, $\hat{y}i$ is the predicted value of the dependent variable for the i^{th} data point.

3.2.2 Ridge Regression Model

RR refers to a technique used for regularizing multicollinearity and improving the predictability of statistical models. The approach imposes a controlled bias on regression results to produce a dramatic reduction in variance [91]. The technique is suitable when the goal is to include all the features in the modelling process for multicollinearity control. The technique works well in scenarios where many coefficients are characterized by small and correlated effects; the approach ensures the coefficients are not associated with excessive variance by systematically reducing their values [106]. In the approach, a penalty term (L2 regularization) is included in the linear regression equation to eliminate overfitting and multicollinearity among the features. The approach uses the regularization parameter (lambda, λ), which regulates the strength of the penalty effect on the features. In RR, the coefficients are shrunk towards zero but do not reach zero even at larger values of the lambda parameter [88]. The cross-validation approach is used to find the best values of λ by evaluating the model's performance at different values of lambda [91]. The RR approach aims to reduce the following objective function [88]:

$$\sum_{i=1}^{n}(y_i - \hat{y}_i)^2 + \lambda \sum_{j=1}^{p} \beta_j^2 \quad (3.4)$$

yi is the observed value of the dependent variable for the i^{th} data point,

ŷi is the predicted value of the dependent variable for the i^{th} data point,

βj is the coefficient for the independent variables,

λ is the lambda, the regularization parameter that controls the overall strength of the penalty,

$\sum_{i=1}^{n}(y_i - \hat{y}_i)^2$: This term measures the sum of the squares of the differences between the observed values *yi* and the predicted values *ŷi*,

$\lambda \sum_{j=1}^{p} \beta_j^2$: This term adds a penalty by the sum of the squares of the coefficients multiplied by the regularization parameter λ. (L2 normalisation penalty)

3.2.3 Lasso Regression Model

LR refers to a machine learning technique used to enhance prediction accuracy and improve the interpretability of models by performing variable selection and

regularization simultaneously. In fact, the LR algorithm is similar to RR based on the concept of regularization. However, the approach used by this technique aims to shrink the coefficients of irrelevant variables towards zero, thus eliminating them from the model while keeping the most relevant features. Because of this selective technique for automatically identifying the most important features, this algorithm has been widely used by researchers for variable selection and solving multicollinearity problems [90]. Furthermore, this technique has been widely used in fields characterized by the presence of a vast amount of data in their databases, requiring rapid algorithms for effective computation and analysis. Also, the approach used in this technique introduces the addition of the L1 normalization penalty to the objective function of the LR algorithm, shrinking some coefficients of the regression equation to zero for an appropriately selected value of the lambda parameter [106]. In order to select the ideal value for the parameter lambda for the LR technique, the cross-validation method is used similar to RR [91]. The LR aims to minimize the objective function given by [88]:

$$\sum_{i=1}^{n}(y_i - \hat{y}_i)^2 + \lambda \sum_{j=1}^{p}|\beta_j| \quad (3.5)$$

yi is the observed value of the dependent variable for the i^{th} data point;
ŷi is the predicted value of the dependent variable for the i^{th} data point;

βj is the coefficient for the independent variables;

λ is the lambda, the regularization parameter that controls the overall strength of the penalty,

$\sum_{i=1}^{n}(y_i - \hat{y}_i)^2$: This term measures the sum of the squares of the differences between the observed values yi and the predicted values ŷi,

$\lambda \sum_{j=1}^{p}|\beta_j|$: This term adds a penalty by the absolute values of the coefficients multiplied by the regularization parameter λ. (L1 normalisation penalty)

3.2.4 Elastic Net Regression Model

The ENR algorithm represents an effective approach which combines the penalizations of RR and LR to leverage the benefits of both strategies. The coefficients are simultaneously shrunk, as in the RR approach, whereas some are set entirely to zero, like in the LR approach [90]. ENR imposes both the L1 and the

L2 norms to the loss function simultaneously. The former, from the LR approach, induces sparsity by turning some coefficients entirely to zero (feature selection). The latter, based on the RR technique, shrinks all coefficients towards zero [107]. It uses the alpha parameter (α), which balances the two penalties without the requirement of two separate lambda values for the two penalty terms. In cases where α=0, the ENR becomes the simple RR approach, and in the cases where α=1, it becomes the LR technique [106]. In the ENR model, cross-validation of both alpha and the lambda values takes place simultaneously to select the best combination for the situation [91]. This model is beneficial in high-dimensional data where the size of the predictor variables exceeds the sample size of observations. In high dimensional data situations, the LR technique only selects a maximum of 'n' features, whereas the ENR technique does not have this restriction and it enables the selection of more than n predictors, including correlated variables. The related objective function for ENR is given below [107]:

$$\sum_{i=1}^{n}(y_i - \hat{y}_i)^2 + \lambda\left(\alpha \sum_{j=1}^{p}|\beta_j| + (1-\alpha)\sum_{j=1}^{p}\beta_j^2\right) \quad (3.6)$$

yi is the observed value of the dependent variable for the i^{th} data point,

$\hat{y}i$ is the predicted value of the dependent variable for the i^{th} data point,

βj is the coefficient for the independent variables,

λ is the lambda, the regularization parameter that controls the overall strength of the penalty,

α is the alpha parameter that governs the ratio between the penalty terms ($0< \alpha <1$),

$\sum_{i=1}^{n}(y_i - \hat{y}_i)^2$: This term measures the sum of the squares of the differences between the observed values yi and the predicted values ŷi,

$\alpha \sum_{j=1}^{p}|\beta_j|$: This term represents the L1 penalty, which encourages sparsity in the coefficients by shrinking some of them to exactly zero.

$(1-\alpha)\sum_{j=1}^{p}\beta_j^2$: This term represents the L2 penalty, which shrink coefficients to the lower values.

4
METHODOLOGY, DATA AND ECONOMIC ANALYSIS

4.1 Methodology and Data for Hybrid Systems

This section primarily focuses on the materials and methods used by the system configurations. The meteorological data of the selected site and load profiles of the systems are also shown to support the analyses. Moreover, approaches to regression models and lists of variables in the regression models in the econometric analyses are presented.

4.1.1 Definition of Hybrid Systems

The techno-economic analysis is conducted by evaluating three configurations that vary in their utilization of EE. Two different WT (XANT L-36 and the combination of XANT L-36 & Vestas V47) are used, for the proposed systems. They were selected due to their compatibility with Schleswig-Holstein's moderate-to-high wind speeds. The XANT L-36 performs efficiently at lower wind speeds, while the Vestas V47 generates higher output under stronger wind conditions, ensuring stable hydrogen production across varying conditions.

In the first system, PV panels and WT renewable sources are used to produce green hydrogen without recovering the surplus energy. In the second system, TLC are added to the system to convert EE into heat, and a boiler is used to compensate the required heat if needed for the thermal load. In the third system, a MGT is incorporated to meet both electricity generation using natural gas and heat production through waste heat recovery. The following configurations are proposed within the study:

(a) PV/XANT L-36 WT / Electrolyser / Hydrogen Tank / Battery System

(b) PV/XANT L-36 WT / Electrolyser / Hydrogen Tank / TLC / Boiler / Battery System

(c) PV/XANT L-36 WT / Electrolyser / Hydrogen Tank / TLC / Boiler / MGT / Battery System

(d) PV/XANT L-36 & Vestas V47 WT / Electrolyser / Hydrogen Tank / Battery System

(e) PV/XANT L-36 & Vestas V47 WT / Electrolyser / Hydrogen Tank / TLC / Boiler / Battery System

(f) PV/XANT L-36 & Vestas V47 WT / Electrolyser / Hydrogen Tank / TLC / Boiler / MGT / Battery System

(g) Biogas generator / Electrolyser / Hydrogen Tank / Battery System

(h) PV/XANT L-36 WT / Biogas generator / Electrolyser / Hydrogen Tank / Battery System

(i) PV/XANT L-36 & Vestas V47 WT / Biogas generator / Electrolyser / Hydrogen Tank / Battery System

4.1.2 HOMER Pro Analysis

HOMER software is an effective tool for designing and arranging HRES to conduct a techno-economic analysis and identify the ideal component size. Recently, more than 80,000 people in 193 countries have downloaded HOMER. As it designs the optimal configuration of HRES and provides techno-economic analysis by evaluating various potential system configurations, HOMER is determined to be the most popular tool [108]. This study is carried out by using HOMER Pro simulation tool to evaluate the technical and economic feasibility of different system configurations.

4.1.2.1 HOMER Pro Input Data

HOMER requires various types of data for simulation and optimization of the HRES. Thus, load data, weather data, optimization constraints, and techno-economic data of the components are introduced into the software. HOMER Pro uses these inputs to simulate a wide range of possible system configurations. Throughout the simulation, the software carries out optimization and sensitivity analyses to identify the most efficient and cost-effective system configuration [109]. The simulation flowchart in HOMER Pro is illustrated in Figure 4.1.

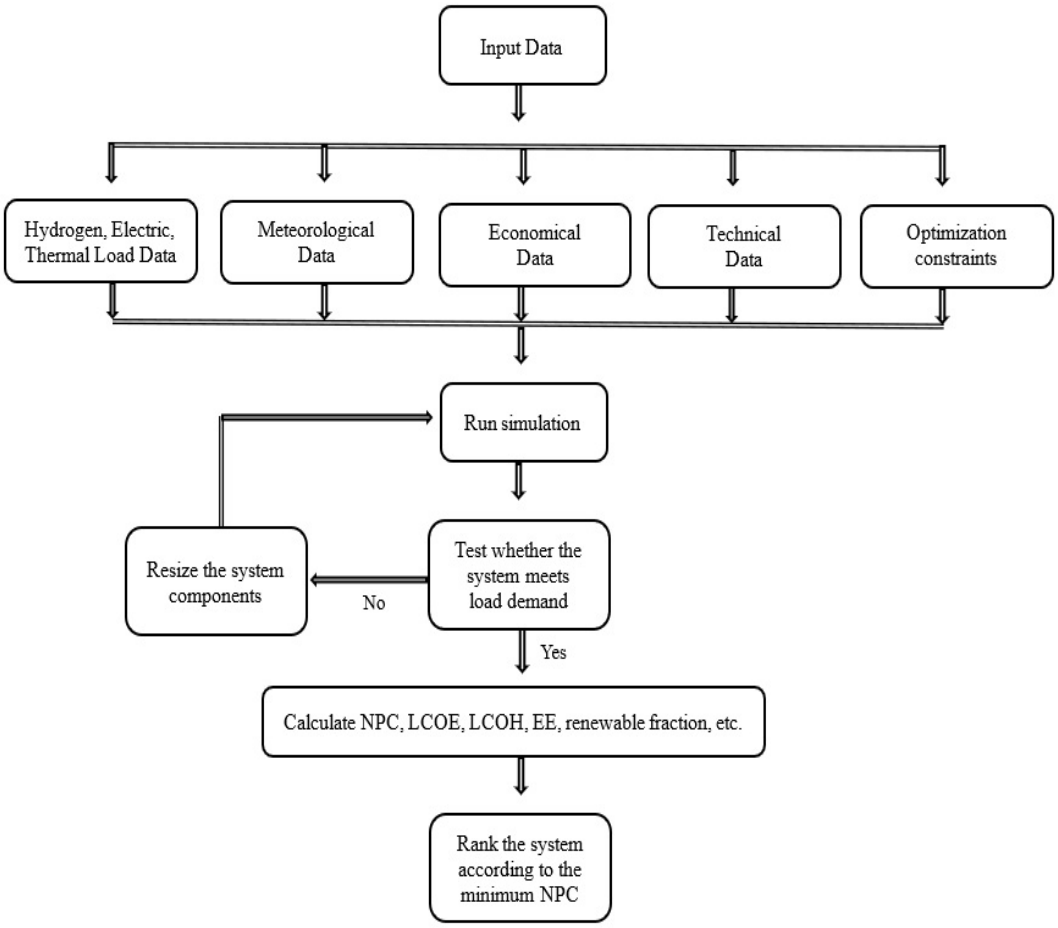


Figure 4.1 Flow Chart of HOMER Pro Optimization Process Steps

4.1.2.2 HOMER Pro Optimization Procedure

The HOMER Pro software can be utilized in the optimization of energy production systems for identifying the most economical configuration to satisfy certain energy requirements [4], [10]. Through the processing of elimination, the HOMER Pro software eliminates non-possible configurations and systematically lists the possible configurations, helping in the identification of the optimum HRES configuration [8]. The optimum sizes of the HRES configurations are identified based on the minimum NPC and the parameters such as LCOE, LCOH, EE, and the renewable fraction are also calculated during the process. If the generated energy does not meet the energy demand, the software helps in resizing the configurations to meet the demand [109]. The HOMER software also presents the results of the

simulation in various tables and charts, helping in comparing configurations based on their technical and economic feasibilities [108].

4.1.3 Description of the selected site

Schleswig-Holstein is located in northern Germany along the Danish border. The geographical coordinates of the area are as follows; 54°13.2'N, 09°41.8'E, and the map of the site is shown in Map 4.1.



Map 4.1 Map of the selected site, Schleswig-Holstein, Germany [110]

Schleswig-Holstein is the Germany's first federal state to achieve its 100% renewable energy target. The region dramatically increased its renewable energy share by 70% within just eight years, beginning from a wind energy of approximately 30% in 2006. Today, the state satisfies its complete electricity needs through a combination of wind, solar, and biomass power. This transformation started in 2010 when regional energy policy set a target to exceed 100% renewable generation by 2020. Energy strategies include substantial wind power expansion targets of 10.5 GW onshore and 2.6 GW offshore, alongside a doubling of solar capacity to 2.9 GW [111]. Schleswig-Holstein also makes use of agricultural by-

products. The major wheat production shows that there is a large amount of straw produced in this state every year. This straw has advantages over other sources of biomass. The harvesting, storage, and transportation of straw are much easier compared to other sources of biomass, making it an economically viable source of energy [27]. Hence, the straw can be effectively utilized in HRES, which can help to reduce the EE. Based on all these factors, Schleswig-Holstein region was selected to determine optimum HRES configuration.

The monthly clearness index and solar radiation in Schleswig-Holstein are given in Figure 4.2. The maximum daily solar radiation is 5.18 kWh/m^2/day, taking place in May. The monthly average wind speed of the considered site is shown in Figure 4.3. The maximum average wind speed is 8.58 m/s, taking place in January [112].

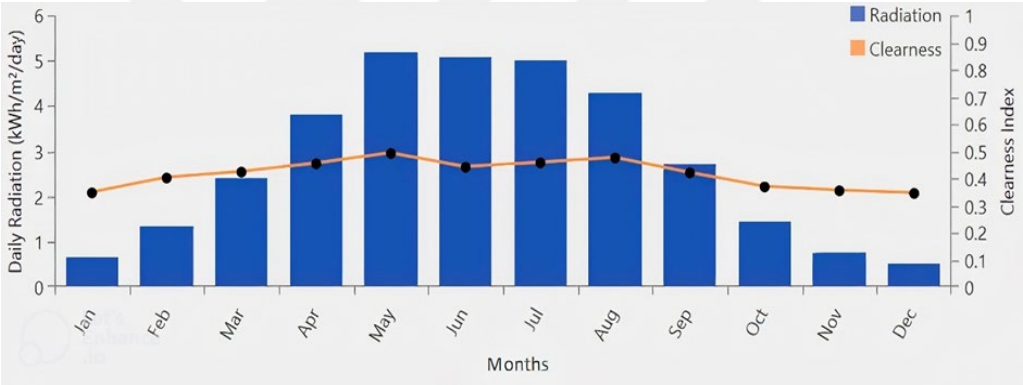


Figure 4.2 The monthly solar radiation and clearness index of Schleswig-Holstein



Figure 4.3 The monthly average wind speed at Schleswig-Holstein

4.1.4 Hybrid System Components

The HRES comprise of PV panels, WT, hydrogen tank, electrolyser, battery, TLC, MGT and boiler components. Techno-economical characteristics of the system components are shown in Table 4.1.

Table 4.1 Techno-economic data of the system components [10], [12], [22], [112], [113], [114]

Components	Technical Data	Economic Data
PV Panels	Type: Flat Plate Derating Factor (%): 80 Lifetime (year): 25	Capital Cost ($/kW): 2500 O&M Cost ($/kW/year): 10
WT -1	Type: XANT L-36 Rated Capacity (kW): 300 Hub Height (m): 55 Lifetime (year): 20	Capital Cost ($/kW): 2500 Replacement Cost ($/kW): 2083 O&M Cost ($/kW/year): 20
WT -2	Type: Vestas V47 Rated Capacity (kW): 660 Hub Height (m): 50 Lifetime (year): 20	Capital Cost ($/kW): 1500 Replacement Cost ($/kW):1500 O&M Cost ($/kW/year): 25
Biogas generator	Minimum load ratio (%): 50 Lifetime (year): 15 Biomass type: Straw	Capital Cost ($/kW): 550 Replacement Cost ($/kW): 500 O&M Cost ($/kW/year): 0.05
Hydrogen Tank	Initial tank level (%): 50 Lifetime (year): 20	Capital Cost ($/kg): 600 O&M Cost ($/kg/year): 3
Electrolyser	Efficiency (%): 85 Lifetime (year): 15	Capital Cost ($/kW): 100 Replacement Cost ($/kW): 100 O&M Cost ($/kW/year): 8
Battery	Nominal voltage (V): 12 Nominal capacity (kWh): 1 Roundtrip efficiency (%): 80 Lifetime (year): 10	Capital Cost ($/kW): 300 Replacement Cost ($/kW): 300 O&M Cost ($/kW/year): 10
Converter	Efficiency (%): 95 Lifetime (year): 15	Capital Cost ($/kW): 300 Replacement Cost ($/kW): 300 O&M Cost ($/kW/year): 10

Table 4.1 Techno-economic data of the system components [10], [12], [22], [112], [113], [114] (continued)

Components	Technical Data	Economic Data
TLC	Lifetime (year): 20	Capital Cost ($/kW): 54 Replacement Cost ($/kW): 54 O&M Cost ($/kW/year): 10
MGT	Lifetime (year): 10	Capital Cost ($/kW): 2000 Natural Gas Fuel Price ($/m^3): 0.3 Replacement Cost ($/kW): 1500 O&M Cost ($/kW/year): 0.01
Boiler	Efficiency (%): 85	Natural Gas Fuel Price ($/m^3): 0.3

4.1.4.1 Solar Photovoltaic Panels

The solar PV source is used in the HRES to generate green electrical energy [12]. It consists of PV panels that utilize solar energy to generate electricity directly and without emitting any pollutants [1]. Generic flat plate PV panels, fixed at a 40° tilt angle, are selected for the analysis, with no tracking system included in the model [2]. The PV array's power output is calculated by the equation below [12]:

$$P_{PV} = Y_{PV} f_{PV} \left(G_T / G_{(T,STC)}\right)\left[1 + a_p\left(T_C - T_{(C,STC)}\right)\right] \quad (3.7)$$

where Y_{PV} is the rated capacity of the PV array, (kW); f_{PV} is the derating factor, (%); G_T is the incident radiation of the PV array, (kW/m^2); and $G_{T,STC}$ is the incident radiation at standard condition, (kW/m^2). The temperature effect on the efficiency of the PV panels is disregarded and thus, it is not included in the power output calculation.

4.1.4.2 Wind Turbine

Wind energy plays a crucial role in electricity generation within HRES [3]. The wind speed at a specified hub height of the WT hub height can be determined by the following equation [4]:

$$\upsilon_{hub} = \upsilon_{anem}(H_{hub}/H_{anem})^m \quad (3.8)$$

where v_{anem} is the wind speed at the anemometer height, (m/s); v_{hub} is the wind speed at the hub height of the WT, (m/s); H_{anem} is the height of the anemometer, (m); H_{hub} the hub height of the WT, (m); and m is the exponent of the power law. HOMER Pro calculates the power output using WT power curves [4], [12]. In this study XANT L-36 and Vestas V47 WT are utilized as renewable energy sources.

4.1.4.3 Biogas generator

In HOMER, biogas is defined as the product obtained from the gasification of biomass. Various biomass feedstocks, including wood residues, agricultural by-products, and energy crops, can be converted into biogas through thermochemical or biological gasification processes. Regardless of the feedstock or the method used, the primary gases in biogas typically consist of carbon monoxide, hydrogen, and CO_2. Minor components of biogas include methane and water vapor [59].

In the present study, biomass energy is utilized by converting straw into biogas through the biogas generator. The straw biomass is assumed to have a carbon content of 40%, a gasification efficiency of 24%, and the resulting biogas has a lower heating value (LHV) of 17.0 MJ/kg [31]. The HOMER software models the biogas generator based on the power produced per unit of fuel consumed and calculates the corresponding electrical output [35].

4.1.4.4 Hydrogen Tank

A hydrogen tank is used for hydrogen storage generated by the electrolyser [4]. The stored hydrogen is then used in hydrogen refuelling stations for cars [10]. Hydrogen is typically stored in tanks operating at a moderate pressure of 200 bar. However, hydrogen refuelling stations are designed to compress and dispense hydrogen at 700 bar to fill the storage tanks of fuel cell vehicles [12]. The equation for the hydrogen tank pressure is as follows [23]:

$$P_t = n_{(g)} RT / V_t \tag{3.9}$$

where n_g is the mole of gas, (mol); R is the gas constant, (Joule/(mol·Kelvin)); T is the input temperature, (K); and V_t is the volume of the tank, (m^3).

4.1.4.5 Electrolyser

The electrolyser is a device which splits hydrogen and oxygen via electrolysis of water. The hydrogen is stored in a tank after separation and is subsequently utilized in the fuel cell to generate power [10]. HOMER Pro operates the electrolyser only when there is EE or when it is necessary to meet the hydrogen demand [22]. The amount of hydrogen produced by the electrolyser is given as follows [23]:

$$m_{H_2} = \left(n_f N_c I_{EI}\right)/\left((2F)\right) \tag{3.10}$$

where N_c is the number of cells; I_{EI} is the current of electrolyser, (A); F is the Faraday Constant, (C/mol); and the η_f is the Faraday efficiency. In this study, a generic electrolyser is used to design the system, with the efficiency set at 85% and a minimum load ratio of 0% [2].

4.1.4.6 Battery and Converter

A battery storage is a backup system, which stores electricity in respect of future usage when needed [10]. The battery storage is used when renewable energy sources cannot provide continuous energy to meet the demand, owing to the intermittent nature of renewable energy sources [12]. The storage capacity of the battery storage is calculated by the equation below [23]:

$$C_{Wh} = (E_L AD)\eta_{inv}\eta_b DOD \tag{3.11}$$

where E_L is total energy demand, (kWh); AD is daily autonomy; DOD is battery depth of discharge, (%); η_{inv} is efficiency of inverter, (%); and η_b is the efficiency of battery, (%). Generic 12-volt lead acid batteries having 1 kWh energy storage are used in the hybrid system configurations [13].

A power converter is used to convert energy from alternating current (AC) to direct current (DC), and conversely from DC to AC [12]. The output power can be calculated by the equation below [10]:

$$P_{out} = P_{in}\eta_{inv} \tag{3.12}$$

where P_{in} is the input power, (kW); and η_{inv} is inverter efficiency, (%). In this study, the converter size and efficiency are determined using the auto-sizing feature in HOMER Pro software, with the converter efficiency set to 95% [21].

4.1.4.7 Thermal Load Controller

TLC is used to meet the thermal need by using the EE produced from renewable energy sources. The TLC works like an electric boiler, in which EE is efficiently converted into heat, thus increasing the efficiency of the system by utilizing the surplus EE, which otherwise is wasted [20].

4.1.4.8 Micro Gas Turbine

A generic MGT is utilized to provide power when both PV and WT cannot meet the desired electrical load, in addition to waste heat recovery to meet the thermal load. The consumption of fuel in MGT is given by the below equation [20], [25]:

$$F_{MGT} = aR_{MGT} + bP_{MGT} \tag{3.13}$$

where a is the fuel curve intercept coefficient, ($m^3hour^{-1}.kW^{-1}$); b is slope of the fuel curve, ($m^3hour^{-1}.kW^{-1}$); R_{MGT} is the generator rated capacity, (kW); and P_{MGT} is power generation of the generator, (kW).

4.1.4.9 Boiler

The boiler is a device that can produce thermal energy when EE that is converted into heat via TLC is not enough to satisfy the thermal load [22]. The boiler has an efficiency of 85% and it is powered by natural gas. The natural gas has a density of 0.79 kg/m^3 and the lower heating value of 45 MJ/kg [18]. Since the boiler is used in the HRES, CO_2 is generated depending on the amount of fuel use [21].

4.1.5 Hydrogen Load Data

In Germany, hydrogen refuelling stations that have already been installed can store 200 kg of hydrogen with a tank capacity of 5 kg, which is enough to refuel 40 vehicles [40]. In order to meet a 200 kg dispensed demand, a 240 kg hydrogen load is utilised, considering both dispensing losses and the required residual hydrogen volume in the storage tanks. It is assumed that refuelling will occur between 20:00 and 8:00, with 240 kg/day distributed equally over a 12-hour period. Figure 4.4 shows the hydrogen load profiles of the systems.

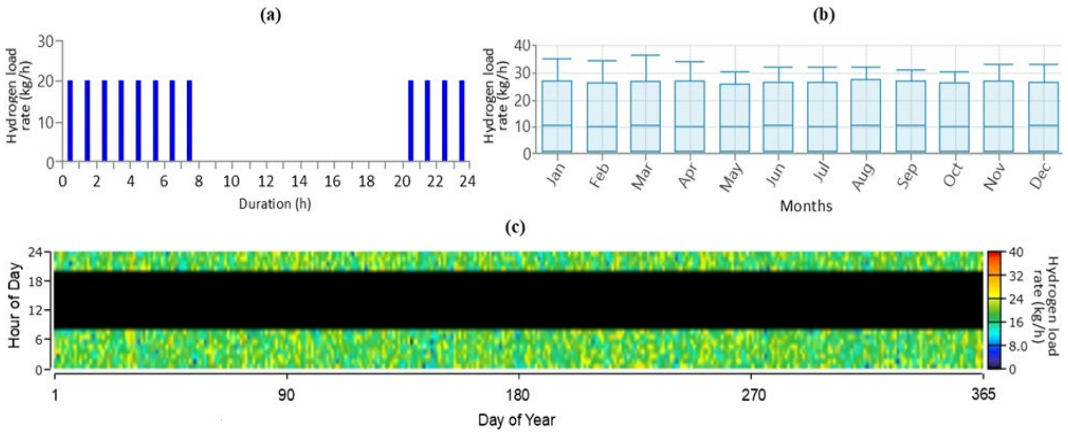


Figure 4.4 Hydrogen load profiles of the systems: (a) daily; (b) seasonal; (c) yearly profiles

The HOMER Pro simulations are carried out to ensure an unmet hydrogen load of 0%, showing that the hydrogen production system satisfies the continuous demand for hydrogen.

4.1.6 Electric Load Data

The electric load consumes 1505 kWh/day electricity, with a peak demand of 188 kW. The hydrogen refuelling station requires electricity for the dispenser, hydrogen compressor and chilling system. Electric load profiles of the HRES are shown in Figure 4.5.

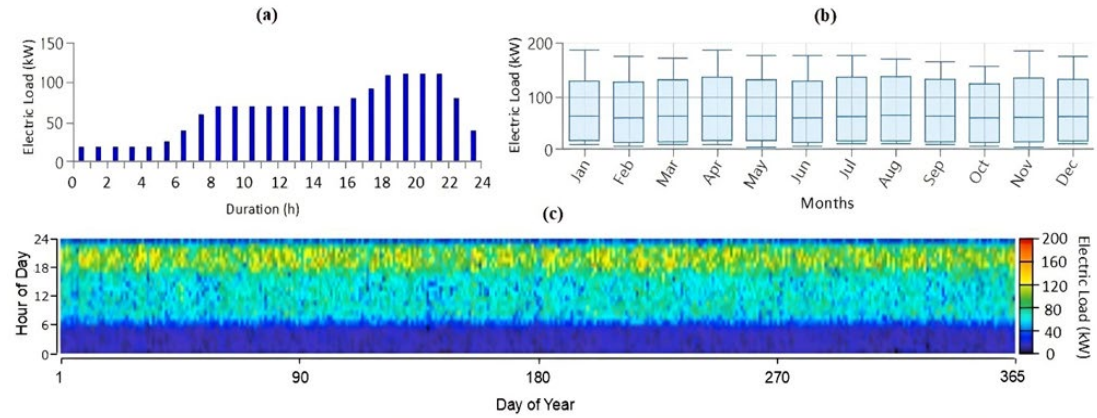


Figure 4.5 Electric load profiles of the systems: (a) daily; (b) seasonal; (c) yearly profiles

4.1.7 Thermal Load Data

Thermal load defines the level of the heat demand of the selected site, where the installation of the hydrogen refuelling station is planned. The demand will be used for facility heating and hot water at the hydrogen refuelling station. The EE recovered by the HRES is used for satisfying the demand, thus enhancing energy efficiency and eliminating the energy dissipation. This thermal load is represented by the scaled annual average energy demand of 4000 kWh/day. The thermal load profiles of the HRES are given in Figure 4.6.

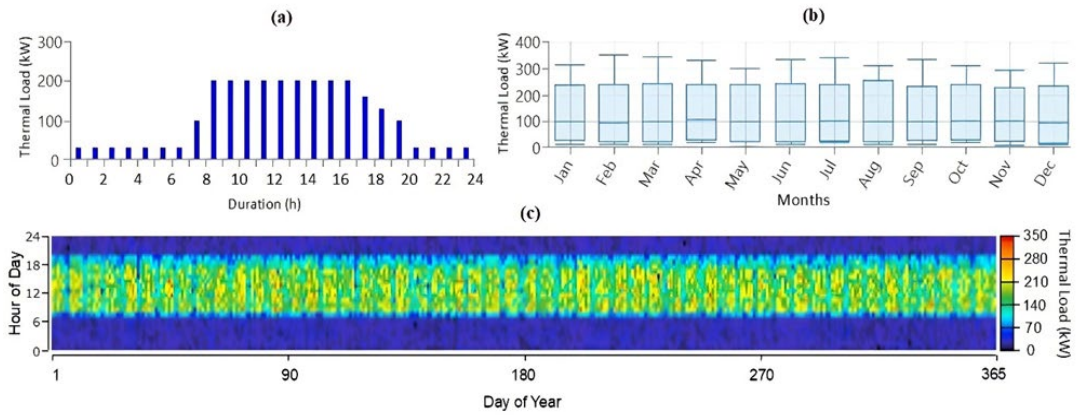


Figure 4.6 Thermal load profiles of the systems: (a) daily; (b) seasonal; (c) yearly profiles

4.1.8 Biomass Load Data

Straw is used as a biomass resource for biogas production, which subsequently fuels a biogas generator. In the hybrid renewable energy system configuration, this generator is specified to operate on biogas to supply electrical power.

The baseline for calculating the accessible straw potential was the officially reported annual wheat production of 1,680,000 tons by the Schleswig-Holstein Ministry for Energy Transition, Agriculture, Environment, Nature and Digitalization [115]. Based on this, the potential straw yield was determined to be 504,000 tons per year. This amount accounts for a straw-to-grain ratio of 50% and allocates 40% of the resulting straw for use in animal husbandry and other agricultural purposes. Finally, the resulting straw amount is integrated into the HOMER simulation as a biomass feedstock, with a specified daily availability

profile in tons/day. The monthly biomass load profile of the HRES is presented in Figure 4.7.

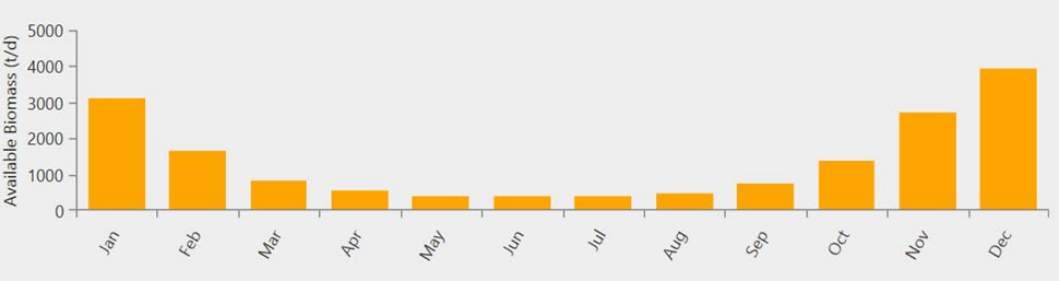


Figure 4.7 Monthly straw biomass distribution of the Schleswig-Holstein in HOMER Pro software

In this study, straw availability is assumed to increase during times when solar energy is low, as presented in Table 4.2. The idea is to rely more on biomass during the winter months, when solar power is limited. Even though wind energy continues to support the system throughout the year, using biomass more actively during these low-solar periods helps improve overall system reliability and makes it more cost-effective by reducing both unmet energy demand and excess electricity generation.

Table 4.2 Daily Biomass Availability Profile Based on 504,000 tons of Annual Straw Supply, Distributed Inversely to Solar Radiation

Month	Solar Radiation	Inverse Proportion	Normalised Proportion (%)	Monthly Biomass (tons/month)	Daily biomass (tons/day)
January	0.64	1.5625	19.01	95,815	3090.8
February	1.33	0.7519	9.15	46,106	1646.7
March	2.41	0.4149	5.05	25,445	820.8
April	3.81	0.2625	3.19	16,095	536.5
May	5.18	0.1931	2.35	11,838	381.9
June	5.06	0.1976	2.40	12,119	404.0

Table 4.2 Daily Biomass Availability Profile Based on 504,000 tons of Annual Straw Supply, Distributed Inversely to Solar Radiation (continued)

Month	Solar Radiation	Inverse Proportion	Normalised Proportion (%)	Monthly Biomass (tons/month)	Daily biomass (tons/day)
July	4.99	0.2004	2.44	12,289	396.4
August	4.29	0.2331	2.84	14,294	461.1
September	2.7	0.3704	4.51	22,712	757.1
October	1.43	0.6993	8.51	42,882	1383.3
November	0.75	1.3333	16.22	81,762	2725.4
December	0.5	2.0000	24.33	122,643	3956.2

4.2 Methodology and Data for Regression Models

R is a programming language that offers extensive tools for data processing and graphical representation. R (version 4.4.0) is used to create regression algorithms for predicting four different regression models. The necessary packages, including “readr”, “caret”, “ggplot”, and “repr”, are installed for all regression models. The process of data partitioning usually involves dividing the data into 30% test data and 70% train data. The model is built using train data, and its performance is assessed and validated using test data. The “preProcess” and “predict” functions are applied to scale the numeric features. The linear regression model is fitted using the primary function “lm”. The “glmnet” package is required to run the functions of RR, LR and ENR models. Since the “glmnet” function does not work with dataframes, a numeric matrix for the training features and target values of vectors is required. The “dummyVars” function from the “caret” library is used to create the model matrix, and the “predict” function generates numeric model matrices for both train and test data. Additionally, the train and test data matrices for the independent variables (X) and dependent variable (Y) are specified. To identify the

optimal lambda values, k-fold cross-validation is carried out using the “cv.glmnet” function. The RR model is constructed by using the “glmnet” function with alpha set to 1. For the LR model, the same procedure is followed, but alpha is set to 0. For the ENR model, the “trainControl” function defines the number of cross-validations and repetitions, and the “train” function is used to determine the optimal alpha and lambda values. Finally, predictions are carried out using the “predict” function on the test data to validate the models. The “eval_results” function calculates RMSE and R^2 metrics for the test data to evaluate model performance [32].

An econometric analysis of green hydrogen production is carried out by data collection, model construction, estimation, analysis and interpretation in R. Lee conducted a comparative econometric assessment of nine different models. He proposed that econometric models help decision-makers optimize strategies for the growth of the bioenergy sector. Furthermore, he concluded that regression models are the most suitable econometric approach for making reliable predictions [116]. Based on Lee`s study, four different regression model including regression, RR, LR and ENR are utilized in this study for econometric assessment of global green hydrogen production. The global green hydrogen energy production (*Y*) is defined as the dependent variable, and its relationship with twelve independent variables is analysed to estimate the influence of these predictors on *Y*. Table 4.3 outlines the dependent variable, global green hydrogen production (*Y*), alongside twelve independent variables (*X1–X12*) considered for the regression analysis.

Table 4.3 Annual variable values used in regression analysis [56], [117], [118], [119], [120], [121], [122]

Year	**2010**	**2011**	**2012**	**2013**	**2014**	**2015**	**2016**	**2017**	**2018**	**2019**	**2020**	**2021**	**2022**
Global green hydrogen production (mio. mt) **(*Y*)**	1.8	2.2	2.6	2.7	2.8	2.9	3.2	3.5	3.8	4.3	4.9	5.4	5.6
Global solar power generation (TWh) **(*X1*)**	32.20	63.58	96.99	131.96	197.74	256	328.11	445.37	575.12	705.52	853.37	1055.7	1323.3
Global solar PV costs ($/kWh) **(*X2*)**	0.445	0.335	0.253	0.193	0.173	0.131	0.114	0.09	0.076	0.067	0.06	0.052	0.049
Global installed solar energy capacity (GW) **(*X3*)**	41.58	73.97	104.23	141.41	180.76	229.06	301.19	396.32	492.64	595.49	728.41	873.86	1073.1
Global wind power generation (TWh) **(*X4*)**	345.9	439.9	529.2	634.1	706.0	829.6	960.0	1139.0	1267.9	1419.8	1590.7	1849.5	2098.5
Global WT costs ($/kWh) **(*X5*)**	0.196	0.205	0.175	0.149	0.181	0.147	0.123	0.112	0.106	0.091	0.088	0.079	0.081
Global installed wind energy capacity (GW) **(*X6*)**	181.08	220.21	267.27	299.91	349.42	416.33	466.96	515.04	563.84	622.77	733.72	824.60	901.23
Global hydrogen refuelling stations **(*X7*)**	213	217	215	186	181	214	274	328	369	434	560	685	814
Global hydrogen demand (mio.mt) **(*X8*)**	62.4	65.7	67.1	68.2	69.2	71.7	71.9	72.2	73.9	91.5	88.5	94.5	95.0
Global hydrogen fuel cell vehicles as a percentage of total vehicles (%) **(*X9*)**	0.11	0.22	0.33	0.55	0.88	1.10	1.65	2.20	2.75	3.30	3.85	4.21	4.63
Global hydrogen production (mio. mt) **(*X10*)**	51.3	53.3	54.6	57.9	59.0	61.8	66.0	70.1	74.5	79.6	83.8	86.7	89.25
Global green hydrogen costs ($/kg) **(*X11*)**	12.50	12.13	11.75	11.38	11.00	10.63	10.25	9.75	9.00	8.25	7.25	6.25	5.25
Global average crude oil price ($/barrel) **(*X12*)**	79.47	111.26	111.63	108.56	98.97	52.32	43.67	54.25	71.34	64.30	41.96	70.86	100.93

4.3 Economic Analysis

The HOMER Pro program is used to assess the hydrogen refuelling station's economic viability, with metrics of NPC, LCOE, and LCOH [4]. The software simulates different system configurations and generates results as a list from lowest to highest NPC [13].

4.3.1 Net Present Cost

The system NPC is represented by subtracting the present value of the total revenues from the present value of the total expenses over the lifetime of the system. The system NPC is determined with the following equation [12]:

$$C_{npc,tot} = C_{ann,tot}/CRF \tag{3.14}$$

where $C_{ann,tot}$ is the total annualised cost of the system, ($/year); and *CRF* is the capital recovery factor. The *CRF* is determined by the equation below [12]:

$$CRF = i(1+i)^n/((1+i)^n - 1) \tag{3.15}$$

where i is the real discount, (%); and n is the project lifetime, (25 years).

4.3.2 Levelised Cost of Energy

The LCOE is calculated by dividing the cost of electricity generated annually by the total electricity produced. The system LCOE is defined by the following equation [13]:

$$LCOE = C_{ann,tot}/E_{served} \tag{3.16}$$

where $C_{ann,tot}$ is the total annualised cost of the system, ($/year); and E_{served} is the total electricity produced, (kWh/year).

4.3.3 Levelised Cost of Hydrogen

The LCOH is calculated by subtracting the annual electricity cost from the total annual cost and dividing the result by the total hydrogen produced annually. The annual LCOH of the system is expressed by using the equation below [13]:

$$LCOH = \left(C_{ann,tot} - C_{electricity}\right)/M_{hydrogen} \tag{3.17}$$

where $C_{ann,tot}$ is the total annual cost, ($/year); $C_{electricity}$ is the revenue from annualised electricity sale, ($/year); and $M_{hydrogen}$ annual hydrogen mass produced, (kg/year).

4.3.4 Operating Cost

The annualized value of all revenue and expenses, except initial capital costs, is known as the operating cost. The following formula is used by HOMER to determine the operating cost [59]:

$$C_{operating} = C_{ann,tot} - C_{ann,cap} \tag{3.18}$$

where $C_{operating}$ is the operating cost, ($/year); $C_{ann,tot}$ is the total annual cost, ($/year); and $C_{ann,cap}$ is the initial capital cost, ($/year).

4.3.5 Initial Capital Cost

A component's initial capital cost is its total installed cost at the beginning of the project [59]. This cost includes the purchase, transportation, installation, and setup of the equipment.

4.3.6 Operational and Maintenance Cost

The cost of operating and maintaining a component is known as its O&M cost. O&M costs of each system component add up to the system's overall O&M cost [59].

4.3.7 Replacement Cost

The replacement cost refers to the expense of substituting a component once it reaches the end of its lifetime, as defined by the component’s lifetime parameter. This cost differs from the component’s initial capital cost in the system [59].

5
RESULTS AND DISCUSSION

5.1 Techno-economic Results of Hybrid Systems

This section presents the simulation results obtained using HOMER Pro software. The technical, economic, and environmental performance of each configuration is compared to identify the optimal system components. The results of the optimization analysis are assessed according to the performance of each system component. The values of NPC, LCOE, LCOH, costs of operation, initial investment costs, EE, and RF are calculated in HOMER Pro software, considering various parameters including solar radiation, wind speed, technical parameters, as well as costs of components of the system. Sensitivity analyses are also carried out to evaluate how changes in costs and electrolyser efficiency affect the techno-economic results. These analyses make the study more reliable by comparing results across different parameters.

5.1.1 Optimization Results of the Systems with Four Different Wind Turbines

A techno-economic analysis was conducted for a hydrogen refuelling station powered by a hybrid system including four different wind turbine models, simulated using HOMER software (Figure 5.1). The results showed that significant variations in the techno-economical results depending on the wind turbine used.

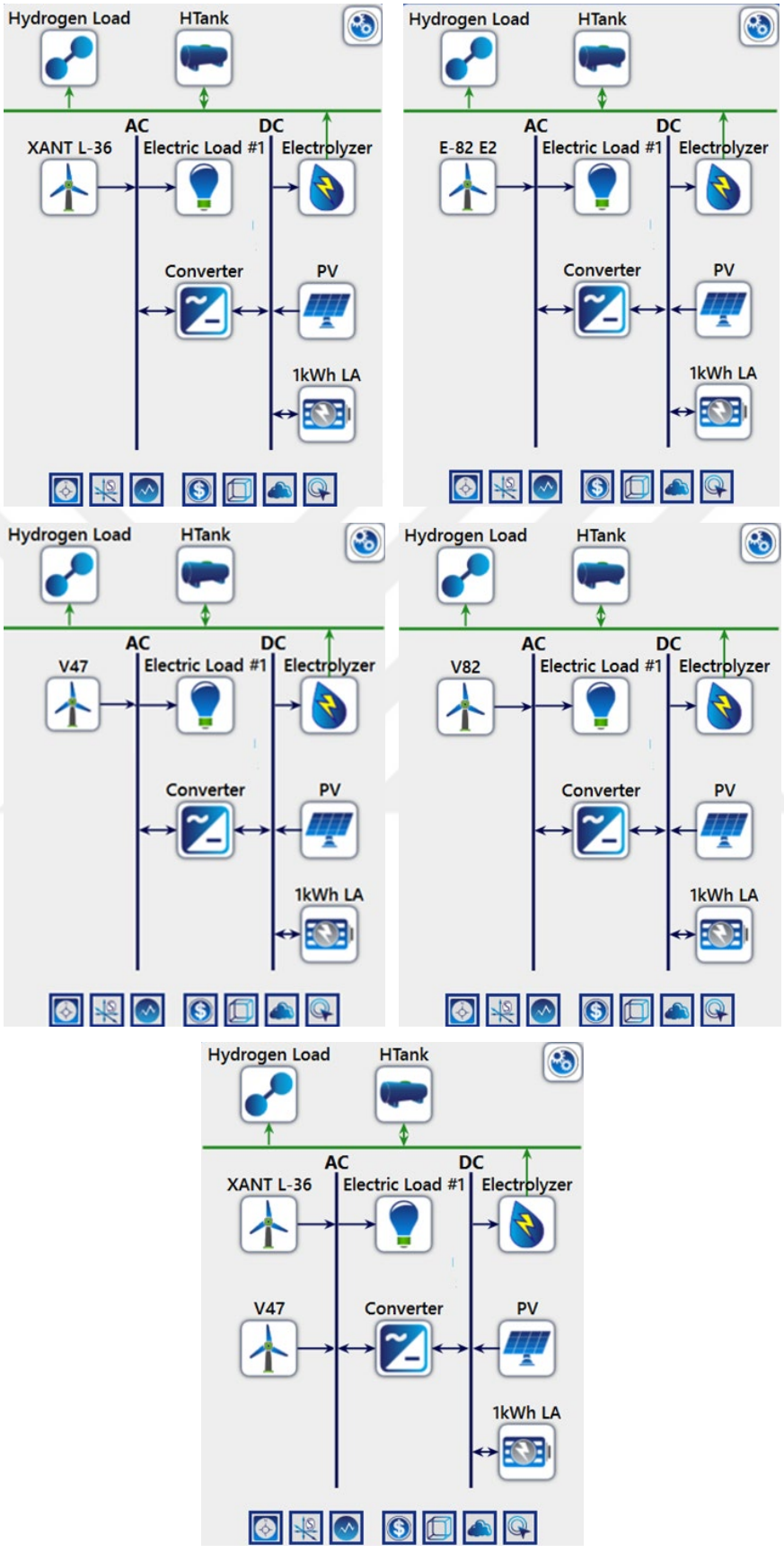


Figure 5.1 HOMER Pro schemes of HRES with various WT

As shown in Table 5.1, configurations utilizing the Enercon E-82 E2, Vestas V47, and Vestas V82 WT generated very high amount of surplus electricity. This excess energy occurs when power production is higher than the station's demand and the battery storage capacity is full. It is crucial to realize that reducing the size of the power generation system to lower the EE was not a good solution since it would negatively impact the system capacity to consistently satisfy the load demand. In comparison, the configurations using the XANT L-36 turbine, both alone and shared with the Vestas V47, demonstrated a significantly lower rate of EE (17.8% and 18.2%, respectively). Based on these results, these two configurations (XANT L-36 and XANT L-36&Vestas V47) were selected for further, more detailed techno-economic and environmental analysis to be evaluated for the final design of the hydrogen refuelling station.

Table 5.1 Renewable fraction and EE results of the HRES with different WT

System	Renewable Fraction (%)	EE (%)
PV / XANT L-36 WT	100	17.8
PV / Enercon E-82 E2 WT	100	57.9
PV / Vestas V47 WT	100	51.2
PV / Vestas V82 WT	100	46.9
PV / XANT L-36 + Vestas V47 WT	100	18.2

5.1.2 Optimization Results of the Systems without Recovering Excess Energy

Two systems are proposed in the optimization process and they are different in terms of WT types: one uses the XANT L-36, while the other employs a combination of the XANT L-36 and Vestas V47. These HRES do not utilize EE and are designed solely to meet electricity and hydrogen demands. Furthermore, the configurations contain PV panels, WT, hydrogen tank, electrolyser, battery and converter components. The optimal configurations of each component of the HRES, simulated with different WT are presented in Table 5.2.

Table 5.2 Optimum configuration of HRES with different WT

System	PV (kW)	WT (number)	Battery (series)	Electrolyser Capacity (kW)	Hydrogen Tank Capacity (kg)	Converter Capacity (kW)
PV/XANT L-36 WT/Battery	287	4	1529	1000	1100	976
PV/XANT L-36 & Vestas V47 WT	332	3	1583	1000	1100	869

In the optimum configuration with the XANT L-36 WT, the system utilizes 4 WT, each with a capacity of 300 kW while the other system utilizes 3 WT: 2 XANT L-36 turbines with a capacity of 300 kW each and 1 Vestas V47 turbine with a capacity of 660 kW. The monthly electricity production for these configurations is shown in Figure 5.2. The high electricity generation of the WT compared to PV panels can be due to the strong wind speeds at the selected site, Schleswig-Holstein, which is the windiest region in Germany because of its geographical location.

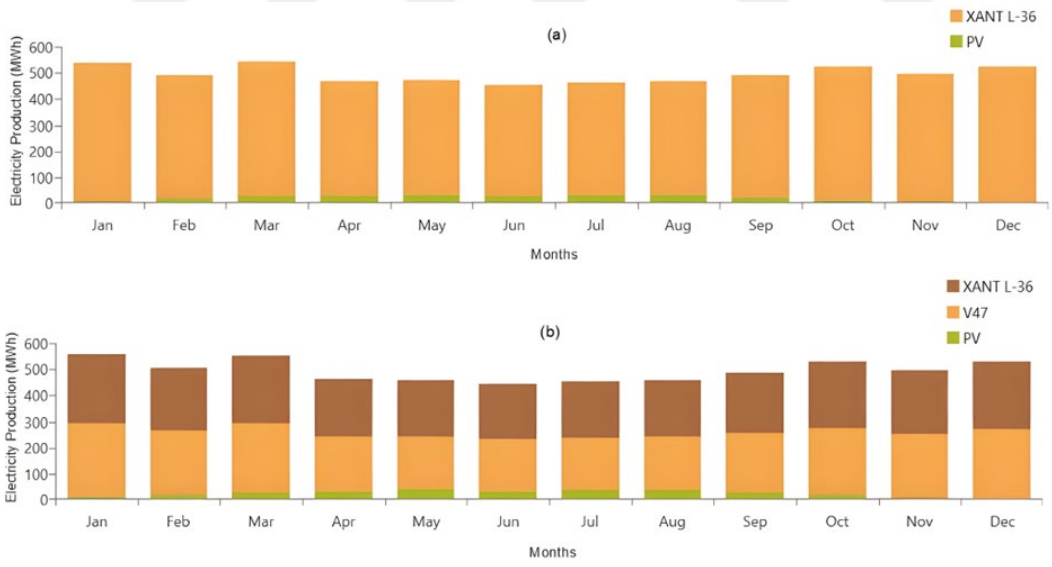


Figure 5.2 The monthly electricity production of: (a) PV/XANT L-36 WT/Battery; (b) PV/XANT L-36 & Vestas V47 WT/Battery systems

For each WT alternative, simulation of the HRES based on minimum NPC are carried out and techno-economical results are given in Table 5.3. The results shows that the systems with the XANT L-36 WT and the combination of XANT L-36 and Vestas V47 WT generate 17.8% and 18.2% EE, respectively.

Table 5.3 Techno-economic analysis results of the HRES with different WT

System	NPC (M$)	LCOE ($)	LCOH ($/kg)	Operating cost ($/y)	Initial capital (M$)	Renewable Fraction (%)	EE (%)
PV/XANT L-36 WT	8.94	0.491	3.04	111,896	5.23	100	17.8
PV/XANT L-36 & Vestas V47 WT	6.89	0.378	2.36	92,048	3.84	100	18.2

The surplus energy is generated when the HRES produces more electricity than needed and the batteries lack sufficient capacity for storage. Though this EE reduces the net efficiency of the systems, it gives a reliability buffer. Reducing the size of the system to minimize EE is not feasible, as it would decrease the system's reliability and fail to meet the energy demand of the hydrogen refuelling station. So, instead of downsizing the system, the surplus energy can be used to run station equipment, meet thermal demand, produce extra hydrogen during low demand, or sell power to nearby microgrids. These approaches turn wasted energy into value and improve the system’s overall performance.

The results further show that both systems produce completely green hydrogen with a 100% renewable fraction and zero greenhouse gas emissions. Furthermore, the configuration with XANT L-36 and Vestas V47 WT has a lower LCOH of $2.36/kg with respect to the LCOH of the system that uses only XANT L-36 WT. Besides, the detailed cost analyses of the components used in both system configurations play an important role for the overall economic performance, as presented in Table 5.4 and Table 5.5.

Table 5.4 The costs of each component for the PV/XANT L-36 WT/Battery system

Component	Capital Cost ($)	Replacement Cost ($)	O&M Cost ($)	Fuel Cost ($)	Salvage Cost ($)	Total Cost ($)
Lead acid Battery	458,700	1,262,702	507,539	0	387,060	1,841,881
Electrolyser	100,000	136,889	265,554	0	56,255	446,188

Table 5.4 The costs of each component for the PV/XANT L-36 WT/Battery system (continued)

Component	Capital Cost ($)	Replacement Cost ($)	O&M Cost ($)	Fuel Cost ($)	Salvage Cost ($)	Total Cost ($)
PV	717,786	0.00	95,305	0	0.00	813,091
Hydrogen Tank	660,000	668,769	109,541	0	556,921	881,389
System Converter	292,750	400,742	0.00	0	164,686	528,807
XANT L-36 WT	3,000,000	3,799,825	796,661	0	3,164,322	4,432,163
System	5,229,236	6,268,927	1,774,599	0	4,329,243	8,943,519

Table 5.5 The costs of each component for the PV/XANT L-36 & Vestas V47 WT/Battery system

Component	Capital Cost ($)	Replacement Cost ($)	O&M Cost ($)	Fuel Cost ($)	Salvage Cost ($)	Total Cost ($)
Lead acid Battery	474,900	1,307,297	525,464	0	400,730	1,906,931
Electrolyser	100,000	136,889	265,554	0	56,255	446,188
PV	830,915	0	110,326	0	0	941,242
Hydrogen Tank	660,000	668,769	109,541	0	556,921	881,389
System Converter	260,810	357,019	0	0	146,717	471,111
Vestas V47	10,000	15,199	16,597	0	12,657	29,139
XANT L-36 WT	1,500,000	1,899,912	398,330	0	1,582,16	2,216,081
System	3,836,625	4,385,086	1,425,812	0	2,755,441	6,892,082

A hydrogen refuelling station in the transportation sector requires the analysis of various LCOH values that are calculated for different sites. It is observed from the reference studies of green hydrogen production for the hydrogen refuelling stations that the LCOH values vary from $3.00/kg to $13.55/kg [4], [10], [11], [12], [13], [14], [15], [16], [17]. It is obvious that the LCOH value of the optimal system, calculated as $2.36/kg, is much more barcompetitive than the production of green hydrogen in other sites given in the literature.

Renewable energy utilization to produce hydrogen offers significant environmental benefits compared to gasoline in the road transport sector. Replacing gasoline with green hydrogen can cause considerable reduction in CO_2 emissions. Based on lower heating values, 2.75 tons of gasoline are equivalent to 1 ton of hydrogen, and the combustion of 1 kg of gasoline emits 3 kg of CO_2 [14]. The hydrogen production, corresponding gasoline replacement, and CO_2 emissions avoided for refuelling stations using different WT are summarized in Table 5.6. The results show that each hydrogen refuelling station can prevent significant amount of CO_2 emissions annually.

Table 5.6 Hydrogen, gasoline replacement, and CO_2 emission reduction values

System	Hydrogen production (kg/year)	Gasoline replaced by hydrogen (kg/year)	CO_2 avoided (kg/year)
PV/XANT L-36 WT	88,548	243,507	730,521
PV/XANT L-36 & Vestas V47 WT	88,054	242,148	726,444

5.1.3 Optimization Results of the Systems with Thermal Components

A TLC is added to recover the EE of the HRES to serve a thermal load. The heat generated by the TLC reduces the system's dependency on fuel for heat production, thereby lowering greenhouse gas emissions. However, a boiler is also utilized in the HRES to satisfy the thermal demand when surplus energy is not available. Thermal load can also be satisfied by MGT through waste heat recovery. Waste heat recovery allows the heat generated by the MGT during electricity production

to be used for a thermal demand. Furthermore, by utilizing waste heat, the system requires less fuel (e.g., for boilers) for heat production. So, integration of the MGT is also carried out to optimize energy utilization and increase the system performance. Schematic representations of the HRES with thermal components in HOMER Pro are shown in Figure 5.3.

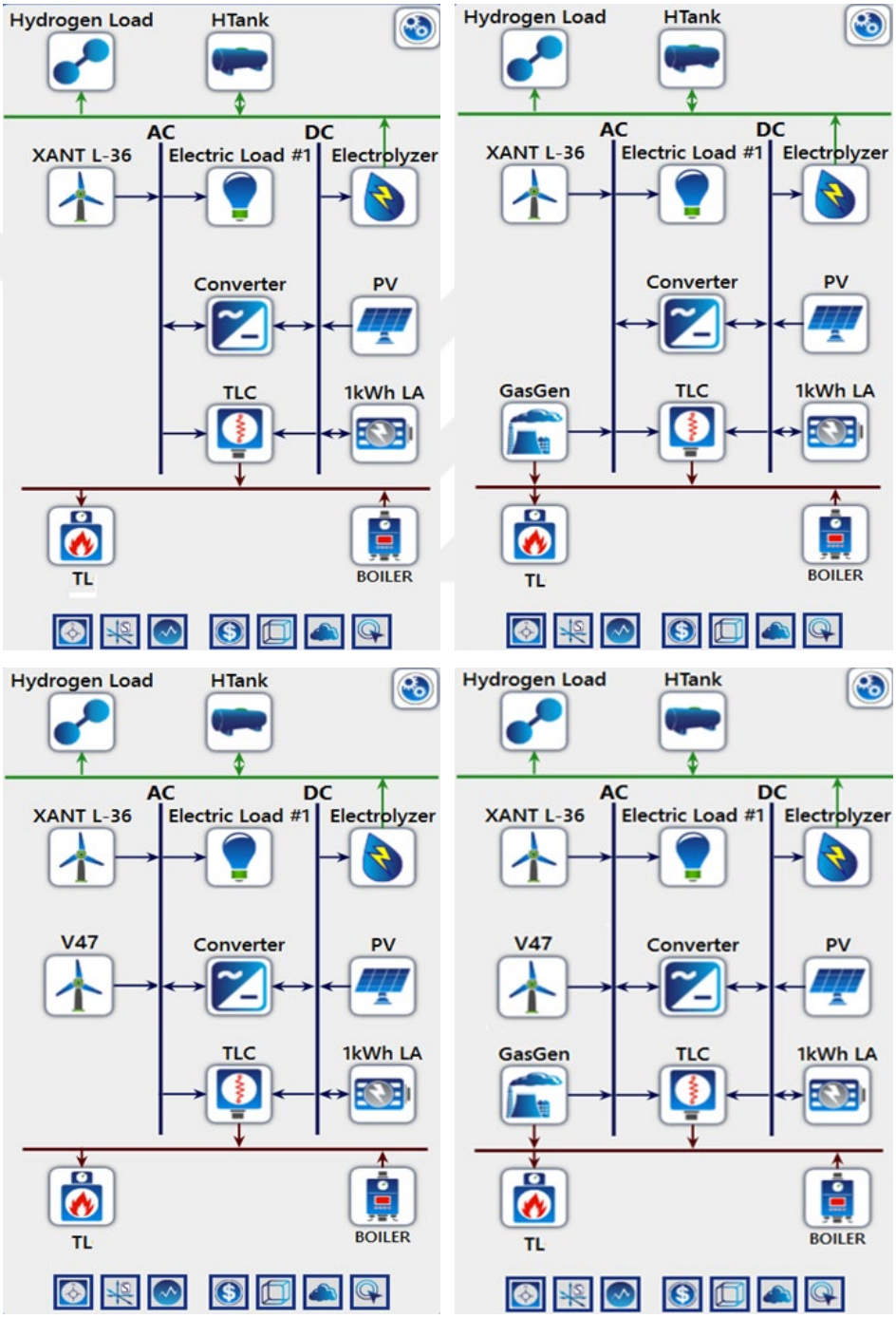


Figure 5.3 HOMER Pro schemes of HRES with thermal components

The optimal configurations of the thermal component integrated systems, simulated with different WT are presented in Table 5.7 and Table 5.8. The capacity of the PV panels in thermal component-integrated systems is low due to the complementary roles of the MGT and boiler. These components reduce the system's reliance on electricity for heating, because the intermittent nature of the renewable sources. Consequently, HOMER Pro optimizes the system by minimizing PV capacity, enhancing both cost-effectiveness and operational efficiency.

Table 5.7 Optimum configuration of thermal component integrated systems with XANT L-36 WT

System	PV Output (kW)	WT (no)	Battery (series)	Electr. Capacity (kW)	Hydrogen Tank Capacity (kg)	Converter Capacity (kW)	TLC Capacity (kW)	MGT Capacity (kW)
PV/XANT L-36 WT /TLC/ Boiler	33.5	4	2389	1000	1100	1435	1200	-
PV/XANT L-36 WT /TLC/ Boiler /MGT	8.86	4	257	1000	1100	887	1200	250

Table 5.8 Optimum configuration of thermal component integrated systems with XANT L-36 & Vestas V47 WT

System	PV Output (kW)	WT (number)	Battery (series)	Electrolyser Capacity (kW)	Hydrogen Tank Capacity (kg)	Converter Capacity (kW)	TLC Capacity (kW)	MGT Capacity (kW)
PV/XANT L-36 & Vestas V47 WT/TLC/ Boiler	184	3	1	2023	1000	1200	900	1380
PV/XANT L-36 &Vestas V47 WT/TLC/ Boiler/MGT	21.8	3	1	226	1000	1100	1009	1380

The integration of the thermal components, such as TLC, boiler, and MGT, may significantly affect the cost of the HRES. Therefore, it is important to consider a detailed evaluation of all component prices, focusing significantly on the prices related to the thermal components. So, the detailed cost results of the components used in the system configurations are tabulated in Table 5.9, Table 5.10, Table 5.11 and Table 5.12.

Table 5.9 The costs of each component for the PV/XANT L-36 WT/TLC/Boiler system

Component	Capital Cost ($)	Replacement Cost ($)	O&M Cost ($)	Fuel Cost ($)	Salvage Cost ($)	Total Cost ($)
Lead acid Battery	716,700	1,972,920	793,00	0	604,765	2,877,864
Boiler	0	0	0	1,352,376	0	1,352,376
Electrolyser	100,000	136,889	265,554	0	56,255	446,188
PV	83,741	0	11,119	0	0	94,860
Hydrogen Tank	660,000	668,769	109,541	0	556,921	881,389
System Converter	430,451	589,239	0	0	242,149	777,541
TLC	64,800	98,491	0	0	82,019	81,272
XANT L-36 WT	3,000,000	3,799,825	796,661	0	3,164,322	4,432,163
System	5,055,692	7,266,133	1,975,883	1,352,376	4,706,431	10,943,653

Table 5.10 The costs of each component for the PV/XANT L-36 WT/TLC/ Boiler/MGT system

Component	Capital Cost ($)	Replacement Cost ($)	O&M Cost ($)	Fuel Cost ($)	Salvage Cost ($)	Total Cost ($)
Lead acid Battery	77,100	212,240	85,309	0	65,058	309,590
Boiler	0	0	0	1,066,145	0	1,066,145
Electrolyser	100,000	136,889	265,554	0	56,255	446,188
PV	22,154	0	2,942	0.00	0.00	25,095
MGT	500,000	0	68,380	270,855	306,939	532,296
Hydrogen Tank	660,000	668,769	109,541	0	556,921	881,389
System Converter	266,158	364,340	0	0	149,726	480,772
TLC	64,800	98,491	0	0	82,019	81,272
XANT L-36 WT	3,000,000	3,799,825	796,661	0	3,164,322	4,432,163
System	4,690,212	5,280,554	1,328,386	1,337,000	4,381,241	8,254,911

Table 5.11 The costs of each component for the PV/XANT L-36 & Vestas V47 WT/TLC/Boiler system

Component	Capital Cost ($)	Replacement Cost ($)	O&M Cost ($)	Fuel Cost ($)	Salvage Cost ($)	Total Cost ($)
Lead acid Battery	606,900	1,670,665	671,518	0	512,114	2,436,969
Boiler	0	0	0	1,185,742	0	1,185,742

Table 5.11 The costs of each component for the PV/XANT L-36 & Vestas V47 WT/TLC/Boiler system (continued)

Component	Capital Cost ($)	Replacement Cost ($)	O&M Cost ($)	Fuel Cost ($)	Salvage Cost ($)	Total Cost ($)
Electrolyser	100,000	136,889	265,554	0	56,255	446,188
PV	459,691	0	61,036	0.00	0.00	520,728
Hydrogen Tank	720,000	729,566	119,499	0	607,550	961,516
System Converter	269,877	369,431	0	0	151,818	487,489
TLC	74,520	113,265	0	0	94,322	93,463
Vestas V47 WT	10,000	15,199	16,597	0	12,657	29,139
XANT L-36 WT	1,500,000	1,899,912	398,330	0	1,582,161	2,216,081
System	3,740,988	4,934,927	1,532,535	1,185,742	3,016,877	8,377,315

Table 5.12 The costs of each component for the PV/XANT L-36&Vestas V47 WT/TLC/Boiler/MGT system

Component	Capital Cost ($)	Replacement Cost ($)	O&M Cost ($)	Fuel Cost ($)	Salvage Cost ($)	Total Cost ($)
Lead acid Battery	67,800	186,639	75,019	0.00	57,211	272,247
Boiler	0	0	0	1,225,253	0	1,225,253
Electrolyser	100,000	136,889	265,554	0	56,255	446,188
PV	54,560	0	7,244	0.00	0.00	61,804

Table 5.12 The costs of each component for the PV/XANT L-36&Vestas V47 WT/TLC/Boiler/MGT system (continued)

Component	Capital Cost ($)	Replacement Cost ($)	O&M Cost ($)	Fuel Cost ($)	Salvage Cost ($)	Total Cost ($)
MGT	480,000	0	66,202	250,465	292,004	504,664
Hydrogen Tank	660,000	668,769	109,541	0	556,921	881,389
System Converter	302,691	414,350	0.00	0	170,278	546,764
TLC	74,520	113,265	$0.00	0	94,322	93,463
Vestas V47 WT	10,000	15,199	16,597	0	12,657	29,139
XANT L-36 WT	1,500,000	1,899,912	398,330	0	1,582,161	2,216,081
System	3,249,571	3,435,024	938,487	1,475,718	2,821,808	6,276,992

The techno-economic analysis results of the solely energy powered and thermal component-integrated HRES with different WT are shown in Table 5.13 and Table 5.14. The results demonstrate that the integration of the TLC and boiler increases NPC, LCOE, and LCOH costs compared to the solely electric-powered system. On the other hand, the configuration with a MGT and two WT has the lowest NPC, LCOE and LCOH costs which are $6.28 M, $0.249 kWh and $2.14/kg, respectively. The optimum configuration of this system contains 21.8 kW PV panels, 2 XANT l-36 WT, 1 Vestas V47 WT, 226 battery strings, 1000 kW electrolyser, 1100 kg hydrogen storage tank, 1009 kW converter, 1380 kW TLC and 240 kW MGT. Notably, the MGT efficiently utilizes waste heat through combined heat and power generation, while also minimizing the need for storage and oversized renewable components by providing cost-effective backup electrical power.

Table 5.13 Techno-economic analysis results of the HRES with XANT L-36 WT

System	NPC (M$)	LCOE ($)	LCOH ($/kg)	Operating cost ($/year)	Initial capital (M$)	Renewable Fraction (%)
PV/XANT L-36 WT	8.94	0.491	3.04	111,896	5.23	100
PV/XANT L-36 WT/TLC/Boiler	10.94	0.506	3.74	177,379	5.06	43.3
PV/XANT L-36 WT/TLC/Boiler/MGT	8.25	0.358	2.83	107,389	4.69	46.1

Table 5.14 Techno-economic analysis results of the HRES with XANT L-36&Vestas V47 WT

System	NPC (M$)	LCOE ($)	LCOH ($/kg)	Operating cost ($/year)	Initial capital (M$)	Renewable Fraction (%)
PV/XANT L-36 & Vestas V47 WT	6.94	0.381	2.38	94,165	3.82	100
PV/XANT L-36 & Vestas V47 WT/TLC/Boiler	8.38	0.365	2.85	139,673	3.74	50.2
PV/XANT L-36 & Vestas V47 WT/TLC/Boiler/MGT	6.28	0.249	2.14	91,203	3.25	40.1

Although the integration of a TLC and heat recovery systems can improve overall system efficiency, the reliance on conventional fuel sources for heat generation introduces a degree of non-renewable energy use. While these components help manage thermal loads and reduce EE, their consumption of natural gas considerably lowers the renewable energy contribution, resulting a significant reduction in the renewable fraction. As a result, these systems exhibit a significantly lower renewable energy fraction, which contributes to the generation of greenhouse emissions. HOMER Pro software can calculate the emissions factor in the simulation and the resulting CO_2 emissions for thermal component integrated systems are presented in Figure 5.4. As indicated in the figure, a considerable quantity of CO_2 is produced annually under various system configurations, between the values of 231.1 tons and 284.4 tons. This high amount of CO_2 produced because

of the burning of fossil fuels in the MGT and the boiler. Therefore, the use of components that depend on fossil fuels in heat recovery and backup power generation makes the systems non-green. The current hybrid system still offers a lower environmental impact compared to conventional systems that rely entirely on fossil fuels. Nonetheless, the use of carbon-neutral fuels in the MGT and the boiler, increasing the use of renewable energy in overall generation and integrating carbon capture technologies would prevent the polluting effect of the fossil-fuel-based components and reduce greenhouse gas emissions to move closer to carbon neutrality.

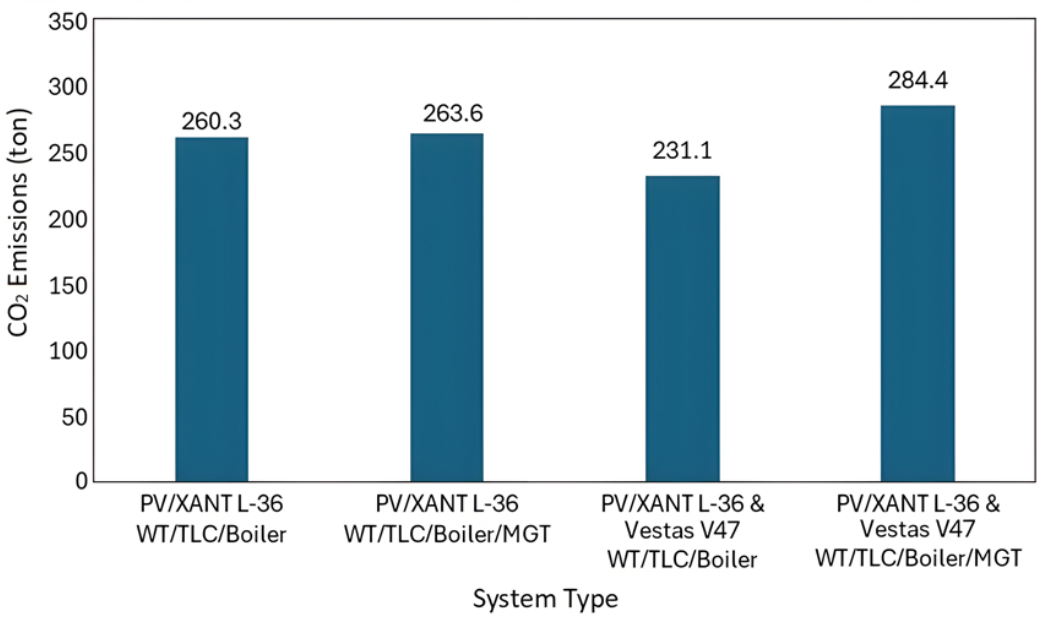


Figure 5.4 CO_2 emissions of the thermal component integrated HRES

5.1.4 Sensitivity Analysis of Capital Costs, O&M Costs, and Electrolyser Efficiency on System Performance

A sensitivity analysis can be carried out by entering multiple values for a specific input variable. For each value of the variable, HOMER Pro restarts its optimization process, allowing users to observe the impact on results. Sensitivity variables are input variables that have many specified values. The users can specify as many sensitivity variables as they require [59].

Sensitivity analysis should be performed to assess how uncertain parameters affect the ideal components configuration for HRES. The most unpredictable factors

should be taken into account in the studies and depending on the location and type of components uncertain parameters may change [109].

A detailed sensitivity analysis was performed for the optimal system configuration (PV/XANT L-36 & Vestas V47 WT/TLC/Boiler/MGT) to assess the impact of capital cost levels with corresponding variations in the O&M costs of each component, on the LCOH and NPC, as shown in Table 5.15. Accordingly, the maximum, minimum, and average values of capital and operational costs were used to evaluate each piece of equipment. This table improves the practical applicability of the study by enabling researchers to adjust cost assumptions to realistic LCOH scenarios for their economic contexts.

Table 5.15 Sensitivity Analysis: Effects of Capital and O&M Cost Changes on System Cost

PV/XANT L-36 & Vestas V47 WT/TLC/Boiler/MGT System										
PV	**Capital Costs**	**700 ($/kW)**			**1600 ($/kW)**			**2500 ($/kW)**		
	O&M Costs	**10**	**17.5**	**25**	**10**	**17.5**	**25**	**10**	**17.5**	**25**
	NPC (M$)	6.11	6.20	6.22	6.25	6.26	6.27	6.28	6.28	6.29
	LCOH ($/kg)	2.08	2.11	2.12	2.12	2.13	2.13	2.14	2.14	2.14
XANT L-36 WT	**Capital Costs**	**1000 ($/kW)**			**1750 ($/kW)**			**2500 ($/kW)**		
	O&M Costs	**20**	**40**	**60**	**20**	**40**	**60**	**20**	**40**	**60**
	NPC (M$)	5.38	5.78	6.17	5.83	6.23	6.62	6.28	6.68	7.07
	LCOH ($/kg)	1.83	1.96	2.10	1.98	2.12	2.25	2.14	2.27	2.41

Table 5.15 Sensitivity Analysis: Effects of Capital and O&M Cost Changes on System Cost (continued)

PV/XANT L-36 & Vestas V47 WT/TLC/Boiler/MGT System										
Vestas V47 WT	**Capital Costs**	**1500 ($/kW)**			**2000 ($/kW)**			**2500 ($/kW)**		
	O&M Costs	**25**	**37.5**	**50**	**25**	**37.5**	**50**	**25**	**37.5**	**50**
	NPC (M$)	6.28	6.51	6.59	6.40	6.63	6.72	6.43	6.67	6.75
	LCOH ($/kg)	2.14	2.21	2.24	2.18	2.26	2.28	2.19	2.27	2.30
Battery	**Capital Costs**	**150 ($/kW)**			**225 ($/kW)**			**300 ($/kW)**		
	O&M Costs	**5**	**12.5**	**20**	**5**	**12.5**	**20**	**5**	**12.5**	**20**
	NPC (M$)	6.18	6.26	6.24	6.21	6.28	6.35	6.24	6.21	6.36
	LCOH ($/kg)	2.10	2.13	2.12	2.11	2.14	2.16	2.12	2.11	2.16
Electrolyser	**Capital Costs**	**80 ($/kW)**			**290 ($/kW)**			**500 ($/kW)**		
	O&M Costs	**5**	**10**	**15**	**5**	**10**	**15**	**5**	**10**	**15**
	NPC (M$)	6.08	6.28	6.45	6.33	6.49	6.66	6.54	6.70	6.87
	LCOH ($/kg)	2.07	2.14	2.19	2.15	2.21	2.27	2.22	2.28	2.34
Hydrogen Tank	**Capital Costs**	**600 ($/kW)**			**900 ($/kW)**			**1200 ($/kW)**		
	O&M Costs	**2**	**5**	**8**	**2**	**5**	**8**	**2**	**5**	**8**
	NPC (M$)	6.24	6.35	6.46	6.57	6.68	6.79	6.90	7.01	7.12
	LCOH ($/kg)	2.12	2.16	2.20	2.24	2.27	2.31	2.35	2.38	2.42

Table 5.15 Sensitivity Analysis: Effects of Capital and O&M Cost Changes on System Cost (continued)

PV/XANT L-36 & Vestas V47 WT/TLC/Boiler/MGT System										
Converter	**Capital Costs**	**200 ($/kW)**			**300 ($/kW)**			**400 ($/kW)**		
	O&M Costs	**10**	**20**	**30**	**10**	**20**	**30**	**10**	**20**	**30**
	NPC (M$)	6.20	6.23	6.28	6.28	6.34	6.38	6.41	6.44	6.47
	LCOH ($/kg)	2.11	2.12	2.14	2.14	2.16	2.17	2.18	2.19	2.20
TLC	**Capital Costs**	**50 ($/kW)**			**100 ($/kW)**			**150 ($/kW)**		
	O&M Costs	**5**	**10**	**15**	**5**	**10**	**15**	**5**	**10**	**15**
	NPC (M$)	6.28	6.29	6.31	6.35	6.36	6.37	6.42	6.43	6.44
	LCOH ($/kg)	2.14	2.14	2.15	2.16	2.16	2.17	2.18	2.19	2.19
MGT	**Capital Costs**	**1000 ($/kW)**			**1500 ($/kW)**			**2000 ($/kW)**		
	O&M Costs	**0.01**	**0.0175**	**0.025**	**0.01**	**0.0175**	**0.025**	**0.01**	**0.0175**	**0.025**
	NPC (M$)	6.04	6.06	6.09	6.16	6.18	6.21	6.28	6.30	6.33
	LCOH ($/kg)	2.05	2.06	2.07	2.09	2.10	2.11	2.14	2.14	2.15

For a PV system, the results reveal that both NPC and LCOH display minimal sensitivity in varying costs, with LCOH narrowly fluctuating between $2.08 & 2.14/kg, indicating that costs of a PV system are of less importance in a system's economy. Furthermore, WT (XANT L-36 & Vestas V47) display higher levels of sensitivity since these components contribute a substantial amount to overall energy of the system. For instance, the LCOH of a XANT L-36 displays considerable

variations of ($1.83-2.41/kg), not only due to a wider range of costs but also the fact that a combination of two turbines is involved in this analysis. The Vestas V47 WT, however, shows LCOH range of ($2.14–2.30/kg), meaning its costs stay more stable because the system uses only one turbine for the configuration. In a further analysis, the electrolysis and the hydrogen tank display considerable variations in LCOH & NPC, indicating the importance of such components in a system's economy. The battery and the converter display minimum impacts in costs and the MGT has also a low range of LCOH ($2.05-2.15/kg). In summary, the analysis emphasizes that a reduction in the costs of WT, electrolysis, and hydrogen storage would be most effective in reducing system costs, as opposed to the costs of PV, batteries, converters, as well as MGT.

Another sensitivity analysis on the PV/XANT L-36 WT, as well as the PV/XANT L-36 & Vestas V47 WT systems emphasizes the importance of electrolyser efficiency on the economics of such systems, as highlighted in Table 5.16 and Table 5.17. This is especially important for the renewable-based systems, where the optimization of electrolyser efficiency becomes a prerequisite to keep the costs minimum.

Table 5.16 Sensitivity Analysis of Electrolyser Efficiency for PV/XANT L-36 WT System

PV/XANT L-36 WT System				
Electrolyser efficiency (%)	**NPC (M$)**	**LCOE ($)**	**LCOH ($/kg)**	**Excess Energy (%)**
65	32.5	1.78	11.1	43.5
70	17.4	0.957	5.94	24.1
75	9.61	0.528	3.27	11.6
80	9.05	0.497	3.08	13.1
85	8.94	0.491	3.04	17.8

Table 5.17 Sensitivity Analysis of Electrolyser Efficiency for PV/XANT L-36 &Vestas V47 WT System

PV/XANT L-36 & Vestas V47 WT System				
Electrolyser efficiency (%)	**NPC (M$)**	**LCOE ($)**	**LCOH ($/kg)**	**Excess Energy (%)**
65	12.7	0.695	4.38	23.7
70	9.47	0.519	3.25	16.3
75	7.67	0.421	2.63	14.2
80	6.95	0.382	2.38	13.6
85	6.89	0.378	2.36	18.2

In both configurations, increasing electrolyser efficiency from 65% to 85% results in substantial reductions in NPC, LCOE, and LCOH. This indicates that while increasing efficiency improves both systems, the hybrid system lowers costs more effectively by utilizing a more stable energy supply. In terms of excess energy, both systems show declining trends as efficiency increases, indicating better utilization of generated renewable energy. Despite the slight increase in excess energy at 85% electrolyser efficiency, the further reductions in NPC and LCOH indicate that operating the system at this efficiency level is still preferable in terms of cost-effectiveness. Overall, the results confirm that improving electrolyser efficiency is a key strategy to lower costs and optimize energy performance in renewable energy systems.

5.1.5 Optimization Results of the Systems with Biogas generator

This section presents three different system configurations that incorporate a biogas generator to harness biomass resources. The first configuration relies solely on biomass as the renewable energy source. The second combines PV panels, the XANT L-36 WT, and biomass to meet the energy demand. The third configuration integrates PV panels, the XANT L-36 and Vestas V47 WT, along with biomass, to supply the energy required for hydrogen production.

5.1.5.1 Hybrid System Design with Biomass as the Sole Renewable Source

In the first configuration of the system, straw biomass is considered as the only renewable fuel source to the biogas generator, which can produce sufficient energy to power a hydrogen refuelling station. This setup shows whether a HRES powered only by biomass can deliver steady and reliable energy without depending on solar or wind sources. A techno-economic analysis is conducted in this scenario to evaluate the viability and overall efficiency of this process. A representation of the system has been developed in HOMER software that has key components, including a biogas generator, electrolyser, hydrogen storage tank, power converter, as well as a battery unit, as shown in Figure 5.5.

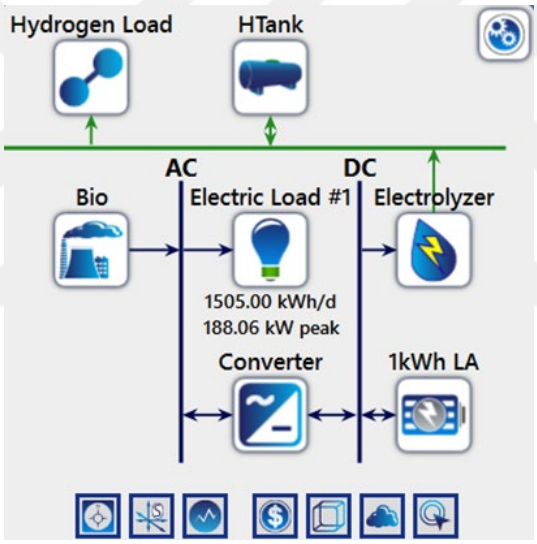


Figure 5.5 HOMER scheme of the biomass-only system

Various capacities of the biogas generator were used to assess the techno-economics of these systems. As shown in Table 5.18, when the only power source in the system is the biogas generator, the values of both the NPC and the LCOH increase considerably, making this economically inefficient. Moreover, there are various systems that display high values of EE generation, showing that energy production and demand are not balanced and that the system design is not feasible.

Table 5.18 Techno-economic analysis results of biomass-only system

Biogas gen. Capacity	NPC (M$)	LCOE ($)	LCOH ($/kg)	Operating cost ($/year)	Initial capital (M$)	Renewable Fraction (%)	EE (%)
1000 kW	-	-	-	-	-	-	-
1500 kW	50.7	2.78	17.4	1,470,000	1.73	100	26.3
2000 kW	67.0	3.68	23.0	1,960,000	2.00	100	44.7
2500 kW	45.1	2.48	15.5	1,280,000	2.57	100	8.49
3000 kW	50.7	2.78	17.5	1,440,000	2.89	100	19.3
3500 kW	60.8	3.34	20.8	1,740,000	3.13	100	34.1
4000 kW	66.9	3.67	23.1	1,910,000	3.42	100	40.8

5.1.5.2 Hybrid System Design Using PV, XANT L-36 Wind Turbine, and Biomass Renewable Sources

In this configuration, the hydrogen refuelling station is powered by renewable sources of energy which include PV panels, XANT L-36 WT, as well as a biogas generator. Each of these systems plays a significant role in ensuring that the station is constantly supplied with sufficient sustainable energy to ensure a continuous hydrogen production at the station. The system diagram is shown in Figure 5.6, which basically represents a HOMER model of the system that incorporates the use of a PV array, XANT L-36 WT, biogas generator, electrolyser, hydrogen storage tank, power converter, as well as a battery bank. This design allows a detailed evaluation of how the system performs technically and economically under various biogas generator capacities.

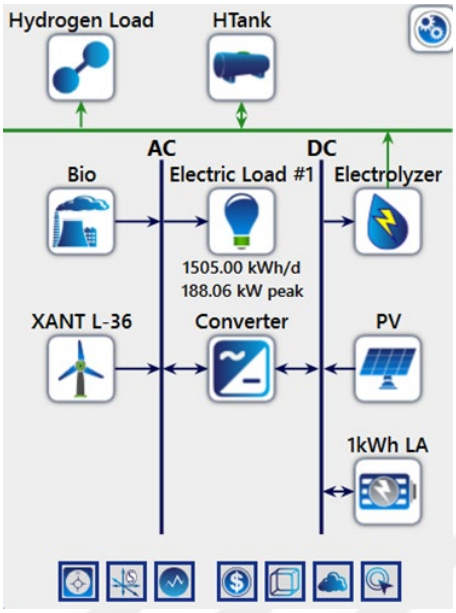


Figure 5.6 HOMER scheme of the PV/XANT L-36 WT /Biogas gen. system

The operational configuration of HRES is shown by the predominance of PV and wind energy due to their high availability and zero variable costs, although their intermittent nature. The biogas generator operates as a dispatchable resource, which is utilized during periods of low solar or wind availability to ensure reliable operation. This backup function operates with a low capacity factor and contributes a small amount to overall production, usually between 1% and 3%. Other restrictions such as high operational costs due to fuel processing and maintenance and biomass availability limitations, are major constraints. The system is optimized to rely mainly on PV and wind power, while biogas is used to provide balanced support when needed.

The techno-economic assessment is carried out with a parametric method where the size of the biogas generator varied between 600 kW to 3000 kW. One of the important results obtained is that the overall system is highly efficient with low EE as indicated in Table 5.19 with a minimum and maximum value of 1.88% and 3.05%, respectively. This range indicated that the hybrid system design successfully balances energy production with demand and storage. The analysis showed that the optimal configuration has a 2000 kW biogas generator capacity resulted in the lowest NPC and LCOH. The optimal configuration consists of a 610 kW PV array,

three XANT L-36 WT, 697 series 1 kW lead-acid batteries, a hydrogen storage capacity of 1100 kg, a 1000 kW electrolyser, and an 852 kW converter.

Table 5.19 Techno-economic analysis results of PV/XANT L-36 WT /Biogas gen. System

Biogas gen. Capacity	NPC (M$)	LCOE ($)	LCOH ($/kg)	Biomass % Energy Prod.	PV % Energy Prod.	WT % Energy Prod.	Renewable Fraction (%)	EE (%)
600 kW	7.97	0.437	2.75	1.73	11.7	86.5	100	2.43
800 kW	7.85	0.431	2.71	1.02	12.4	86.6	100	2.45
1000 kW	7.81	0.428	2.70	1.55	11.4	87.0	100	1.88
1200 kW	7.82	0.429	2.70	1.35	11.8	86.9	100	2.07
1400 kW	7.80	0.428	2.70	1.35	11.9	86.8	100	2.17
1600 kW	7.80	0.428	2.69	1.60	11.6	86.8	100	2.08
1800 kW	7.80	0.428	2.69	1.73	11.6	86.7	100	2.16
2000 kW	7.78	0.427	2.69	1.73	11.6	86.7	100	2.13
2200 kW	7.81	0.428	2.69	1.81	11.9	86.3	100	2.52
2400 kW	7.82	0.429	2.70	2.00	11.7	86.3	100	2.49
2600 kW	7.83	0.430	2.70	2.27	11.4	86.4	100	2.42
2800 kW	7.83	0.430	2.71	2.06	12.0	86.0	100	3.05
3000 kW	7.83	0.430	2.71	2.21	11.8	86.0	100	2.97

To further reduce the NPC, LCOH, and EE of the optimum system with a 2000 kW biogas generator, simulations with different electrolyser capacities are conducted. This parametric analysis is essential because the electrolyser's capacity is a key cost driver; its sizing critically affects the system's ability to utilize EE, thereby determining overall efficiency and economic performance. As given in Table 5.20, when the electrolyser capacity is 1200 kW, both NPC and LCOH decrease even further, and EE drops to nearly zero at 0.787%.

Table 5.20 Techno-economic analysis results of PV/XANT L-36 WT /Biogas gen. (2000kW) system with different electrolyser capacities

Electrolyser Capacity	NPC (M$)	LCOE ($)	LCOH ($/kg)	Biomass % Energy Prod.	PV % Energy Prod.	WT % Energy Prod.	Renewable Fraction (%)	EE (%)
1000 kW	7.78	0.427	2.69	1.73	11.6	86.7	100	2.13
1100 kW	7.73	0.424	2.67	1.91	10.7	87.4	100	1.26
1200 kW	7.72	0.424	2.67	1.69	10.5	87.8	100	0.787
1300 kW	7.77	0.426	2.68	1.80	10.5	87.7	100	0.896
1400 kW	7.77	0.426	2.68	1.71	10.6	87.7	100	0.953
1500 kW	7.82	0.429	2.70	1.71	10.6	87.7	100	0.953

The integration of a biogas generator into the HRES system, along with the determination of the optimal capacities for the biogas generator and the electrolyser, represents key factors influencing the system’s overall feasibility. Therefore, the individual costs of each component are presented in the Table 5.21 below.

Table 5.21 The costs of each component for the PV/XANT L-36 WT /Biogas gen. system

Component	Capital Cost ($)	Replacement Cost ($)	O&M Cost ($)	Fuel Cost ($)	Salvage Cost ($)	Total Cost ($)
Lead acid Battery	212,100	583,866	234,683	0	178,974	851,674
Biogas generator	1,100,000	0	272,192	163,521	1,456,995	78,719
Electrolyser	120,000	164,266	318,664	0	67,506	535,425
PV	1,363,582	0	181,052	0	0	1,544,634
Hydrogen Tank	660,000	668,769	109,541	0	556,921	881,389
System Converter	281,249	384,998	0	0	158,216	508,032
XANT L-36 WT	2,250,000	2,849,869	597,495	0	2,373,242	3,324,122
System	5,986,931	4,651,768	1,713,628	163,521	4,791,852	7,723,996

Table 5.22 summarizes the techno-economic results of different hybrid renewable energy system configurations that integrate PV panels, the XANT L-36 wind turbine, and a biogas generator. Comparing the optimal PV/XANT L-36 WT/Biogas generator (2000 kW) configuration with the PV/XANT L-36 WT-only system reveals that incorporating the biogas generator substantially lowers both the NPC and LCOH values. Furthermore, the share of EE decreases notably from 17.8% to 0.787%, reflecting enhanced system efficiency and more effective use of generated power.

Table 5.22 Techno-economic analysis comparison of PV/XANT L-36 WT system with/without biogas generator

System	NPC (M$)	LCOE ($)	LCOH ($/kg)	Operating cost ($/year)	Initial capital (M$)	Renewable Fraction (%)	EE (%)
PV/XANT L-36 WT	8.94	0.491	3.04	111,896	5.23	100	17.8
PV/XANT L-36 WT/Biogas gen. (2000 kW)	7.72	0.424	2.67	52,330	5.99	100	0.787

5.1.5.3 Hybrid System Design Using PV, XANT L-36&Vestas V47 Wind Turbine, and Biomass Renewable Sources

In this system configuration, PV panels, XANT L-36 and Vestas V47 WT, and a biogas generator serve as the primary energy sources supplying the hydrogen refuelling station. The integration of these renewable and dispatchable technologies aims to ensure a stable and continuous power supply. As illustrated in Figure 5.7, the HOMER Pro scheme presents the main system components, including PV panels, XANT L-36 WT, Vestas V47 WT, biogas generator, electrolyser, hydrogen storage tank, power converter, and battery bank, all interconnected to support the efficient production and storage of green hydrogen.

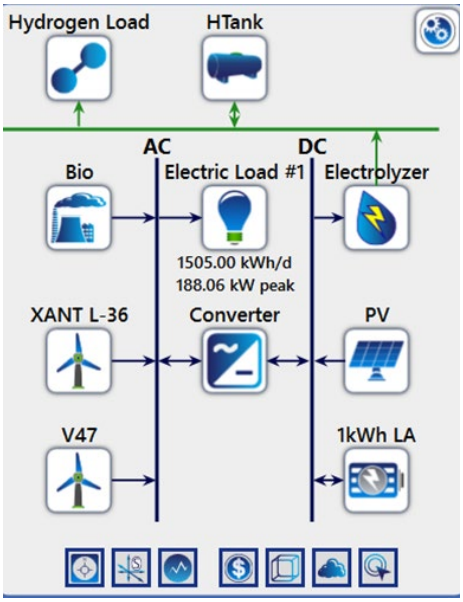


Figure 5.7 HOMER scheme of the PV/ XANT L-36&Vestas V47 WT/Biogas gen. system

Techno-economic analyses are performed by evaluating various biogas generator capacities to determine their effect on the system performance. The EE amount is observed between 3.75% and 5.36%, which displays a high level of system efficiency and effective utilization of energy. As presented in Table 5.23, the configuration with a biogas generator capacity of 1000 kW yields the lowest NPC and LCOH. The optimal configuration consists of a 753 kW PV array, one XANT L-36 WT, one Vestas V 47 WT, 561 series 1 kW lead-acid batteries, a hydrogen storage capacity of 1100 kg, a 1000 kW electrolyser, and an 868 kW converter.

Table 5.23 Techno-economic analysis results of PV/ XANT L-36&Vestas V47 WT/Biogas gen. system

Biogas gen. Capacity	NPC (M$)	LCOE ($)	LCOH ($/kg)	Biomass % Energy	PV % Energy	XANT L-36 WT % Energy	VESTAS V47 WT % Energy	EE (%)
600 kW	6.45	0.354	2.22	1.64	15.3	28.0	55.1	5.24
800 kW	6.24	0.342	2.15	1.45	14.7	28.3	55.6	4.27
1000 kW	6.17	0.338	2.13	1.86	14.0	28.4	55.7	3.99
1200 kW	6.20	0.340	2.14	1.89	14.0	28.4	55.7	3.98
1400 kW	6.22	0.341	2.14	2.03	13.7	28.4	55.8	3.75
1600 kW	6.22	0.341	2.14	1.63	14.7	28.2	55.5	4.38
1800 kW	6.21	0.341	2.14	1.62	14.7	28.2	55.5	4.42
2000 kW	6.21	0.341	2.14	2.11	14.0	28.3	55.6	4.10
2200 kW	6.22	0.341	2.14	1.81	14.6	28.2	55.4	4.51
2400 kW	6.26	0.343	2.15	2.11	14.6	28.1	55.2	4.74
2600 kW	6.24	0.342	2.15	1.98	15.0	28.0	55.1	5.07
2800 kW	6.25	0.342	2.15	2.04	15.1	27.9	54.9	5.36
3000 kW	6.26	0.343	2.15	2.34	14.6	28.0	55.1	5.04

Additional simulations were conducted by varying the electrolyser capacity to further optimize the system performance and NPC, LCOH and EE in the configuration containing a 1000 kW biogas generator. As presented in Table 5.24, increasing the electrolyser capacity to 1300 kW results in additional reductions in both NPC and LCOH, while EE decreases to 1.98%, indicating an improvement in overall energy utilization and economic efficiency.

Table 5.24 Techno-economic analysis results of PV/XANT L-36&Vestas V47 WT/Biogas gen. (1000kW) system with different electrolyser capacities

Electrolyser Capacity	NPC (M$)	LCOE ($)	LCOH ($/kg)	Biomass % Energy Prod.	PV % Energy Prod.	XANT L-36 WT % Energy Prod.	VESTAS V47 WT % Energy Prod.	EE (%)
1000 kW	6.17	0.338	2.13	1.86	14.0	28.4	55.7	3.99
1100 kW	6.05	0.332	2.08	1.66	13.4	28.6	56.3	2.98
1200 kW	6.01	0.330	2.07	1.60	12.9	28.8	56.7	2.28
1300 kW	6.01	0.330	2.07	1.28	12.9	28.9	56.9	1.98
1400 kW	6.04	0.331	2.08	1.22	12.9	28.9	56.9	1.91
1500 kW	6.07	0.333	2.09	1.40	12.8	28.9	56.8	1.97

The capacities of the biogas generator, electrolyser and the costs of the other system components, significantly affect the overall techno-economic feasibility of the HRES configuration. Hence, detailed cost information for each component is presented in Table 5.25 to support the evaluation of the economic viability.

Table 5.25 The costs of each component for the PV/XANT L-36 WT/Vestas V47 WT/Biogas gen. system

Component	Capital Cost ($)	Replacement Cost ($)	O&M Cost ($)	Fuel Cost ($)	Salvage Cost ($)	Total Cost ($)
Lead acid Battery	211,200	581,388	233,687	0	178,215	848,060
Biogas generator	550,000	0	182,568	124,999	689,119	168,448
Electrolyser	130,000	177,955	345,220	0	73,131	580,044
PV	1,702,546	0	226,059	0	0	1,928,605
Hydrogen Tank	660,000	668,769	109,541	0	556,921	881,389
System Converter	258,708	354,143	0	0	145,535	467,316
Vestas V47	10,000	15,199	16,597	0	12,657	29,139
XANT L-36 WT	750,000	949,956	199,165	0	791,081	1,108,041
System	4,272,455	2,747,411	1,312,836	124,999	2,446,659	6,011,043

Table 5.26 presents the techno-economic performance of various hybrid renewable energy system configurations composed of different combinations of PV panels, XANT L-36 and Vestas V47 WT, and a biogas generator.

Table 5.26 Techno-economic analysis comparison of PV/XANT L-36 WT/Vestas V47 WT system with/without biogas generator

Energy Source	NPC (M$)	LCOE ($)	LCOH ($/kg)	Operating cost ($/year)	Initial capital (M$)	Renewable Fraction (%)	EE (%)
PV/XANT L-36 & Vestas V47 WT	6.94	0.381	2.38	94,165	3.82	100	18.2

Table 5.26 Techno-economic analysis comparison of PV/XANT L-36 WT/Vestas V47 WT system with/without biogas generator (continued)

Energy Source	NPC (M$)	LCOE ($)	LCOH ($/kg)	Operating cost ($/year)	Initial capital (M$)	Renewable Fraction (%)	EE (%)
PV/XANT L-36 & Vestas V47 WT/Biogas Gen. (1000 kW)	6.01	0.330	2.07	52,376	4.27	100	1.98

A comparison between the optimal PV/XANT L-36 WT/Vestas V47 WT/Biogas generator (1000 kW) configuration and the PV/XANT L-36 & Vestas V47 WT system reveals that the former has lower NPC and LCOH values. Furthermore, the proportion of EE decreases significantly from 18.2% to 1.98%, demonstrating more effective utilization of the available renewable energy resources.

5.2 Regression Model Results

Regression models use RMSE and R^2 metrics to compare the model performance in R. These metrics help to determine the alignment of the regression model with the data and how accurately it predicts the dependent variable.

5.2.1 Linear Regression Results

The results of the final linear regression model show that only 8 independent variables can be determined because 4 variables have singularity problem because of the multicollinearity between the independent variables (Table 5.27).

Table 5.27 Linear regression model results created in R

Coefficients	Estimate	Standard Error	t value
Intercept	3.5556	NA	NA
X1	8.9467	NA	NA
X2	0.8422	NA	NA
X3	- 4.3772	NA	NA

Table 5.27 Linear regression model results created in R (continued)

Coefficients	Estimate	Standard Error	t value
X4	- 6.3502	NA	NA
X5	- 1.7824	NA	NA
X6	2.8660	NA	NA
X7	- 0.7781	NA	NA
X8	- 0.1653	NA	NA
X9	NA	NA	NA
X10	NA	NA	NA
X11	NA	NA	NA
X12	NA	NA	NA

The multicollinearity issue cause overfitting in the model. As a result, this model is not reliable in terms of determining the RMSE and R^2. Furthermore, regularization techniques must be used to resolve the singularity problem since they include a penalty term in the loss function that removes multicollinearity.

5.2.2 Ridge, Lasso, Elastic Net Regression Results

The optimal lambda for each of the regression models is identified by cross-validation using training data. On the other hand, the results of the final regression models can be evaluated using test data with determination of RMSE and R^2 values. The optimal lambda was found as 0.251 with RMSE of 0.182 and R^2 of 0.983 in the RR model. For the LR model, the optimal lambda was calculated as 0.0158 with the RMSE of 0.286 and R^2 of 0.958. For the ENR model, the optimal alpha and lambda parameters were obtained as 0.961 and 0.00213. From the evaluation of the test data, the RMSE and R^2 values obtained for this model were 0.293 and 0.956,

respectively. The coefficients of the final RR model, LR model, and ENR model in R programming are given in Table 5.28.

Table 5.28 RR, LR and ENR model results created in R

Coefficients	Estimate in RR	Estimate in LR	Estimate in ENR
Intercept	3.55556	3.55556	3.55556
X1	0.11677	NA	NA
X2	- 0.04118	NA	- 0.00614
X3	0.11717	NA	NA
X4	0.09935	NA	NA
X5	- 0.07734	- 0.25261	- 0.25288
X6	0.10576	NA	NA
X7	0.15745	0.46932	0.45573
X8	0.10663	0.06860	0.06795
X9	0.08793	NA	NA
X10	0.08981	NA	NA
X11	- 0.12034	- 0.33401	- 0.36447
X12	0.03000	NA	0.01236

The optimal lambda for each of the regression models is identified by cross-validation using training data. On the other hand, the results of the final regression models can be evaluated using test data with determination of RMSE and R^2 values. The optimal lambda is identified as 0.251 with RMSE of 0.182 and R^2 of 0.983 in

the RR model. For the LR model, the optimal lambda is identified as 0.0158. Also, the RMSE is 0.286 and R^2 is 0.958 for this model.

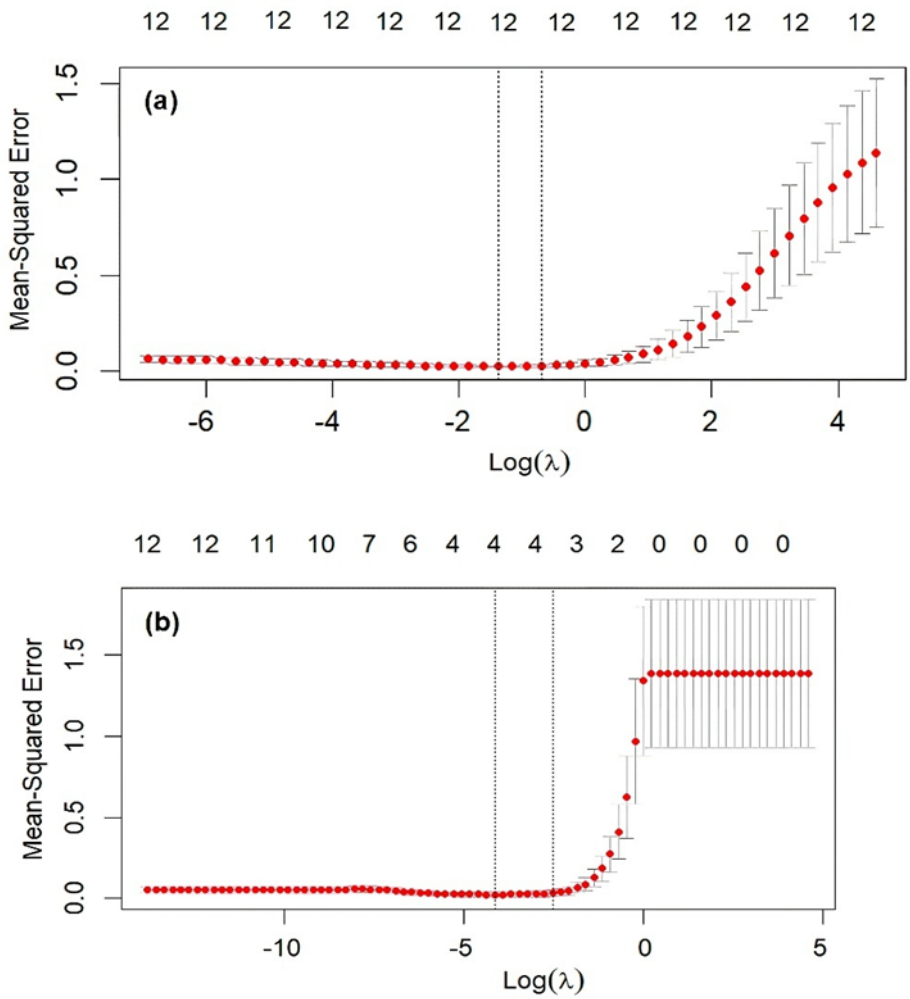


Figure 5.8 Mean squared error vs log (λ) for the train data in (a) RR; (b) LR

The plot of mean squared error (MSE) against log lambda for the training data is shown in Figure 5.8. The lambda within one standard error of the the minimum MSE (lambda.1se) is indicated by the vertical line to the right, while the lambda with the minimum MSE (lambda.min) is indicated by the vertical line to the left. The latter is used to produce a more regularized model with high accuracy. From Figure 5.8 (a), as the logarithmic value of lambda increases beyond 0, the MSE increases because the coefficients are constrained too much. As a result, underfitting occurs in the RR model. It can be seen from Figure 5.8 (b), when logarithmic lambda equals 0, the MSE increases significantly because it removes

coefficients beyond this value in the LR model. So, further model predictions is not possible in this region. The optimal parameters, showing the lowest prediction error, are identified at the lambda.min vertical line, corresponding to the final regression models.

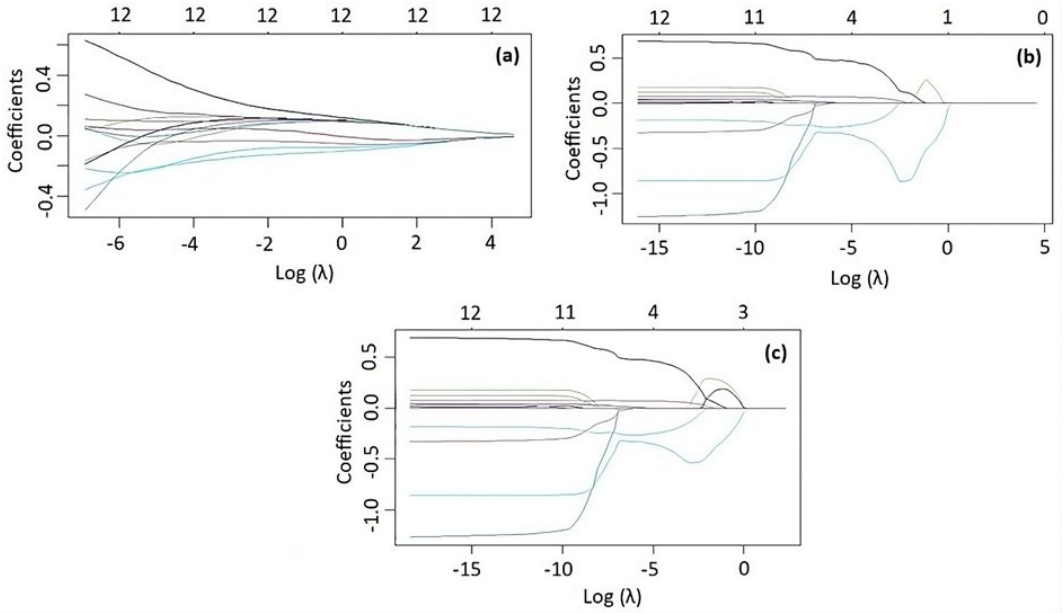


Figure 5.9 Coefficients vs log (λ) for the train data in (a) RR; (b) LR; (c) ENR

Figure 5.9 illustrates the change in the coefficients with log lambda for the train data. As log lambda increases, the coefficients move towards zero due to the regularization penalty. At lower log lambda values, the coefficients are larger, which correspond to higher ordinary least squares values. This indicates less regularization and a higher risk of overfitting the model. At the top of the graph, the number of remaining coefficients as a function of log lambda can be seen. In Fig. 5.9 (a), all coefficients shrink but remain in the RR model, even at higher lambda values. In Fig. 5.9 (b) and (c), some coefficients shrink exactly to zero as lambda increases, which is due to the specific penalty terms used in the LR and ENR models. These penalty terms enable feature selection by identifying the most important predictors and eliminating irrelevant ones. As shown in the graphs, the final LR model retains 4 coefficients, while the final ENR model retains 6 coefficients after the cross-validation steps.

5.2.3 Model Comparison

Table 5.29 presents the comparison of the regression models to evaluate model performance. Since the linear regression model has a multicollinearity problem, it is not included in the comparison of the models. On the other hand, the RR model achieves the lowest RMSE value for the test data compared to the other models. Lower RMSE values demonstrate better model performance, as the predictions are more accurate and closer to the actual observed values. The RR model has also the highest R^2 value for the test data which indicates a good fit. A higher R^2 means that the model captures more of the variability in the dependent variable. Moreover, since the RR shrinks the coefficients to lower values, all independent variables remain in the model. Hence, only 4 and 6 independent variables remain in the LR and ENR models, respectively. Therefore, the best model is determined to be RR, as it has the lowest RMSE, the highest R^2, and retains all the coefficients in the model.

Table 5.29 Comparison of Model Performance Based on Different Regression Parameters

Parameters	Linear Regression Model	RR Model	LR Model	ENR Model
RMSE of test data	NA	0.182	0.286	0.293
R^2 of test data	NA	0.983	0.958	0.956
Coefficients Shrinkage	NA	Coefficients shrink towards zero	Some coefficients shrink to zero	Some coefficients shrink to zero
Number of Coefficients	8	12	4	6
Multicollinearity	Multicollinearity present	Handles multicollinearity	Handles multicollinearity	Handles multicollinearity

The final RR model that best fits our data is given by the equation below:

$$Y = 3.55556 + 0.11677\mathbf{X1} - 0.04118\mathbf{X2} + 0.11717\mathbf{X3} + 0.09935\mathbf{X4} - 0.07734\mathbf{X5} + 0.10576\mathbf{X6} + 0.15745\mathbf{X7} + 0.10663\mathbf{X8} + 0.08793\mathbf{X9} + 0.08981\mathbf{X10} - 0.12034\mathbf{X11} + 0.03000\mathbf{X12} \quad (3.19)$$

The final model indicates that the number of global hydrogen refuelling stations (X7) have the strongest impact on global green hydrogen production (Y). As more refuelling stations are established, the demand for green hydrogen is expected to increase. This growing demand can encourage companies to build new green hydrogen production facilities, as refuelling stations require a consistent supply to meet the demand. On the other hand, the global average fuel oil price (X12) seems to have the least impact on global green hydrogen production. This is because fluctuations in fuel oil prices do not directly affect the global production of green hydrogen, since it is largely based on renewable energy sources rather than fossil fuels. Moreover, global solar PV costs (X2), global wind costs (X5), and global green hydrogen costs (X11) have a negative relationship with global green hydrogen production (Y). This means that when global solar PV costs, wind costs, or green hydrogen costs increase, the production of green hydrogen becomes more expensive and less feasible. As a result, investment is discouraged, and generation capacity is limited, decreasing the green hydrogen production.

6
CONCLUSION

6.1 Conclusion

In this study, several HRES configurations are proposed to produce green hydrogen for a hydrogen refuelling station. The configurations powered by renewable sources incorporate PV panels and two distinct WT models (XANT L-36 and Vestas V47) to achieve fully renewable electricity generation and green hydrogen production. Techno-economic assessments of each configuration are performed using HOMER software, considering the parameters such as NPC, LCOE, LCOH, renewable energy fraction and EE. The renewable energy configuration with PV panels, XANT L-36 and Vestas V47 WT provides a highly competitive LCOH of $2.36/kg, which is significantly lower than the LCOH values reported in the literature. According to the simulation results, more than 700 tons of CO_2 emissions can be avoided annually through the operation of these system configurations.

Alternative systems include a TLC and a boiler to recover EE and meet thermal demands. A MGT is also integrated to recover waste heat and optimize the system design. The results indicate that systems with a TLC and boiler have higher NPC, LCOE, and LCOH compared to systems without EE recovery. However, these costs are significantly reduced with the incorporation of a MGT, which improves system performance. It supports the system by reducing the reliance on renewable energy for the electrical load and supporting the thermal load by waste heat recovery. Nonetheless, the renewable fraction of configurations with thermal load components is substantially reduced by more than 40% due to the fuel consumption of the boiler and MGT. The optimal system configuration includes 21.8 kW PV panels, 2 XANT L-36 WT (300 kW each), 1 Vestas V47 WT (660 kW), 226 battery

strings, a 1000 kW electrolyser, 1100 kg hydrogen storage tank, 1009 kW converter, 1380 kW TLC, and a 240 kW MGT. This configuration provides minimum NPC, LCOE and LCOH costs which are $6.28 M, $0.249 kWh and $2.14/kg, respectively.

Furthermore, an econometric analysis of green hydrogen production is conducted using regression models. In this respect, linear regression, RR, LR and ENR models are evaluated to identify the optimal model that fits the data well. According to the RMSE and R^2 results, the RR model provides the best fit, and the relationship between global green hydrogen production and the independent variables is given by the equation derived from the coefficients of this model. The regression equation exhibits a statistically significant and substantially higher coefficient for the variable representing global hydrogen refuelling stations (X7) relative to other independent variables. This indicates that, within the specified model, the expansion of refuelling infrastructure is the most robust predictor and a primary driver of scaled green hydrogen production. Conversely, it shows that the global average price of fuel oil (X12) does not demonstrate a significant relationship with the expansion of green hydrogen production on a global scale as its regression coefficient is small.

The biomass-integrated HRES that combine a biogas generator with PV and wind turbine renewable sources are also analysed within this study. These HRES components create a strong synergistic effect, significantly improving the system's overall performance and economic efficiency. The analysis results shows that a configuration relying only on straw biomass as the main energy source is not cost-effective, exhibiting very high NPC and LCOH values. This configuration also produces high EE which results inefficient resource utilization. Alternatively, the optimized hybrid system that integrates PV panels, XANT L-36 wind turbine, and a biogas generator is found to be the most technically and economically suitable option. This configuration substantially reduces both NPC and LCOH while lowering EE generation to less than 1%. On the other hand, the similar system including both XANT L-36 and Vestas V47 WT produces approximately 2% surplus energy, which still represents an efficient energy utilization. This low excess energy indicates a highly efficient a system and the variability of solar and

wind resources is effectively compensated by the controllable output of the biogas generator. Consequently, the study demonstrates that HRES with biomass resource offer a simple, practical, and economically sustainable way for developing efficient and reliable hydrogen refuelling station.

REFERENCES

[1] O. Nematollahi, P. Alamdari, M. Jahangiri, A. Sedaghat, and A. A. Alemrajabi, "A techno-economical assessment of solar/wind resources and hydrogen production: A case study with GIS maps," *Energy*, vol. 175, pp. 914–930, May 2019, doi: 10.1016/J.ENERGY.2019.03.125.

[2] J. Li, P. Liu, and Z. Li, "Optimal design and techno-economic analysis of a hybrid renewable energy system for off-grid power supply and hydrogen production: A case study of West China," *Chemical Engineering Research and Design*, vol. 177, pp. 604–614, Jan. 2022, doi: 10.1016/j.cherd.2021.11.014.

[3] H. S. Das, C. W. Tan, A. H. M. Yatim, and K. Y. Lau, "Feasibility analysis of hybrid photovoltaic/battery/fuel cell energy system for an indigenous residence in East Malaysia," 2017, *Elsevier Ltd*. doi: 10.1016/j.rser.2017.01.174.

[4] T. R. Ayodele, T. C. Mosetlhe, A. A. Yusuff, and M. Ntombela, "Optimal design of wind-powered hydrogen refuelling station for some selected cities of South Africa," *Int J Hydrogen Energy*, vol. 46, no. 49, pp. 24919–24930, Jul. 2021, doi: 10.1016/j.ijhydene.2021.05.059.

[5] International Energy Agency, "Sources of electricity generation." [Online]. Available: https://www.iea.org/countries

[6] World Health Organization, *Health risk assessment from the nuclear accident after the 2011 Great East Japan earthquake and tsunami, based on a preliminary dose estimation*. 2013.

[7] A. John, S. Basu, Akshay, and A. Kumar, "Design and evaluation of stand-alone solar-hydrogen energy storage system for academic institute: A case study," in *Materials Today: Proceedings*, Elsevier Ltd, 2021, pp. 5918–5922. doi: 10.1016/j.matpr.2021.04.461.

[8] V. M. Phap *et al.*, "Feasibility analysis of hydrogen production potential from rooftop solar power plant for industrial zones in Vietnam," *Energy Reports*, vol. 8, pp. 14089–14101, Nov. 2022, doi: 10.1016/j.egyr.2022.10.337.

[9] O. M. Babatunde, J. L. Munda, and Y. Hamam, "Off-grid hybrid photovoltaic – micro wind turbine renewable energy system with hydrogen and battery storage: Effects of sun tracking technologies," *Energy Convers Manag*, vol. 255, Mar. 2022, doi: 10.1016/j.enconman.2022.115335.

[10] S. Praveenkumar *et al.*, “Techno-economic optimization of PV system for hydrogen production and electric vehicle charging stations under five different climatic conditions in India,” *Int J Hydrogen Energy*, vol. 47, no. 90, pp. 38087–38105, Nov. 2022, doi: 10.1016/j.ijhydene.2022.09.015.

[11] E. M. Barhoumi, P. C. Okonkwo, I. Ben Belgacem, M. Zghaibeh, and I. Tlili, “Optimal sizing of photovoltaic systems based green hydrogen refueling stations case study Oman,” *Int J Hydrogen Energy*, vol. 47, no. 75, pp. 31964–31973, Sep. 2022, doi: 10.1016/j.ijhydene.2022.07.140.

[12] M. Gökçek and C. Kale, “Optimal design of a Hydrogen Refuelling Station (HRFS) powered by Hybrid Power System,” *Energy Convers Manag*, vol. 161, pp. 215–224, Apr. 2018, doi: 10.1016/j.enconman.2018.02.007.

[13] M. Gökçek and C. Kale, “Techno-economical evaluation of a hydrogen refuelling station powered by Wind-PV hybrid power system: A case study for İzmir-çeşme,” *Int J Hydrogen Energy*, vol. 43, no. 23, pp. 10615–10625, Jun. 2018, doi: 10.1016/j.ijhydene.2018.01.082.

[14] S. H. Siyal, D. Mentis, and M. Howells, “Economic analysis of standalone wind-powered hydrogen refueling stations for road transport at selected sites in Sweden,” *Int J Hydrogen Energy*, vol. 40, no. 32, pp. 9855–9865, Aug. 2015, doi: 10.1016/j.ijhydene.2015.05.021.

[15] P. C. Okonkwo *et al.*, “Utilization of renewable hybrid energy for refueling station in Al-Kharj, Saudi Arabia,” *Int J Hydrogen Energy*, vol. 47, no. 53, pp. 22273–22284, Jun. 2022, doi: 10.1016/j.ijhydene.2022.05.040.

[16] Q. Chen, Y. Gu, Z. Tang, D. Wang, and Q. Wu, “Optimal design and techno-economic assessment of low-carbon hydrogen supply pathways for a refueling station located in Shanghai,” *Energy*, vol. 237, Dec. 2021, doi: 10.1016/j.energy.2021.121584.

[17] R. P. Micena, O. R. Llerena-Pizarro, T. M. de Souza, and J. L. Silveira, “Solar-powered Hydrogen Refueling Stations: A techno-economic analysis,” *Int J Hydrogen Energy*, vol. 45, no. 3, pp. 2308–2318, Jan. 2020, doi: 10.1016/j.ijhydene.2019.11.092.

[18] M. Jahangiri, R. A. Rizi, and A. A. Shamsabadi, “Feasibility study on simultaneous generation of electricity and heat using renewable energies in Zarrin Shahr, Iran,” *Sustain Cities Soc*, vol. 38, pp. 647–661, Apr. 2018, doi: 10.1016/j.scs.2018.01.043.

[19] M. Jahangiri, F. K. Shahmarvandi, and R. Alayi, “Renewable Energy-Based Systems on a Residential Scale in Southern Coastal Areas of Iran: Trigeneration of Heat, Power, and Hydrogen,” *Journal of Renewable Energy and Environment*, vol. 8, no. 4, pp. 67–76, Oct. 2021, doi: 10.30501/jree.2021.261980.1170.

[20] B. K. Das and M. Hasan, “Optimal sizing of a stand-alone hybrid system for electric and thermal loads using excess energy and waste heat,” *Energy*, vol. 214, Jan. 2021, doi: 10.1016/j.energy.2020.119036.

[21] B. K. Das, M. S. H. K. Tushar, and R. Hassan, “Techno-economic optimisation of stand-alone hybrid renewable energy systems for concurrently meeting electric and heating demand,” *Sustain Cities Soc*, vol. 68, May 2021, doi: 10.1016/j.scs.2021.102763.

[22] M. R. Akhtari and M. Baneshi, “Techno-economic assessment and optimization of a hybrid renewable co-supply of electricity, heat and hydrogen system to enhance performance by recovering excess electricity for a large energy consumer,” *Energy Convers Manag*, vol. 188, pp. 131–141, May 2019, doi: 10.1016/j.enconman.2019.03.067.

[23] S. Di Micco, F. Romano, E. Jannelli, A. Perna, and M. Minutillo, “Techno-economic analysis of a multi-energy system for the co-production of green hydrogen, renewable electricity and heat,” *Int J Hydrogen Energy*, vol. 48, no. 81, pp. 31457–31467, Sep. 2023, doi: 10.1016/j.ijhydene.2023.04.269.

[24] N. M. Isa, H. S. Das, C. W. Tan, A. H. M. Yatim, and K. Y. Lau, “A techno-economic assessment of a combined heat and power photovoltaic/fuel cell/battery energy system in Malaysia hospital,” *Energy*, vol. 112, pp. 75–90, Oct. 2016, doi: 10.1016/j.energy.2016.06.056.

[25] M. Ramesh and R. P. Saini, “Dispatch strategies based performance analysis of a hybrid renewable energy system for a remote rural area in India,” *J Clean Prod*, vol. 259, Jun. 2020, doi: 10.1016/j.jclepro.2020.120697.

[26] H. Liu, G. M. Jiang, H. Y. Zhuang, and K. J. Wang, “Distribution, utilization structure and potential of biomass resources in rural China: With special references of crop residues,” Jun. 2008. doi: 10.1016/j.rser.2007.01.011.

[27] U. und ländliche R. des L. S.-H. Ministerium für Landwirtschaft, “Energiepotenzial aus Biomasse und Versorgungsbeitrag,” 2020.

[28] S. O. Sanni, J. Y. Oricha, T. O. Oyewole, and F. I. Bawonda, “Analysis of backup power supply for unreliable grid using hybrid solar PV/diesel/biogas system,” *Energy*, vol. 227, Jul. 2021, doi: 10.1016/j.energy.2021.120506.

[29] S. G. Sigarchian, R. Paleta, A. Malmquist, and A. Pina, “Feasibility study of using a biogas engine as backup in a decentralized hybrid (PV/wind/battery) power generation system - Case study Kenya,” *Energy*, vol. 90, pp. 1830–1841, 2015, doi: 10.1016/j.energy.2015.07.008.

[30] H. Al-Najjar, H. J. El-Khozondar, C. Pfeifer, and R. Al Afif, “Hybrid grid-tie electrification analysis of bio-shared renewable energy systems for domestic application,” *Sustain Cities Soc*, vol. 77, Feb. 2022, doi: 10.1016/j.scs.2021.103538.

[31] J. Li, P. Liu, and Z. Li, “Optimal design and techno-economic analysis of a solar-wind-biomass off-grid hybrid power system for remote rural electrification: A case study of west China,” *Energy*, vol. 208, Oct. 2020, doi: 10.1016/j.energy.2020.118387.

[32] Y. Kirim, H. Sadikoglu, and M. Melikoglu, “Technical and economic analysis of biogas and solar photovoltaic (PV) hybrid renewable energy

system for dairy cattle barns," *Renew Energy*, vol. 188, pp. 873–889, Apr. 2022, doi: 10.1016/j.renene.2022.02.082.

[33] Y. Kirim, H. Sadikoglu, and M. Melikoglu, "Development of a Hybrid Renewable Energy System with Co-Firing Option," *Energy Sources, Part A: Recovery, Utilization and Environmental Effects*, vol. 47, no. 1, pp. 10560–10575, 2025, doi: 10.1080/15567036.2021.1967521.

[34] T. A. Boghdady, A. J. Alamer, M. M. Yousef, A. M. Elshafee, M. A. Mostafa Hassan, and A. M. Seif, "Technical and economic study of powering poultry farm in Egypt using PV-biomass on-grid energy generation system: Case study," *WSEAS Transactions on Power Systems*, vol. 16, pp. 67–77, Apr. 2021, doi: 10.37394/232016.2021.16.7.

[35] T. Sarkar, A. Bhattacharjee, H. Samanta, K. Bhattacharya, and H. Saha, "Optimal design and implementation of solar PV-wind-biogas-VRFB storage integrated smart hybrid microgrid for ensuring zero loss of power supply probability," *Energy Convers Manag*, vol. 191, pp. 102–118, Jul. 2019, doi: 10.1016/j.enconman.2019.04.025.

[36] M. A. V. Rad, R. Ghasempour, P. Rahdan, S. Mousavi, and M. Arastounia, "Techno-economic analysis of a hybrid power system based on the cost-effective hydrogen production method for rural electrification, a case study in Iran," *Energy*, vol. 190, Jan. 2020, doi: 10.1016/j.energy.2019.116421.

[37] H. El-houari *et al.*, "Feasibility evaluation of a hybrid renewable power generation system for sustainable electricity supply in a Moroccan remote site," *J Clean Prod*, vol. 277, Dec. 2020, doi: 10.1016/j.jclepro.2020.123534.

[38] P. Malik, M. Awasthi, and S. Sinha, "Techno-economic and environmental analysis of biomass-based hybrid energy systems: A case study of a Western Himalayan state in India," *Sustainable Energy Technologies and Assessments*, vol. 45, Jun. 2021, doi: 10.1016/j.seta.2021.101189.

[39] F. Bayrak, "Prediction of photovoltaic panel cell temperatures: Application of empirical and machine learning models," *Energy*, vol. 323, p. 135764, May 2025, doi: 10.1016/J.ENERGY.2025.135764.

[40] H2 MOBILITY Deutschland GmbH & Co KG, "Filling up with H2," 2025.

[41] M. H. Nehrir *et al.*, "A review of hybrid renewable/alternative energy systems for electric power generation: Configurations, control, and applications," Oct. 2011. doi: 10.1109/TSTE.2011.2157540.

[42] P. G. Arul, V. K. Ramachandaramurthy, and R. K. Rajkumar, "Control strategies for a hybrid renewable energy system: A review," 2015, *Elsevier Ltd*. doi: 10.1016/j.rser.2014.10.062.

[43] J. C. León Gómez, S. E. De León Aldaco, and J. Aguayo Alquicira, "A Review of Hybrid Renewable Energy Systems: Architectures, Battery Systems, and Optimization Techniques," Jun. 01, 2023, *Multidisciplinary Digital Publishing Institute (MDPI)*. doi: 10.3390/eng4020084.

[44] L. Olatomiwa, S. Mekhilef, M. S. Ismail, and M. Moghavvemi, “Energy management strategies in hybrid renewable energy systems: A review,” 2016, *Elsevier Ltd*. doi: 10.1016/j.rser.2016.05.040.

[45] Y. S. Mohammed, M. W. Mustafa, and N. Bashir, “Hybrid renewable energy systems for off-grid electric power: Review of substantial issues,” 2014, *Elsevier Ltd*. doi: 10.1016/j.rser.2014.04.022.

[46] K. E. Bassey, “HYBRID RENEWABLE ENERGY SYSTEMS MODELING,” 2024, doi: 10.51594/estj/v4i6.1255.

[47] M. K. Deshmukh and S. S. Deshmukh, “Modeling of hybrid renewable energy systems,” Jan. 2008. doi: 10.1016/j.rser.2006.07.011.

[48] Q. Hassan, S. Algburi, A. Z. Sameen, H. M. Salman, and M. Jaszczur, “A review of hybrid renewable energy systems: Solar and wind-powered solutions: Challenges, opportunities, and policy implications,” Dec. 01, 2023, *Elsevier B.V.* doi: 10.1016/j.rineng.2023.101621.

[49] B. Bhandari, K. T. Lee, G. Y. Lee, Y. M. Cho, and S. H. Ahn, “Optimization of hybrid renewable energy power systems: A review,” *International Journal of Precision Engineering and Manufacturing - Green Technology*, vol. 2, no. 1, pp. 99–112, 2015, doi: 10.1007/s40684-015-0013-z.

[50] P. Roy, J. He, T. Zhao, and Y. V. Singh, “Recent Advances of Wind-Solar Hybrid Renewable Energy Systems for Power Generation: A Review,” 2022, *Institute of Electrical and Electronics Engineers Inc.* doi: 10.1109/OJIES.2022.3144093.

[51] P. Bajpai and V. Dash, “Hybrid renewable energy systems for power generation in stand-alone applications: A review,” Jun. 2012. doi: 10.1016/j.rser.2012.02.009.

[52] D. Neves, C. A. Silva, and S. Connors, “Design and implementation of hybrid renewable energy systems on micro-communities: A review on case studies,” Mar. 2014. doi: 10.1016/j.rser.2013.12.047.

[53] D. P. Kaundinya, P. Balachandra, and N. H. Ravindranath, “Grid-connected versus stand-alone energy systems for decentralized power-A review of literature,” Oct. 2009. doi: 10.1016/j.rser.2009.02.002.

[54] J. F. Manwell, “Hybrid Energy Systems,” *Encyclopedia of Energy*, 2004.

[55] International Renewable Energy Agency, “Renewable Generation.” [Online]. Available: https://www.irena.org/Energy-Transition/Technology

[56] Our World in Data, “Global Installed Renewable Energy Capacity by Technology.” [Online]. Available: https://ourworldindata.org/search?q=Installed%20Solar%20and%20Wind%20Capacity

[57] M. R. Maghami, A. G. O. Mutambara, C. Gomes, and J. Pasupuleti, “Impact of heat recovery and thermal load control on combined heat and power (CHP) performance,” *Energy Convers Manag*, vol. 307, May 2024, doi: 10.1016/j.enconman.2024.118388.

[58] B. K. Das, M. S. H. K. Tushar, and F. Zaman, “Techno-economic feasibility and size optimisation of an off-grid hybrid system for supplying electricity and thermal loads,” *Energy*, vol. 215, Jan. 2021, doi: 10.1016/j.energy.2020.119141.

[59] Homer Energy, “Homer Pro Version 3.7 User Manual,” 2016.

[60] R. Banihabib and M. Assadi, “The Role of Micro Gas Turbines in Energy Transition,” Nov. 01, 2022, *MDPI*. doi: 10.3390/en15218084.

[61] S. Saib, A. Gherbi, R. Bayindir, and A. Kaabeche, “Multi-objective Optimization of a Hybrid Renewable Energy System with a Gas Micro-turbine and a Storage Battery,” *Arab J Sci Eng*, vol. 45, no. 3, pp. 1553–1566, Mar. 2020, doi: 10.1007/s13369-019-04066-4.

[62] J. Li, Z. Liu, and R. Ye, “Current Status and Prospects of Gas Turbine Technology Application,” in *Journal of Physics: Conference Series*, IOP Publishing Ltd, Nov. 2021. doi: 10.1088/1742-6596/2108/1/012009.

[63] R. De Robbio, “Micro Gas Turbine Role in Distributed Generation with Renewable Energy Sources,” Jan. 01, 2023, *MDPI*. doi: 10.3390/en16020704.

[64] I. Aslanidou, M. Rahman, V. Zaccaria, and K. G. Kyprianidis, “Micro Gas Turbines in the Future Smart Energy System: Fleet Monitoring, Diagnostics, and System Level Requirements,” Jun. 01, 2021, *Frontiers Media S.A.* doi: 10.3389/fmech.2021.676853.

[65] J. Millward-Hopkins, J. K. Steinberger, N. D. Rao, and Y. Oswald, “Providing decent living with minimum energy: A global scenario,” *Global Environmental Change*, vol. 65, Nov. 2020, doi: 10.1016/j.gloenvcha.2020.102168.

[66] E. Baker, A. P. Goldstein, and I. M. Azevedo, “A perspective on equity implications of net zero energy systems,” *Energy and Climate Change*, vol. 2, Dec. 2021, doi: 10.1016/j.egycc.2021.100047.

[67] B. E. Lebrouhi, J. J. Djoupo, B. Lamrani, K. Benabdelaziz, and T. Kousksou, “Global hydrogen development - A technological and geopolitical overview,” Feb. 05, 2022, *Elsevier Ltd*. doi: 10.1016/j.ijhydene.2021.12.076.

[68] Z. Abdin, A. Zafaranloo, A. Rafiee, W. Mérida, W. Lipiński, and K. R. Khalilpour, “Hydrogen as an energy vector,” Mar. 01, 2020, *Elsevier Ltd*. doi: 10.1016/j.rser.2019.109620.

[69] I. K. Muritala, D. Guban, M. Roeb, and C. Sattler, “High temperature production of hydrogen: Assessment of non-renewable resources technologies and emerging trends,” *Int J Hydrogen Energy*, vol. 45, no. 49, pp. 26022–26035, Oct. 2020, doi: 10.1016/j.ijhydene.2019.08.154.

[70] Republic of Turkey Ministry of Energy and Natural Resources, “Hydrogen Technologies Strategy and Roadmap of Turkey,” 2023.

[71] M. Hermesmann and T. E. Müller, “Green, Turquoise, Blue, or Grey? Environmentally friendly Hydrogen Production in Transforming Energy Systems,” May 01, 2022, *Elsevier Ltd*. doi: 10.1016/j.pecs.2022.100996.

[72] S. G. Nnabuife, A. K. Hamzat, J. Whidborne, B. Kuang, and K. W. Jenkins, “Integration of renewable energy sources in tandem with electrolysis: A technology review for green hydrogen production,” *Int J Hydrogen Energy*, vol. 107, pp. 218–240, Mar. 2025, doi: 10.1016/j.ijhydene.2024.06.342.

[73] F. Zhang, P. Zhao, M. Niu, and J. Maddy, “The survey of key technologies in hydrogen energy storage,” Sep. 07, 2016, *Elsevier Ltd*. doi: 10.1016/j.ijhydene.2016.05.293.

[74] I. A. Gondal, S. A. Masood, and R. Khan, “Green hydrogen production potential for developing a hydrogen economy in Pakistan,” *Int J Hydrogen Energy*, vol. 43, no. 12, pp. 6011–6039, Mar. 2018, doi: 10.1016/j.ijhydene.2018.01.113.

[75] A. Ajanovic, M. Sayer, and R. Haas, “The economics and the environmental benignity of different colors of hydrogen,” *Int J Hydrogen Energy*, vol. 47, no. 57, pp. 24136–24154, Jul. 2022, doi: 10.1016/j.ijhydene.2022.02.094.

[76] International Renewable Energy Agency, “Green Hydrogen Cost Reduction: Scaling up Electrolysers to Meet the 1.5 0C Climate Goal,” 2020.

[77] Bloomberg Finance L.P., “‘Green’ Hydrogen to Outcompete ‘Blue’ Everywhere by 2030.” [Online]. Available: https://about.bnef.com/insights/clean-energy/green-hydrogen-to-outcompete-blue-everywhere-by-2030

[78] R. Angelico, F. Giametta, B. Bianchi, and P. Catalano, “Green Hydrogen for Energy Transition: A Critical Perspective,” Jan. 01, 2025, *Multidisciplinary Digital Publishing Institute (MDPI)*. doi: 10.3390/en18020404.

[79] B. S. Zainal *et al.*, “Recent advancement and assessment of green hydrogen production technologies,” Jan. 01, 2024, *Elsevier Ltd*. doi: 10.1016/j.rser.2023.113941.

[80] D. Wickham, A. Hawkes, and F. Jalil-Vega, “Hydrogen supply chain optimisation for the transport sector – Focus on hydrogen purity and purification requirements,” *Appl Energy*, vol. 305, Jan. 2022, doi: 10.1016/j.apenergy.2021.117740.

[81] S. Singh *et al.*, “Hydrogen: A sustainable fuel for future of the transport sector,” Jul. 18, 2015, *Elsevier Ltd*. doi: 10.1016/j.rser.2015.06.040.

[82] A. Murugan *et al.*, “Measurement challenges for hydrogen vehicles,” *Int J Hydrogen Energy*, vol. 44, no. 35, pp. 19326–19333, Jul. 2019, doi: 10.1016/j.ijhydene.2019.03.190.

[83] A. Iqbal, H. Malik, A. Riyaz, K. Abdellah, and S. Bayhan, *Renewable Power for Sustainable Growth*. 2020. [Online]. Available: http://www.springer.com/series/7818

[84] N. Qin and P. Brooker, “Hydrogen Fueling Stations Infrastructure,” 2014.

[85] O. Ehret and K. Bonhoff, “Hydrogen as a fuel and energy storage: Success factors for the German energiewende,” *Int J Hydrogen Energy*, vol. 40, no. 15, pp. 5526–5533, Apr. 2015, doi: 10.1016/j.ijhydene.2015.01.176.

[86] Federal Ministry for Economic Affairs and Energy, “The National Hydrogen Strategy.” [Online]. Available: https://www.bundeswirtschaftsministerium.de/Redaktion/EN/Hydrogen/Dossiers/national-hydrogen-strategy.html

[87] F. Cuevas, J. Zhang, and M. Latroche, “The Vision of France, Germany, and the European Union on Future Hydrogen Energy Research and Innovation,” Jun. 01, 2021, *Elsevier Ltd*. doi: 10.1016/j.eng.2021.04.010.

[88] G. James, D. Witten, T. Hastie, and R. Tibshirani, *An Introduction to Statistical Learning*. 2017.

[89] N. Shrestha, “Detecting Multicollinearity in Regression Analysis,” *Am J Appl Math Stat*, vol. 8, no. 2, pp. 39–42, Jun. 2020, doi: 10.12691/ajams-8-2-1.

[90] H. M. Nayem, S. Aziz, and B. M. G. Kibria, “Comparison among Ordinary Least Squares, Ridge, Lasso, and Elastic Net Estimators in the Presence of Outliers: Simulation and Application,” *International Journal of Statistical Sciences*, pp. 25–48, Dec. 2024, doi: 10.3329/ijss.v24i20.78212.

[91] Netti Herawati, Ameliana Wijayanti, Agus Sutrisno, Nusyirwan, and Misgiyati, “The Performance of Ridge Regression, LASSO, and Elastic-Net in Controlling Multicollinearity: A Simulation and Application,” *Journal of Modern Applied Statistical Methods*, vol. 23, Jan. 2024, doi: 10.56801/jmasm.v23.i2.4.

[92] J. I. Daoud, “Multicollinearity and Regression Analysis,” in *Journal of Physics: Conference Series*, Institute of Physics Publishing, Jan. 2018. doi: 10.1088/1742-6596/949/1/012009.

[93] J. Y. Le Chan *et al.*, “Mitigating the Multicollinearity Problem and Its Machine Learning Approach: A Review,” Apr. 01, 2022, *MDPI*. doi: 10.3390/math10081283.

[94] V. N. Gudivada, A. Apon, and J. Ding, “Data Quality Considerations for Big Data and Machine Learning: Going Beyond Data Cleaning and Transformations,” *International Journal on Advances in Software*, 2017, [Online]. Available: www.iaria.org

[95] J. Hoey, “Bias and Variance in Machine Learning,” 2018.

[96] B. Ghojogh and M. Crowley, “The Theory Behind Overfitting, Cross Validation, Regularization, Bagging, and Boosting: Tutorial,” 2023.

[97] Swathi P, “Analysis on Solutions for Over-fitting and Under-fitting in Machine Learning Algorithms,” *Int J Innov Res Sci Eng Technol*, vol. 7, 2018, doi: 10.15680/IJIRSET.2018.0712086.

[98] D. Berrar, “Cross-Validation,” *Encyclopedia of Bioinformatics and Computational Biology: ABC of Bioinformatics*, vol. 1–3, pp. 542–545, Jan. 2019, doi: 10.1016/B978-0-12-809633-8.20349-X.

[99] I. K. Nti, O. Nyarko-Boateng, and J. Aning, “Performance of Machine Learning Algorithms with Different K Values in K-fold CrossValidation,” *International Journal of Information Technology and Computer Science*, vol. 13, no. 6, pp. 61–71, Dec. 2021, doi: 10.5815/ijitcs.2021.06.05.

[100] T. Chai and R. R. Draxler, “Root mean square error (RMSE) or mean absolute error (MAE)?,” Feb. 28, 2014. doi: 10.5194/gmdd-7-1525-2014.

[101] T. O. Hodson, “Root-mean-square error (RMSE) or mean absolute error (MAE): when to use them or not,” Jul. 19, 2022, *Copernicus GmbH*. doi: 10.5194/gmd-15-5481-2022.

[102] L. Saunders, R. Russell, and D. Crabb, “The coefficient of determination: What determines a useful R2 statistic?,” Oct. 2012. doi: 10.1167/iovs.12-10598.

[103] O. Renaud and M. P. Victoria-Feser, “A robust coefficient of determination for regression,” *J Stat Plan Inference*, vol. 140, no. 7, pp. 1852–1862, Jul. 2010, doi: 10.1016/j.jspi.2010.01.008.

[104] G. Simon and C. Aliferis, *Artificial Intelligence and Machine Learning in Health Care and Medical Sciences*. 2024.

[105] D. M. Lane, D. Scott, M. Hebl, R. Guerra, D. Osherson, and H. Zimmer, *Introduction to Statistics*. 2003.

[106] J. O. Ogutu, T. Schulz-Streeck, and H. P. Piepho, “Genomic selection using regularized linear regression models: Ridge regression, lasso, elastic net and their extensions,” *BMC Proc*, vol. 6, no. SUPPL. 2, 2012, doi: 10.1186/1753-6561-6-S2-S10.

[107] M. Usman, S. I. S. Doguwa, and B. B. Alhaji, “Comparing the Prediction Accuracy of Ridge, Lasso and Elastic Net Regression Models with Linear Regression Using Breast Cancer Data,” *Bayero Journal of Pure and Applied Sciences*, vol. 14, no. 2, pp. 134–149, Jul. 2021, doi: 10.4314/bajopas.v14i2.16.

[108] S. Sinha and S. S. Chandel, “Review of software tools for hybrid renewable energy systems,” Apr. 2014. doi: 10.1016/j.rser.2014.01.035.

[109] S. Bahramara, M. P. Moghaddam, and M. R. Haghifam, “Optimal planning of hybrid renewable energy systems using HOMER: A review,” 2016, *Elsevier Ltd*. doi: 10.1016/j.rser.2016.05.039.

[110] Shutterstock, “Schleswig-Holstein State Map.” Accessed: Dec. 15, 2025. [Online]. Available: https://www.shutterstock.com/de/image-vector/schleswigholstein-state-map-germany-vector-silhouette-528630562

[111] W. und V. des L. S. H. Ministerium für Wissenschaft, “Energiepolitik für Schleswig-Holstein,” 2010.

[112] HOMER Energy, “HOMER Pro (Version 3.18.4),” 2016.

[113] J. D. Ampah, S. Afrane, E. B. Agyekum, H. Adun, A. A. Yusuf, and O. Bamisile, “Electric vehicles development in Sub-Saharan Africa: Performance assessment of standalone renewable energy systems for hydrogen refuelling and electricity charging stations (HRECS),” *J Clean Prod*, vol. 376, p. 134238, Nov. 2022, doi: 10.1016/J.JCLEPRO.2022.134238.

[114] E. B. Agyekum, J. D. Ampah, S. Afrane, T. S. Adebayo, and E. Agbozo, “A 3E, hydrogen production, irrigation, and employment potential assessment of a hybrid energy system for tropical weather conditions – Combination of HOMER software, shannon entropy, and TOPSIS,” *Int J Hydrogen Energy*, vol. 47, no. 73, pp. 31073–31097, Aug. 2022, doi: 10.1016/j.ijhydene.2022.07.049.

[115] A. E. N. and D. Schleswig-Holstein Ministry for Energy Transition, “Agriculture in Schleswig-Holstein,” 2016.

[116] D. H. Lee, “Econometric assessment of bioenergy development,” *Int J Hydrogen Energy*, vol. 42, no. 45, pp. 27701–27717, 2017, doi: 10.1016/j.ijhydene.2017.08.055.

[117] Q. Hassan, I. D. J. Azzawi, A. Z. Sameen, and H. M. Salman, “Hydrogen Fuel Cell Vehicles: Opportunities and Challenges,” *Sustainability (Switzerland)*, vol. 15, no. 15, Aug. 2023, doi: 10.3390/su151511501.

[118] Our World in Data, “Renewable electricity generation, World.” [Online]. Available: https://ourworldindata.org/grapher/modern-renewable-energy-consumption

[119] Aleasoft Energy Forecasting, “Levelized Cost of Electricity for Wind and Solar Photovoltaic.” [Online]. Available: https://aleasoft.com/drop-lcoe-renewable-energies-past-decade-drives-energy-transition/

[120] Flanders Investment & Trade in Poznan, “Hydrogen sector in Poland,” 2022. [Online]. Available: https://export.flandersinvestmentandtrade.com/sites/fit_domains/files/media/report/2022_Hydrogen%2520in%2520Poland_2.pdf

[121] E. B. Agyekum, C. Nutakor, A. M. Agwa, and S. Kamel, “A Critical Review of Renewable Hydrogen Production Methods: Factors Affecting Their Scale-Up and Its Role in Future Energy Generation,” *Membranes (Basel)*, 2022, doi: 10.3390/membranes12020173.

[122] Statista, “Average annual brent crude oil price from 1976 to 2025.” [Online]. Available: https://www.statista.com/statistics/262860/uk-brent-crude-oil-price-changes-since-1976/

PUBLICATIONS FROM THE THESIS

Conference Paper

1. B. B. Kalyoncu, Y. Kirim, and H. Sadikoglu, "Techno-Economic Optimization of Hybrid Renewable Energy Systems for Electricity and Heat Co-Production at a Hydrogen Refuelling Station," in Proceedings of the Grad Symposium 2025 Sustainable Solutions in Engineering, Yildiz Technical University, 2025, p. 51.

Paper

1. B. B. Kalyoncu, Y. Kirim, and H. Sadikoglu, "Optimization study of a hybrid renewable energy system for co-production of electricity and heat at a hydrogen refuelling station," *Int J Hydrogen Energy*, vol. 148, Jul. 2025, doi: 10.1016/j.ijhydene.2025.06.134.